SEISMIC PERFORMANCE EVALUATION OF NOVEL COLD-FORMED STEEL FRAMED SHEAR WALLS SHEATHED WITH CORRUGATED STEEL SHEETS

Xing Lan

Thesis Prepared for the Degree of

MASTER OF SCIENCE

UNIVERSITY OF NORTH TEXAS

August 2017

APPROVED:

Cheng Yu, Major Professor
Michael Shenoda, Committee Member
Haifeng Zhang, Committee Member
Enrique Barbieri, Chair of the Department of Engineering Technology
Costas Tsatsoulis, Dean of the College of Engineering
Victor Prybutok, Dean of the Toulouse Graduate School

Lan, Xing. *Seismic Performance Evaluation of Novel Cold-Formed Steel Framed Shear Walls Sheathed with Corrugated Steel Sheets*. Master of Science (Engineering Technology), August 2017, 116 pp., 19 tables, 20 figures, references, 24 titles.

This thesis presents experiments and numerical analysis of a novel cold-formed steel framed shear wall sheathed with corrugated steel sheets. The objective of this newly designed shear wall is to meet the growing demand of mid-rise buildings and the combustibility requirement in the International Building Code. The strength of the novel shear wall is higher than currently code certified shear wall in AISI S400-15 so that it could be more favorable for mid-rise building in areas that are prone to earthquakes and hurricanes. Full-scale monotonic and cyclic tests were conducted on bearing walls and shear walls under combined lateral and gravity loads. Though the gravity loads had negative effects on the strength and stiffness of the shear wall due to the buckling of the chord framing members, it still shows promise to be used in mid-rise buildings. The objective of numerical analysis is to quantify the seismic performance factors of the newly design shear wall lateral-force resisting system by using the recommended methodology in FEMA P695. Two groups of building archetypes, story varied from two to five, were simulated in OpenSees program. Nonlinear static and dynamic analysis were performed in both horizontal directions of each building archetype. Finally, the results of the performance evaluation verified the seismic performance factors($R=C_d=6.5$ and $\Omega=3.0$) were appropriate for the novel shear wall system.

ACKNOWLEDGEMENTS

Massive thanks to all the individuals who accompanied me in the journey of study and research in the University of North Texas (UNT), the journey could not be completed without their help, advice, counsel and dedication.

First and foremost, so much thank you Dr. Cheng Yu for giving me the opportunity to join the research group and participating in the exciting innovative shear wall project. I am so grateful for your academic and financial support throughout the years. Your guidance, working attitude, and creative thinking influenced me a lot and I firmly believe they will benefit me in the future.

Second, thank you to my professors Dr. Michael Shenoda, Dr. Haifeng Zhang, Dr. Seifollah Nasrazadani and all other faculty and staff in UNT who provided assistance in my study and research. I would also especially say thanks to ETEC Lab Manager Bobby Grime who provided precious technical suggestions to the lab work.

Thanks to the hard work and dedication of all my friends who helped me perform the wall tests. We developed incredible friendship during the work. These friends are Mahsa Mahdavian, Nathan Derrick, Nick O'Connor, Zhishan Yan, Jeremy Artman, Adam Johnson and Dawson Guerrettaz. Special credit to Ph.D student Wenying Zhang, who assisted me tremendously in the aspects of test and numerical analysis.

I would also like to thank our donors, Steel Stud manufacturers Association, Nucor Vulcraft and Simpson Strong-Tie.

Finally, tremendously thanks to my parents and brother who always support me and help me go through all the difficulties in this journey.

TABLE OF CONTENTS

Page

LIST OF TABLES

Page

LIST OF FIGURES

Page

CHAPTER 1

INTRODUCTION

In contrary to the hot-rolled steel member, cold-formed steel member is made in room temperatures by feeding sheet steel through roll forming machines. Cold-formed steel members can be formed from a wide range of material thickness that enables them to meet the requirements of nearly all structural and non-structural applications.

Cold-formed steel is widely used in interior and exterior walls systems, floor systems and roof truss systems for low-rise and mid-rise (4-9 stories) structures. Due to its light weight, high strength, non-combustible nature, fast and ease of installation, it has gain popularity in recent years. As a recognized green building material, steel framing projects can also earn credits or points for green building rating programs as well as other government incentives.

Cold-formed steel shear wall, by definition, is a wall with structural sheathing attached to cold-formed steel structural members and designed to primarily resist lateral forces parallel to the wall (AISI S400-15). The CFS framed walls sheathed by flat steel sheets or wood-based panels are the common types of shear walls. Figure 1.1 shows a typical 4 ft. by 8 ft. CFS shear wall with sheathing. The sheathing is usually fastened to the frame. Hold-downs are commonly used in CFS shear walls to resist the overturning forces.

As population is growing in cities, the demand of housing is expected to grow as well. However, less and less land can be developed for housing. Mid-rise building (4-9 stories), especially built out of cold-formed steel structure, is one of the economic solutions for housing demand. Most of these mid-rise residential and commercial buildings fall under the International Building Code (IBC 2015)'s Types I and II construction categories. IBC 602.2 states "Type I and

II construction are those types of construction in which the building elements listed in Table 601 are of noncombustible materials, …" Part of contents is shown in Table 1.1.

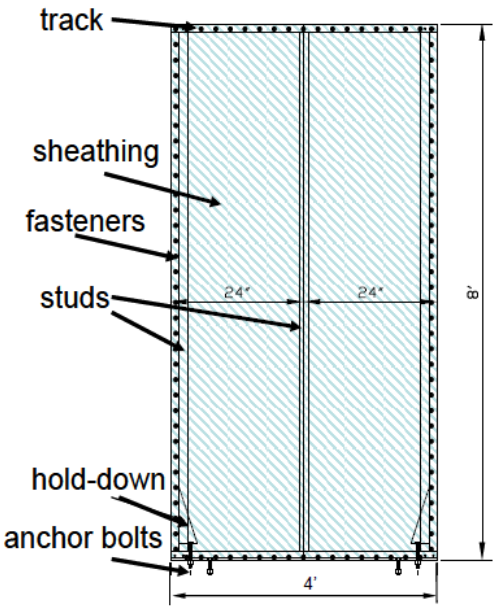

Figure 1.1 - A Typical 4 ft by 8 ft Cold-Formed Steel Shear Wall

Table 1.1 - Fire Resistance Rating Requirements for Building Elements (part of the Table 60-IBC)

BUILDING ELEMENT	TYPE I		TYPE II	
	A	B	A	B
Primary structural frame[f] (see Section 202)	3[a]	2[a]	1	0
Bearing walls	3	2	1	0
Exterior[e, f]				
Interior	3[a]	2[a]	1	0

a. Roof supports: Fire-resistance ratings of primary structural frame and bearing walls are permitted to be reduced by 1 hour where supporting a roof only.

Due to the non-combustibility material requirement by IBC for Types I and II construction, the shear wall with flat steel sheets and the flat straps cross bracing shear wall are the only choices for mid-rise building. The "x" straps generally require special plate brackets to be installed at the corners of the wall and the straps are difficult to install without resulting in a sagging or loose fit.

The cross bracing wall also requires interior drywall or exterior finishing material to be attached over the straps, there may be undesirable bumps or bulges in the wall surfaces. Further, such a cross bracing wall structure is labor intensive to build and requires higher design loads as specified by the building code (IBC 2015) due to it less ductility and lower reliability than shear walls with flat steel sheets. So, shear wall with flat steel sheets is therefore the only available economic lateral system for mid-rise Type I and II buildings. However, the shear wall with flat steel sheets provides low shear strength as its strength is close to the shear wall with wood-based sheathing. The low strength of the shear wall with flat steel sheets significantly obstructs the application of CFS members in mid-rise buildings, particularly in areas subjected to high seismic or strong wind hazards. Non-combustible CFS shear walls with high structural performances are in great need by the industry for the mid-rise construction market.

CHAPTER 2

LITERATURE REVIEW

The cold-formed steel (CFS) corrugated sheet is widely used as the floor decking and roofing materials in both residential and commercial buildings. In order to take advantage of its rigidity and incombustibility, the corrugated steel sheet used as shear wall sheathing was investigated by a few researchers. Fülöp and Dubina (2004) initiated a testing program to investigate the structural characteristics of 2.44 m high × 3.66 m wide CFS shear walls with different sheathing materials including corrugated steel sheet, gypsum boards, and OSB. A total of 7 monotonic tests and 8 cyclic tests were conducted. Fülöp and Dubina (2004) observed that the hysteretic behavior is characterized by very significant pinching, and reduced energy dissipation. And most of the damages concentrated on seam fasteners. But most importantly, they concluded that corrugated steel sheets could effectively resist lateral loads.

Stojadinovic and Tipping (2007) conducted a total of 44 cyclic shear wall tests with corrugated sheet steel sheathing, and a wide range of parameters were studied, such as thickness of the corrugated steel sheet and framing members, size and spacing of the fasteners, wall aspect ratio, etc. The authors reported that in all the tests, the failure mode was the screws pull out due to warping in the corrugated steel sheet. However, the boundary elements of all the shear walls were reinforced by rectangular steel tube which excluded failures in the boundary framing members, it was not the real engineering design and engineering practice.

In order to investigate the performance of shear walls with corrugated steel sheet by using common framing configurations in terms of the framing member thickness, the fastener size and spacing, and the boundary stud configurations, 4 full-scale monotonic and 4 cyclic shear wall tests were conducted at University of North Texas (Yu et al. 2009) by using the testing methods

recommended by the International Code Council,. The test results indicated that the CFS framed shear walls using 27 mil corrugated steel sheathings yielded higher strength and greater initial stiffness compared with the CFS walls using conventional sheathing materials including flat steel sheets, plywood panels and OSB boards. However, the tested specimens did not yield desirable ductility compared to the shear wall with OSB and flat sheet sheathing.

Guowang Yu (2013) conducted his research at University of North Texas aiming to improve the ductility of CFS shear walls with corrugated steel sheathings. Guowang Yu and Dr. Cheng Yu proposed a method of creating openings (perforation) on the corrugated sheathing to improve the wall's ductility and to control the failure mechanism and failure locations on the shear wall. A total of 9 types of openings and patterns were tested in Yu's research including: different diameter circular holes, different lengths of horizontal slits and vertical slits. Based on the results, Yu recommended further research on shear walls with 24×2 in. vertical slits and 24×3 in. vertical slits on corrugated sheathings.

Follow up Yu's research, Mahsa Mahdavian (2016) conducted 36 shear wall tests to further explore the structural performance of shear walls with different configurations in University of North Texas. She found that 12x2 in. vertical lists on corrugated steel sheets yielded the best performance. She also suggested to use 68 mil framing member and 27 mil corrugated steel sheets instead of 54 mil framing member and 18 mil corrugated steel sheets because the thinner members caused weak sheathing connections. In Mahdavian's (2016) research, she introduced three new shear wall configurations that the corrugated steel sheets were installed inside the frame (sheet-in shear wall), instead of outside frame (sheet-out shear wall). The disadvantages of sheet-out shear wall was that it would cause trouble when installing the finish materials because this type of shear

wall is thinker than the adjacent walls. Mahdavian's concluded that sheet-in shear wall with 300T field framing member and 12x2 in. vertical slits show the best performance.

Extensive finite element analysis models have been studied and compared in OpenSees (McKenna, 2015) by Leng (2015) in order to develop a high fidelity computational model of CFS Structure with wood sheathing shear walls. The results were calibrated according to full shake table test results and the suggested modeling methods for CFS framed buildings were given. However, the CFS-NEES building was the only building archetype for the performance evaluation, while FEMA requires more archetypes with different design parameters for the performance evaluation.

In order to test the wall in a more realistic condition, Zhang (2016) conducted 4 sheet-out shear wall and 4 sheet-out bearing wall tests under a combined lateral and gravity loading. She found that the gravity load would increase the shear strength and initial stiffness of the wall. She suggested that 7% drift as the collapsed drift for this new type wall system with corrugated steel sheathing. In the modeling part, Zhang utilized Leng's (2015) modeling approaches to study a modified 2-story CFS-NEES building archetype's seismic performance with the newly proposed sheet out shear wall by using FEMA P695 Methodology. She concluded that the seismic performance factors ($R=C_d=6.5$ and $\Omega = 3.0$) is appropriate for the new shear wall type with the framing members specified in her research. However, more building archetypes with varied design parameters needs to be studied per FEMA P695 Methodology.

Zhang (2017) followed up her previous research, and conducted the performance evaluation of two groups of total 6 building archetypes to verify the seismic performance factors ($R=C_d=6.5$ and $\Omega = 3.0$) of the cold-formed steel structure with newly proposed sheet-out shear wall. The building archetype design parameters varied in story height, number of stories,

occupancy type, seismic intensity, and plan configuration, etc. She concluded that the seismic performance factors ($R=C_d=6.5$ and $\Omega = 3.0$) obtained from the structure seismic performance evaluation were appropriate for his newly proposed sheet-out shear wall system.

CHAPTER 3

RESEARCH OBJECTIVES

3.1 Conduct Sheet-in Wall Tests under Combined Lateral and Gravity Loads

Mahdavian (2016) proposed the sheet-in wall in her research, however, the test did not consider the effects of gravity loads on the wall. Zhang (2016) pointed out that the gravity load had positive effects on the performance of the sheet-out shear wall. So, in my research, monotonic and cyclic tests on sheet-in shear wall and bearing walls would be conducted. Then, the effects of gravity loads on sheet-in shear wall would be discussed.

3.2 Performance Evaluation of CFS Structure with Sheet-in Shear Wall

The method of modeling of shear wall and building archetype referred to Leng's (2015) and Zhang's (2016) modeling methods, two groups of CFS building archetypes with sheet-in shear walls would be modeled in OpenSees program. According to FEMA P695 Methodology, seismic performance factors of this newly proposed sheet-in shear wall lateral-force-resisting systems would be evaluated.

CHAPTER 4

TEST PROGRAM

4.1 Test Setup

Wall shear tests were conducted on a 16 ft. by 13.3 ft. high self-equilibrating steel testing frame located in the Structural Laboratory at the University of North Texas. The testing frame was equipped with a MTS 35 kip hydraulic actuator with a 10 in. stroke. A MTS 407 controller and a 20-GPM MTS hydraulic power unit were used to drive the loading system. A 30 kip TRANSDUCER TECHNIQUES SWO universal compression/tension load cell was used to measure the forces. One out of five NOVOTECHNIC 10 position transducers were used to measure the horizontal displacement at the top of the shear wall, and the other four were used to measure the vertical and horizontal displacements at the bottom of the two boundary frame members. The data acquisition system consisted of a National Instruments unit and an HP Compaq computer. 5,384 pounds of gravity load applied on wall was calculated based on the two-story CFS-NEES office building. This weight was divided into two equal parts and added on each side of the wall by using weight boxes with sand bags held by steel chains from the top of the shear wall. Weight boxes were 5 inches off the ground. Contact between weight boxes and shear wall was eliminated by using a support frame. The applied force and the five displacements were recorded instantaneously during each test. Details of the testing frame and the location of the position transducers are shown in Figure 4.1.

The wall specimens were bolted to the base of the testing frame and loaded horizontally at the top. The base beam is a 5 in. × 5 in. × ½ in. structural steel tube and is bolted to a W16×67 structural steel beam which is anchored to the floor. One web of the base beam has openings in several locations to provide access of the anchor bolts for the connection of hold-downs to the base

beam. Figure 4.2 and Figure 4.3 demonstrate the testing setup with an 8 ft. × 4 ft. shear wall installed.

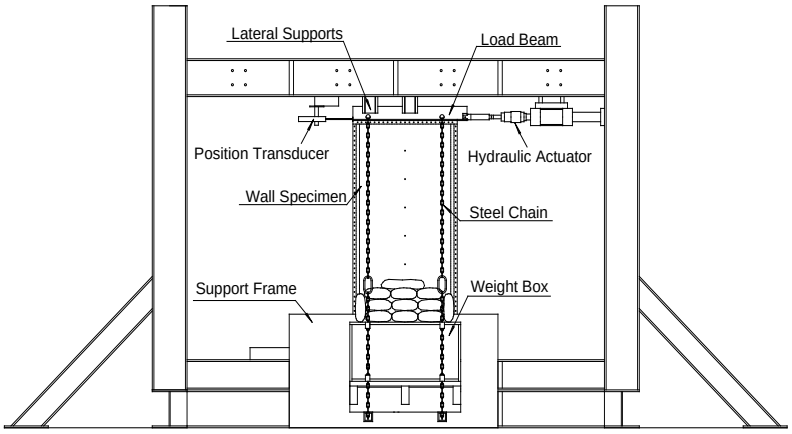

(a) Elevation View

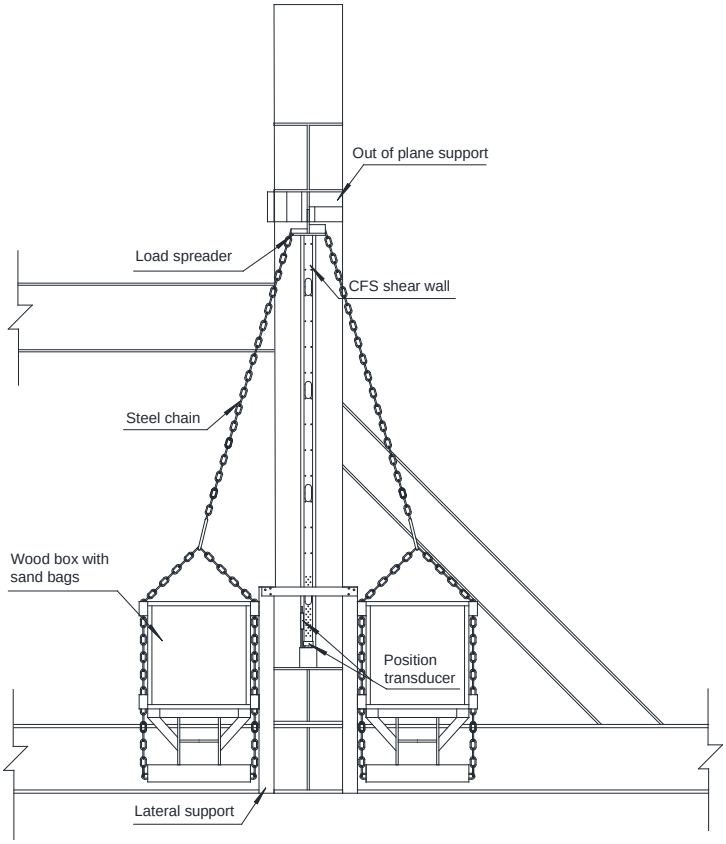

(b) Side View

Figure 4.1 - Testing Frame and Position Transducer Layout

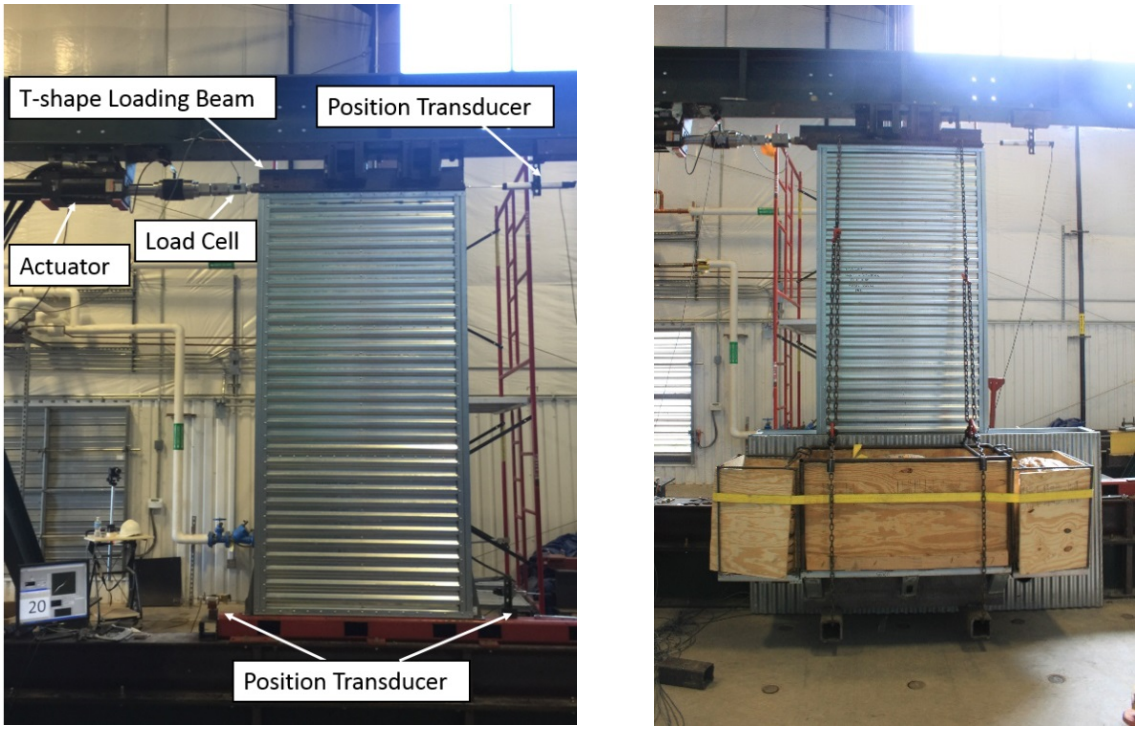

(a) Wall specimen without gravity load (b)Wall specimen with gravity load

Figure 4.2 - Front View of Test Setup

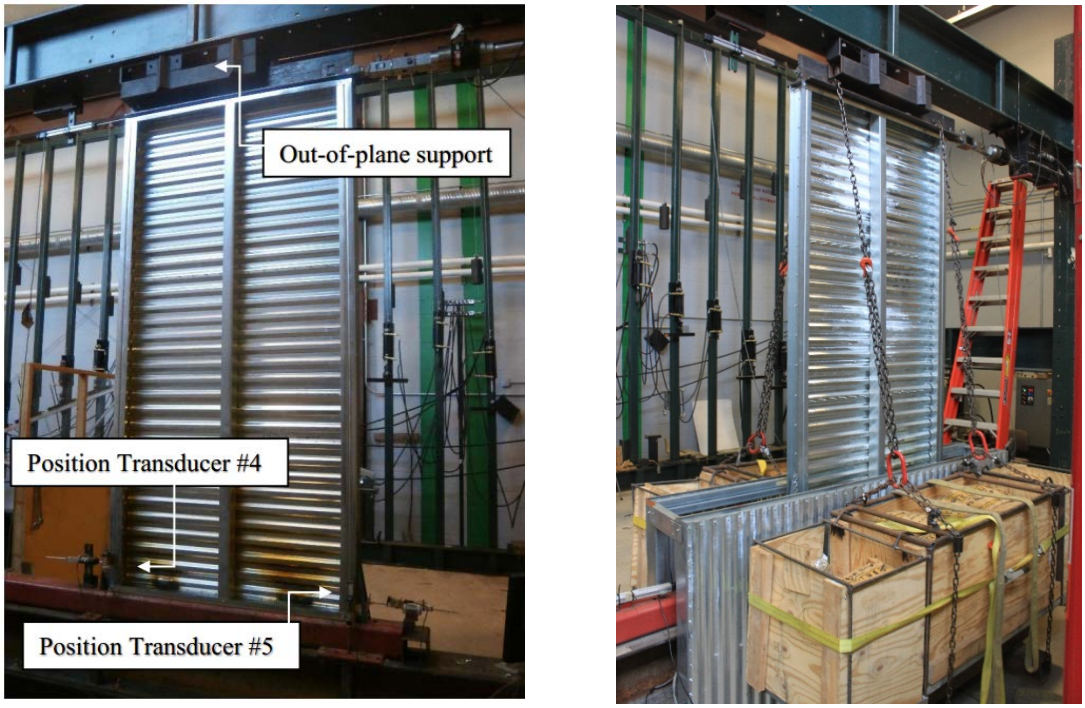

(a) Wall specimen without gravity load (b)Wall specimen with gravity load

Figure 4.3 - Back View of Test Setup

The lateral loading was applied directly to the T-shaped loading beam by the actuator. The loading beam was attached to the web of the top track using a pair of No. 12× 1 ¼ in. hex head self-drilling screws every 3 in. on center so that a uniform horizontal force could be transmitted to the top track of the wall. The web of the T-shape beam was placed in the gap between the rollers located at the top of the testing frame to prevent out-of-plane movement of the wall. The rotation of the rollers were able to reduce the friction generated by the movement of the T-shape beam during the loading process and were also able to guide the loading T-shape beam. To anchor the specimen to the base beam of the testing frame, two Simpson Strong-Tie S/HD15S hold-downs with 33 pre-drilled holes corresponding to No. 14-14 × 1 in. hex washer head self-drilling screws were used. In addition, two Grade-8 3/4 in. shear bolts and two Grade-8 5/8 in. anchor bolts were used in the anchorage system.

4.2 Test Method

Both monotonic test and cyclic test were conducted. In all tests, the gravity load was applied to the wall specimens prior to the lateral loading and the gravity load remained constant during the test. The lateral loading was applied to the wall top using displacement controlled loading method.

The procedure of the monotonic tests is in accordance with ASTM E564 (2012) “Standard Practice for Static Load Test for Shear Resistance of Framed Walls for Buildings”. The displacement was applied to the top of the wall at a uniform rate of 0.0075 in/sec. The cyclic tests referred to CUREE protocol with 0.2 Hz (5 seconds) loading frequency which was in accordance with Method C in ASTM E2126 (2012) “Standard Test Methods for Cyclic (Reversed) Load Test for Shear Resistance of Vertical Elements of the Lateral Force Resisting Systems for Buildings.” The standard CUREE loading history includes 40 cycles with specific displacement amplitudes. 3

more cycles were added to the standard CUREE method with total of 43 cycles in order to fully investigate post peak behavior of the walls, the CUREE loading history is shown in Figure 4.4 and the parameters of each cycle is given in Table 4.1.

Monotonic tests are for determining the nominal shear strength for wind loads, it is also safe approach to explore the performance of a new shear wall with unknown strength. Cyclic tests are for determining the shear strength for seismic loads.

According to the testing method mentioned above, it is required to have at least two identical tests for each wall configuration for each testing method. However, it is found that in the past research (Yu(2013), Mahdavian (2016) & Zhang (2016), the results of the two monotonic tests usually were consistent. Therefore, only one specimen were tested by monotonic test method in author's research. For cyclic test, two identical specimens were tested.

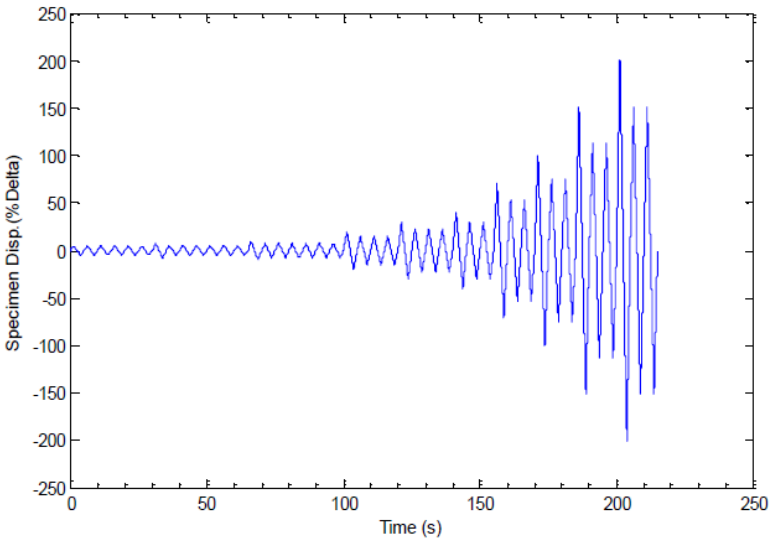

Figure 4.4 - CUREE Loading History Diagram (0.2 Hz)

Table 4.1 - CUREE Basic Loading History

Cyclic No.	*% Δ*	Cyclic No.	*% Δ*	Cyclic No.	*% Δ*	Cyclic No.	*% Δ*
1	*5*	12	*5.6*	23	*15*	34	*53*

2	*5*	13	*5.6*	24	*15*	35	*100*
3	*5*	14	*10*	25	*30*	36	*75*
4	*5*	15	*7.5*	26	*23*	37	*75*
5	*5*	16	*7.5*	27	*23*	38	*150*
6	*5*	17	*7.5*	28	*23*	39	*113*
7	*7.5*	18	*7.5*	29	*40*	40	*113*
8	*5.6*	19	*7.5*	30	*30*	41	*200*
9	*5.6*	20	*7.5*	31	*30*	42	*150*
10	*5.6*	21	*20*	32	*70*	43	*150*
11	*5.6*	22	*15*	33	*53*	-	-

4.3 Test Specimens

Test specimens are labeled by following rules: “Wall Width (ft.) x Wall Height (ft.) x Framing Member Thickness (mil) x Sheathing Thickness (mil) – Test Number.” Text Matrix is given in Table 3.

Though Mahsa suggested that sheet-in shear wall with 12x2 slits openings were the best configuration, author chose sheet-in shear wall without opening for this research as the shear strength of the sheet-in shear wall with openings dropped nearly 25% while the ductility did not improve too much for sheet-in shear wall with 12x2 slits openings. Tracks are used as studs in sheet-in wall, which is different from the engineering practice. This is because the corrugated steel sheets were designed inside of the CFS frame, the lips of the standardized stud will be in the way for the installation of corrugated steel sheets. All 350T125-68 vertical chord tracks are connected using a pair of No. 12 x 1 ¼ in. hex washer head self-drilling screws every 6 in. on center starting from above the hold-downs. Simpson Strong-tie S/HD 15S Hold-downs in shear walls are screwed outside of the vertical chord tracks by No. 14x1 in. hex washer head self-drilling screws. Top and bottom tracks are 362T150-68. Middle vertical track 300T200-68. 27 mil Verco Decking SV36 is

used for the sheathing, no opening is created in the sheathing, and the deck profile is shown in Figure 4.5. The sectional view of the sheet-in shear wall is shown in Figure 4.6.

Table 4.2 - Test Matrix

Test Label	Wall Type	Test protocol (M/C)	Gravity Load	Hold-down	Vertical chord tracks
4x8x68x27 - T#1	Bearing wall	M	Y	N	1
4x8x68x27 - T#1	Bearing wall	C	Y	N	1
4x8x68x27 - T#2	Bearing wall	C	Y	N	1
4x8x68x27 - T#1	Shear wall	M	Y	Y	2
4x8x68x27 - T#1	Shear wall	C	Y	Y	2
4x8x68x27 - T#2	Shear wall	C	Y	Y	2

Note: M-Monotonic loading, C-Cyclic loading.

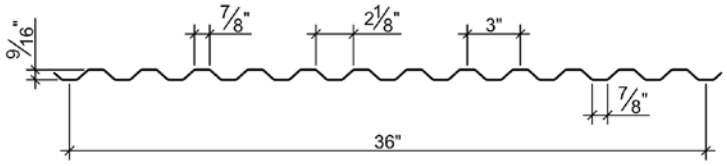

Figure 4.5 - Verco Decking SV36 Sheathing Profile

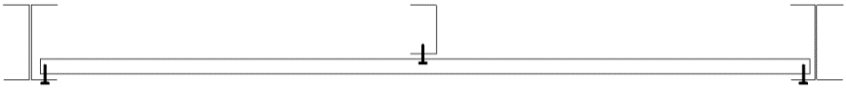

Figure 4.6 - Sectional View of Sheet-in Shear Wall (8 ft. x 4 ft.)

4.4 Material Properties

Coupon tests of each member were conducted according to the ASTM A370 (2006) "Standard Test Methods and Definitions for Mechanical Testing of Steel Products" to obtain the actual properties of the test materials in this project. The coating of the steel samples was removed by hydrochloric wash prior to coupon tests.

The tensile test of coupons were conducted on an INSTRON 4482 Universal Testing Machine and an INSTRON 2630-106 extensometer was used to measure the tensile strain. The coupon tests were conducted in displacement control mode at a constant tension rate of 0.05 in./min. A total of three coupon tests were performed for each member, and the average results are provided in Table 4.3.

Table 4.3 - Material properties of Wall Components

Member	Uncoated Thickness (in.)	Yield Stress Fy (ksi)	Tensile Strength Fu (ksi)
362T150-68-Track	-	53.15	70.07
350T125-68-Stud	0.0711	57.49	74.42
27mil Verco Decking SV36	0.0294	86.09	89.93

4.5 Test Results and Discussions

4.5.1 Wall Behaviors under Monotonic Loading

Though bearing wall is not designed to resist gravity loads instead of lateral loads, it still shows capabilities to resist lateral forces. During the test, it was observed that the vertical chord tracks and the bottom track in the tension side was lift up due to no hold-downs were installed which was in accordance with the engineering practice, while the vertical chord tracks and the bottom track in the compression side buckled. No screws failures were observed. The maximum displacement was set to 7.2 in., which was equivalent to 7.5% story drift. It was observed that the bearing wall specimen was able to carry the gravity load without collapse during the entire loading process. The failures of the bearing wall specimen in monotonic test are shown in Figure 4.7.

(a) Tension Side (b) Compression Side

Figure 4.7 - Failures of Bearing Wall Specimen in Monotonic Test

For the shear wall monotonic test, the vertical chord tracks were not lift up in the tension side thanks to the assistance of hold-downs. Local buckling in the vertical chord tracks in the compression side was observed right above the hold-down area. This failure was not observed in Mahdavian's (2016) research, where no gravity loads were applied on the shear wall. The reason that caused the new failure could be that the hold-downs obstructed the lateral movement of vertical chord tracks at the lower part, while the vertical chord tracks at the upper part was free to move laterally. So, the second-order effects would be acted on the vertical chord tracks, this was proved by the local twisting of the vertical chord studs shown in Figure 9. The new failure proved that having gravity loads in the shear test can more realistic reflect the actual behaviors of the wall. Other failures were screws pull-out on the bottom corrugated steel sheet, middle vertical track local buckling. A tension field observed on the bottom sheet. The test was stopped at 7.5% story drift, the shear wall could carry the gravity load without collapse during the whole loading process. The failures of the shear wall specimen in monotonic test are shown in Figure 4.8.

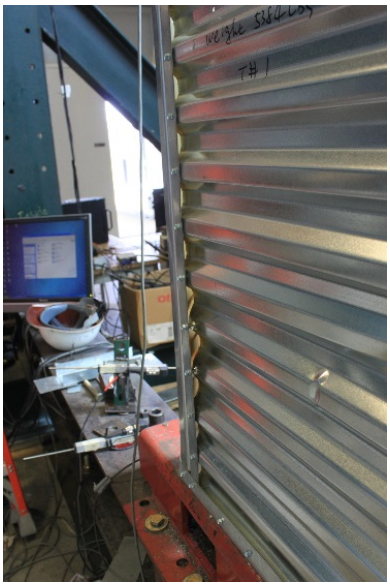

(a) Screw pull-out

(b) Screw pull-out

(c) Chord framing member buckles

(d) Middle framing member buckles

Figure 4.8 - Failures of the Shear Wall Specimen in Monotonic Test

4.5.2 Wall Behaviors under Cyclic Loading

For bearing wall specimens in the cyclic tests, vertical chord tracks buckled at the bottom ends at the cycle of 38 during the test. Unlike bearing wall in the monotonic test, screws were pull-

out in the vertical chord track-to-bottom track connection. Maximum drift in the cyclic test reached 4.79%, bearing walls were able to carry gravity load without collapse during the test. The failures of the bearing wall specimen in cyclic test are shown in Figure 4.9.

(a) Screw pull-out (b) Chord framing member lift up

Figure 4.9 - Failures of the Bearing Wall Specimen in Cyclic Test

For the first shear wall specimen in the cyclic tests. One side of the vertical chord tracks buckled above the hold-downs at the cycle of 35 and another side of vertical chord tracks buckled above the hold-downs at the cycle of 38. For the second shear walls specimen, minor local buckling was observed on the vertical chord tracks. For both tests, screws broke and screws pull-out were observed on the middle and bottom sheets. Screws pull-out in the overlap between middle sheet and bottom sheets were also observed. The failures of the shear wall specimen in cyclic test are shown in Figure 4.10.

(a) Screw shear failure

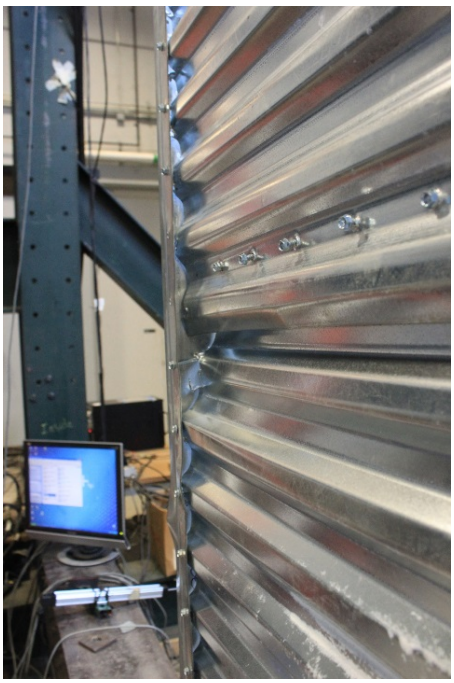

(b) Screw pull-out

(c) Chord framing member buckles

(b) Vertical Framing member buckle

Figure 4.10 - Failures of the Shear Wall Specimen in Cyclic Test

Table 4.4 - Results of Each Wall Specimen

Test label	Wall Type	Test protocol (M/C)	Gravity Load	Hold-down	Vertical chord trackss	Average Peak Load (plf)	Average Disp @ Peak Load (in.)	Ductility Factor	Drift	Initial Stiffness k (lbs/in)
4x8x68x27 - T#1	Bearing wall	M	Y	N	1	1186.9	2.58	2.873	7.50%	4066
4x8x68x27 - T#1	Bearing wall	C	Y	N	1	1380.18	3.02	2.09	3.15%	2845
4x8x68x27 - T#2	Bearing wall	C	Y	N	1	1211.92	2.87	3.99	2.98%	4561
4x8x68x27 - T#1	Shear wall	M	Y	Y	2	3380.9	2.3	1.8	7.50%	8561
4x8x68x27 - T#1	Shear wall	C	Y	Y	2	3459.28	2.12	2.01	2.21%	8493
4x8x68x27 - T#2	Shear wall	C	Y	Y	2	3586.65	2.1	2.2	2.19%	10461

Note: M – Monotonic, C – Cyclic, plf – pound linear foot

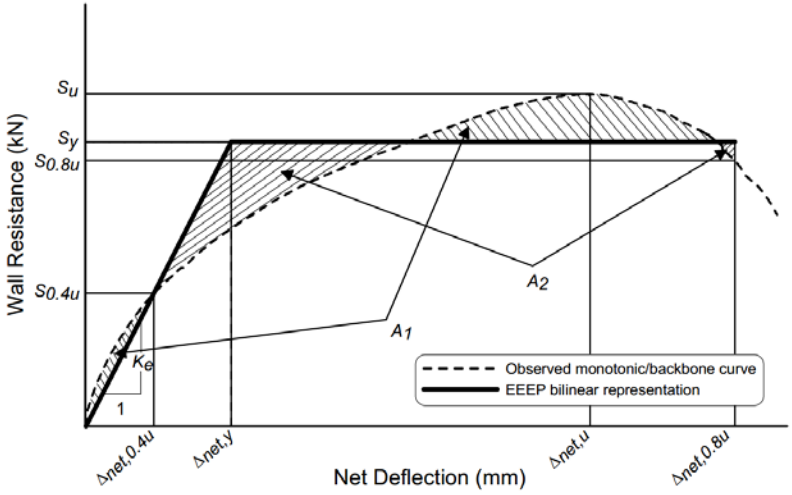

Figure 4.11 - Equivalent Energy Elastic-Plastic (EEEP) Analysis Mode

4.5.3 Wall Properties Calculation

The results of each wall specimen under monotonic loading and cyclic loading are provided respectively in Table 4.4. The results include the test peak load, lateral displacement at peak load, initial stiffness as well as the ductility factor. Ductility factor was calculated using the equivalent energy elastic plastic model (EEEP) according to AISI S213 (2012). The EEEP method was first proposed by Park (1989), and was improved by Foliente (1996), Each Test details can be found in Appendix A. The procedure for calculating ductility factor is that a backbone curve plotted first, and then a bold line (shown in Figure 4.11) plotted to make the area of A1 equal to the area of A2. The equation of ductility factor calculation is $\mu = \Delta_u/\Delta_y$.

4.5.4 Discussion of Test Results

A few of key points of the test results would be discussed in this section. There were the effects of gravity loads on the structural performance of the wall, the lateral resistance contribution of the sheet-in bearing wall, and the determination of collapse drift limit.

Firstly, the effects of gravity loads on the walls. For sheet-in bearing wall, gravity loads would cause the bottom end of the vertical chord tracks local bucking; for sheet-in shear wall, gravity loads would cause severe local buckling on the vertical chord studs right above the hold-down area. But for the shear wall without gravity loads. Only minor buckling on the chord vertical tracks. It is believed that due to the severe buckling happened on the sheet-in shear wall test with gravity loads, the shear strength dropped 11.56% and initial stiffness dropped 7.72% compared to sheet-in shear wall without gravity load, see the comparison in Table 4.5 and Figure 4.12. So, gravity loads had negative effects on the structural performance of the sheet-in shear wall. In Mahdavian's (2016) research, she did not do tests on sheet-in bearing wall. The only two tests she

conducted were cyclic tests on sheet-in shear wall without gravity loads. So, the difference of gravity loads effects on wall only could be made on sheet-in shear walls in cyclic tests.

Secondly, the lateral resistance contribution of the sheet-in bearing wall was significant. For monotonic tests, the shear strength of sheet-in bearing walls equal to 35.11% of the sheet-in shear wall. For cyclic tests, the shear strength of sheet-in bearing walls equal to 36.79% of the sheet-in shear wall. Considering the amount of bearing walls in the CFS structure, their contribution to the lateral-force-resisting system should not be ignored. Details of the comparison between sheet-in bearing wall and sheet-in shear wall is given in Table 4.6.

Table 4.5 - Comparison between Sheet-in Shear Wall with and Without Gravity Loads

Test label	Wall Type	Test protocol (M/C)	Gravity Load	Average Peak Load (plf)	Average Disp @ Peak Load (in.)	Ductility Factor	Drift	Initial Stiffness k (lbs/in)
4x8x68x27 - T#1	Shear wall	C	Y	3459.28	2.12	2.01	2.21%	8493
4x8x68x27 - T#2	Shear wall	C	Y	3586.65	2.1	2.2	2.19%	10461
Average				3522.96	2.11	2.11	2.20%	9477
4x8x68x27 - T#1	Shear wall	C	N	3969	2.05	2.34	2.13%	11332
4x8x68x27 - T#2	Shear wall	C	N	3998	2.33	2.17	2.43%	9208
Average				3983.5	2.19	2.26	2.28%	10270

Note: plf – pound linear foot

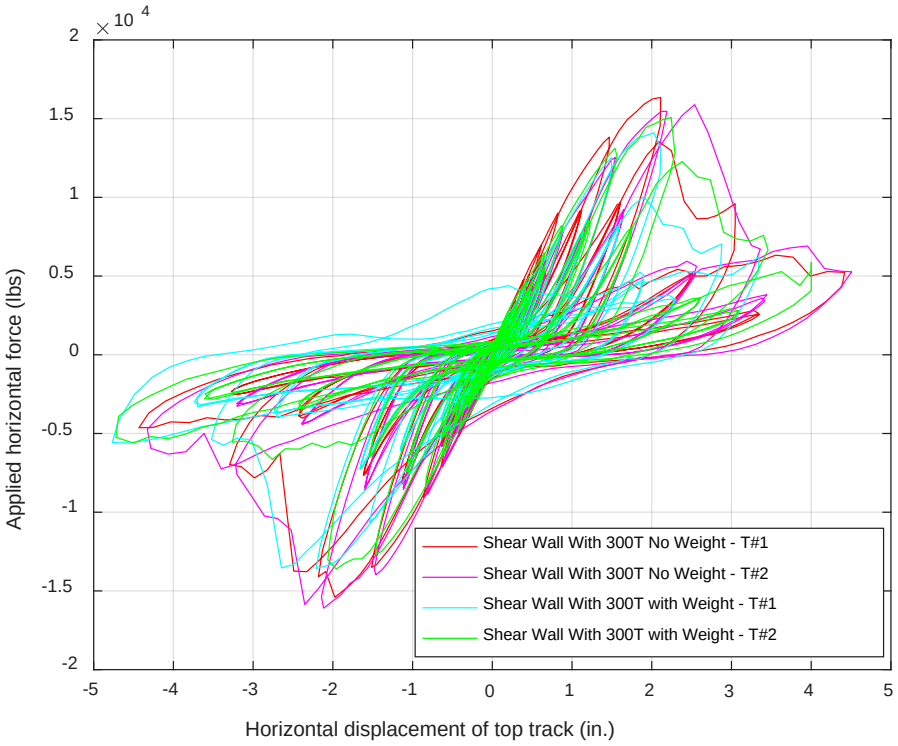

Figure 4.12 - Illustration of the 2-Story Office Building and 2-Story Hotel Building

For the determination of collapse drift limit, the bearing walls and shear walls were able to carry the gravity loads without collapse though the loading process at a maximum drift of 7.5%. In Chapter 9 of FEMA P695 (2009), the Example adopts a 7% drift as the collapse drift limit for the light wood framed structures. FEAM P695 (2009) does not provide a recommended drift limit for light steel framed structures. However, these two CFS framed structure systems were considered to have similar seismic performances by the research communities. For instance, the same seismic performance factors was adopted on both systems in IBC (2015) and ASCE -7 (2010) in similar light-framed structures. In addition, Zhang (2016) considered a collapse drift limit of 7% was appropriate and conservative for the CFS structure system with sheet-out shear wall. Therefore, 7% drift limit was also used as the collapse drift limit in the following finite element (FE) modeling and seismic performance evaluation.

Table 4.6 - Comparison between Sheet-in Bearing Wall and Sheet-in Shear Wall

Test label	Wall type	Test protocol (M/C)	Gravity Load	Hold-down	Average Peak Load (plf)	Average Disp @ Peak Load (in.)	Ductility Factor	Drift	Initial Stiffness k (lbs/in)
4x8x68x27 - T#1	Bearing Wall	M	Y	N	1186.9	2.58	2.873	7.50%	4066
4x8x68x27 - T#1	Shear wall	M	Y	Y	3380.9	2.3	1.8	7.50%	8561
4x8x68x27 - T#1	Bearing wall	C	Y	N	1380.18	3.02	2.09	3.15%	2845
4x8x68x27 - T#2	Bearing wall	C	Y	N	1211.92	2.87	3.99	2.98%	4561
Average					1296.05	2.95	3.04	0.03	3703
4x8x68x27 - T#1	Shear wall	C	Y	Y	3459.28	2.12	2.01	2.21%	8493
4x8x68x27 - T#2	Shear wall	C	Y	Y	3586.65	2.1	2.2	2.19%	10461
Average					3522.96	2.11	2.11	0.02	9477

Note: plf – pound linear foot

CHAPTER 5

FINITE ELEMENT MODELING

5.1 Introduction of OpenSees

The Open System for Earthquake Engineering Simulation (OpenSees) (Mckenna, 2015) is a software framework for simulating the seismic response of structural and geotechnical systems. It has advanced capabilities for modeling and analyzing the nonlinear response of systems using a wide range of material models, elements, and solution algorithms.

OpenSees provides a wide range of materials and elements users, such as uniaxial material, beam-column element and truss element, etc. In particularly, the Pinching4 uniaxial material, which is used in truss element of the wall model to define the hysteretic characteristics of shear walls and bearing walls under cyclic loading.

For the analysis features of OpenSees, it provides nonlinear static and dynamic methods, equation solvers, and methods for handling constraints for nonlinear analysis. In my research, the nonlinear static (pushover) analysis and nonlinear dynamic analysis (incremental dynamic analysis-IDA) were used for the structural analysis.

5.2 Introduction of FEMA P695

The Quantification of Building Seismic Performance Factors, known as FEMA P695, provides a methodology for reliably quantifying building system performance and response parameters for use in seismic design. These factors include the response modification coefficient ($R\ factor$) , the system overstrength factor (Ω_0), and the deflection amplification factor (C_d), collectively referred to as “seismic performance factors”.

Today’s building code includes more than 80 individual structural systems, each with individual system response coefficients somewhat arbitrarily assigned. Many of these recently

defined structural systems have never been subjected to significant level of earthquake ground shaking and the potential response characteristics and the ability to meet the design performance objectives is untested and unknown. Based on these facts, this publication provides a methodology to quantify the seismic performance factors for untested structural systems and for newly proposed structural systems. The methodology provided by FEMA P695 would be used for the performance evaluation of the newly proposed sheet-in shear wall system.

5.3 Building Archetype

Behaviors of a proposed seismic-force-resisting system are investigated through the use of archetypes. An archetype (FEMA P695) is a prototypical representation of a seismic-force-resisting system. Archetypes are intended to reflect the range of design parameters and system attributes that are judged to be reasonable representations of the feasible design space and have a measurable impact on system response. They are used to bridge the gap between collapse performance of a single specific building and the generalized predictions of behavior needed to quantify performance for an entire class of buildings.

It is expected that the set of index archetype configurations will generally include about twenty to thirty specific structural configurations. The configuration design variables could be occupancy and use, elevation and plan configurations, building height and seismic design category, etc. Index archetype configurations are assembled into performance groups that reflect major differences in configurations.

Two groups of archetypes were studied in this research. They were a group of office building archetypes and a group of hotel building archetypes, shown in Table 5.1.

Table 5.1 - Two Groups of Building Archetypes

Group	Arch. ID	No. of Stories	Key Archetype Design Parameters				
			Occupancy	Shear wall Aspect Ratio	S_{MT}(g)	T(s)	V/W(g)
Group 1	1	2	Hotel	2.46	1.5	0.262	0.154
	2	4	Hotel	2.46	1.5	0.44	0.154
	3	5	Hotel	2.46	1.5	0.52	0.154
Group 2	4	2	Office	2.57	1.39	0.245	0.143
	5	3	Office	2.57	1.39	0.332	0.143
	6	5	Office	2.57	1.39	0.486	0.143

The office building used in the NEES-CFS project (Madsen, Nakata, Schafer, 2011) was chosen as a reference office building in this research. The NEES-CFS building was redesigned by Zhang (2016) to fit the layout of sheet-out shear wall. According to the Building Structural Design Narrative (Madsen, Nakata, Schafer, 2011), the 2-story office building was assumed to be located in Orange County, California which had a plan dimension of 49.75 ft. x 23 ft. Site Class D was chosen as is typical for sites in the vicinity of this project. For the office occupancy chosen, IE = 1.0 was used. The response modification coefficient, R, and overstrength factor Ω_0 were derived from ASCE 7-10 Table 12.2-1 for light-framed walls systems sheathed with wood structural panels, and were set as R = 6.5 and Ω_0= 3.0.

For office building archetypes, the quantity and length of shear walls were redesigned based on the author's test results. The bearing walls of the office building were mainly designed the on the exterior side, which allowed the flexible arrangement of the partition walls inside the building. Figure 14-a illustrates the schematic drawing of a 2-story office building model used in OpenSees.

The hotel building archetypes were designed according to ASCE 7-10. For the hotel building, the bearing walls were mainly the interior walls, which allowed the window openings on the exterior walls. Figure 14-b illustrates the schematic drawing of a 2-story hotel building model used in OpenSees.

Window sills and headers would help to transfer the force around the wall openings, but they are not part of the lateral-force-resisting systems. So, they were not considered in the modeling.

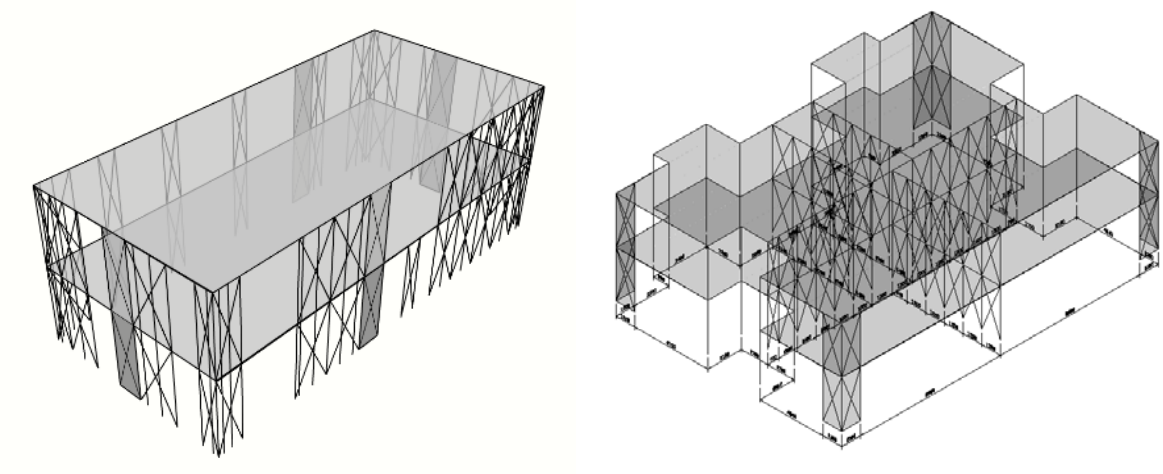

(a) Office Building (b) Hotel Building

Figure 5.1 - Illustration of the 2-Story Office Building and 2-Story Hotel Building

5.4 Design of Shear Walls

The earthquake loads were calculated in accordance with Chapter 11 of ASCE 7-10. In this section, the example of shear wall design for the 2-story office building was given. Same design procedures apply to all other building archetypes in this research.

Firstly, Site Class needs to be determined. As mentioned above, the office building was assumed in Site Class D. Then, the Maximum Considered Earthquake (MCE) spectral response acceleration parameter for short periods (S_{MS}) and at 1 s (S_{M1}) were calculated by the following equations, respectively.

$$S_{MS} = F_a S_S = 1.39 \times 1.0 = 1.39$$

$$S_{M1} = F_v S_1 = 0.5 \times 1.5 = 0.75$$

Where

S_S = the mapped MCE spectral response acceleration parameter at short periods.

S_1= the mapped MCE spectral response acceleration parameter at a period of 1 s.

Design earthquake spectral response acceleration parameter at short period, S_{DS}, and at 1 s period, S_{D1} were two thirds are the mapped MCE spectral response acceleration.

$$S_{DS} = \frac{2}{3} S_{MS} = 0.927\ (g)$$

$$S_{D1} = \frac{2}{3} S_{M1} = 0.500(g)$$

The seismic response coefficient, C_S, is determined by

$$C_S = \frac{S_{DS}}{\left(\frac{R}{I_e}\right)} = \frac{0.927}{\left(\frac{6.5}{1.0}\right)} = 0.143$$

Next, the seismic base shear, V, is calculated by

$$V = C_S W = 0.143 \times 77585 = 11061\ (pound)$$

W = the effective seismic weight

Note: The calculation of the effective seismic weight can refer to the Design Narrative (Madsen, Nakata, Schafer, 2011).

The lateral seismic force F_x induced at any level of the building shall be determined by the section of 12.8.3 of ASCE 7-10. The vertical distribution of seismic forces at each floor level is given in Table 5.2.

Table 5.2 - Vertical Distribution of Seismic Forces

Level	Effective Seismic Weight w_x (lb)	Height h_x (ft)	$w_x h_x^k$	Vertical Distribution Factor C_{vx}	Seismic Force F_x (lb)
Roof	32451	18	584123	0.59	6524
2nd	45134	9	406206	0.41	4537

Once seismic force applied on each floor was determined, the quantity and length of shear wall could be calculated. The Load Resistance Factor Design (LRFD) method was applied and the trial seismic force modification factors were referred to the light-framed walls systems with wood structural panels (ASCE 7-10). Hence, R = 6.5 and Ω_0 = 3.0 were used in all building archetype design, and were subjected to be verified.

The nominal shear wall strength was based on the test results by the author. It should be noted that the width of the shear wall used in the building archetype was 3.5 in. wide, which was different from the 4 in. width of test specimens. As per AISI S240 (2015), for Type I shear walls with aspect ratios (h/w) greater than 2:1, but no exceeding 4:1, the nominal strength shall be multiplied by (2w/h). In addition, a resistance factor of ϕ = 0.6 was considered according to the provisions in AISI S400 (2015). The shear wall design calculation is given in Table 5.3.

5.5 Modeling of Shear Walls and Bearing Walls

5.5.1 Modeling of Shear Walls

The shear walls and bearing walls were simulated in OpenSees as two diagonal truss elements and elastic beam-column elements as illustrated in Figure 5.2. EqualDOF command was used to ensure the displacement of the top two ends of the wall were the same.

Table 5.3 - Shear Wall Design for 2-Story Office Building Archetype

Location	Distributed Force V(lb)	Shear Wall Width B(ft)	Design Shear Force v(lb/ft)	Nominal Strength Vn(lb/ft)	H (ft)	Adjustment Factor (2w/h)	Design Strength φVn(lb/ft)	v/(φVn)
2S	3262	3.5	932	3584	9	0.778	1673	0.557
2N	3262	3.5	932	3584	9	0.778	1673	0.557
2W	3262	3.5	932	3584	9	0.778	1673	0.557
2E	3262	3.5	932	3584	9	0.778	1673	0.557
1S	5530	3.5	1580	3584	9	0.778	1673	0.945
1N	5530	3.5	1580	3584	9	0.778	1673	0.945
1W	5530	3.5	1580	3584	9	0.778	1673	0.945
1E	5530	3.5	1580	3584	9	0.778	1673	0.945

Note: 2S means side shear wall on the 2nd floor, 1E means east side shear wall on the 1st floor. Same rules applies to others.

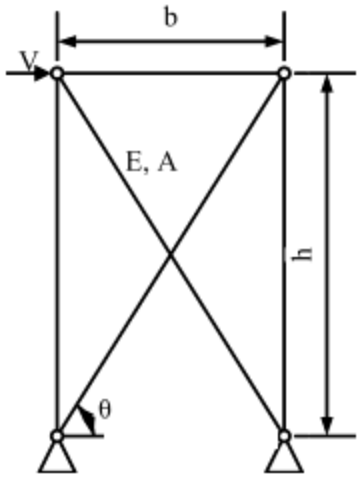

Figure 5.2 - Shear wall Numerical Model

Pinching effect is a load-deformation response and exhibits stiffness and strength degradation under cyclic loading. To achieve the pinching effect, pinching4 uniaxial hysteretic material was used for the diagonal truss elements. To obtain the backbone curve of pinching4 material, the load vs. displacement in the horizontal direction was first converted to the stress-strain relationship in the truss elements according to the basic equilibrium and geometry.

The axial force in the diagonal truss element *F* can be expressed as:

$$F = V / (2\cos\theta)$$

The stress and strain in the diagonal truss element are calculated as:

$$\sigma = F / A = V / (2A\cos\theta)$$

$$\varepsilon = d / l = (\Delta\cos\theta) / l$$

Where $\cos\theta = \frac{b}{\sqrt{b^2+h^2}}$, and $l = \sqrt{b^2 + h^2}$. Herein b *and* h are the width and height of the shear wall respectively.

After the backbone curve is defined by 4 positive and 4 negative points, it is required to input the parameters that can define the strength and stiffness degradation, as well as the pinching effect under cyclic loading, as shown in Figure 5.3. The complete set of Pinching4 parameters,

was listed in Table 5.4. The definition of the parameters can be found in the OpenSees Command Language Manual.

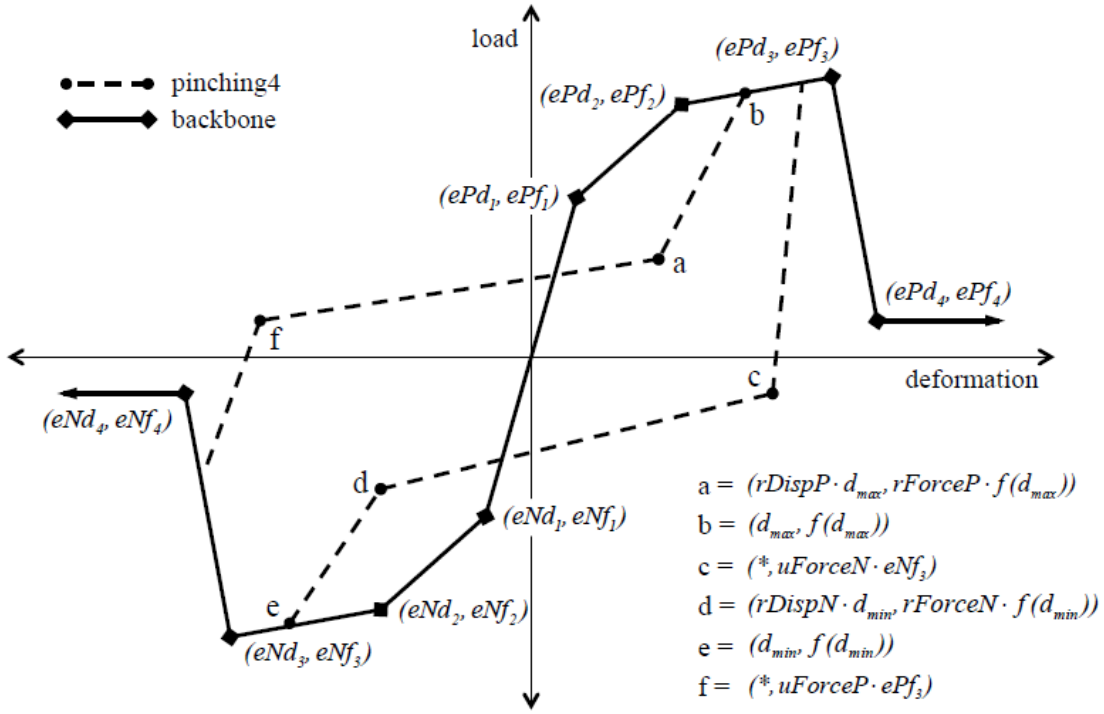

Figure 5.3 - The Parameter Definition of Pinching4 Material

Table 5.4 - Pinching4 Material Parameters Used for Shear Wall

ePd1	ePd2	ePd3	ePd4	ePf1	ePf2	ePf3	ePf4
0.41	0.82	1	1.44	0.47	0.74	1	0.33
eNd1	eNd2	eNd3	eNd4	eNF1	eNF2	eNF3	eNF4
0.41	0.82	1	1.44	0.47	0.74	1	0.33
rDisp	rForce	uForce	gK1	gK2	gK3	gK4	gKlim
0.1	0.3	-0.05	-0.2	-0.2	0.3	0.2	0.9
gD1	gD2	gD3	gD4	gDLim	gF	gE	
0.35	0.74	1	1.75	0.1	0	10	

The comparison between the shear wall simulation results and the shear wall test results is shown in Figure 5.4. It shows that they have a good match. Also, the shear wall model is able to simulate the post-peak behaviors of the shear wall. Please note that only last 15 cycles of the 43

cycles were plotted in the Figure 5.4 as they were the most important cycles as the force and displacement of the previous cycles were not significant.

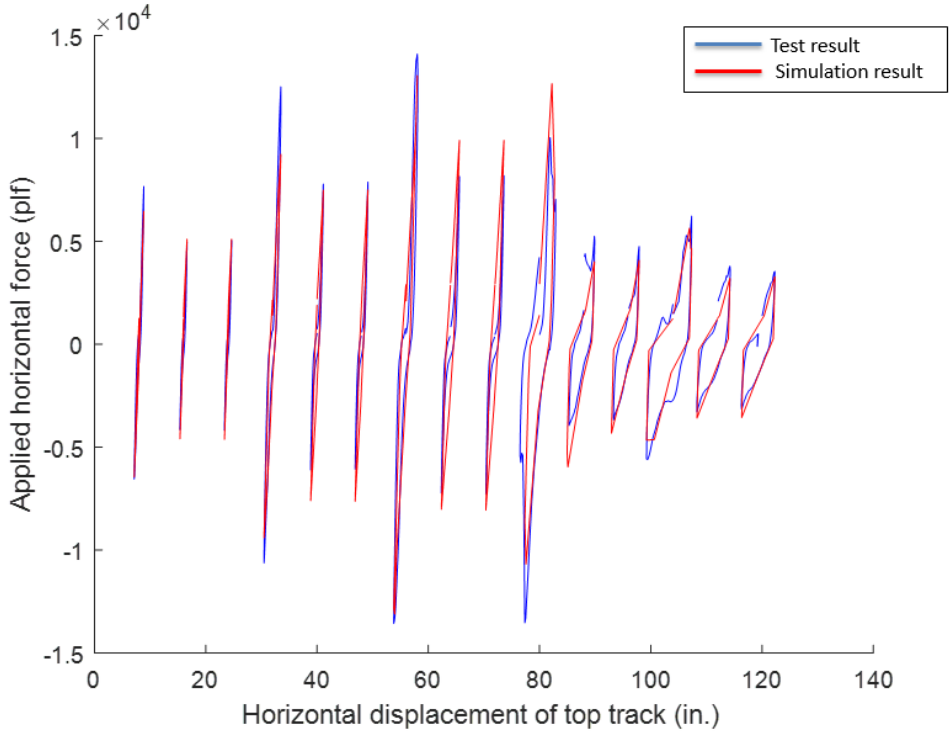

Figure 5.4 - Comparison between the Shear Wall Simulation Results and the Test Results

5.5.2 Modeling of Bearing Walls

Test results showed that the shear strength of bearing wall was about 1/3 of the shear wall. Considering the quantity of the bearing walls in the wall systems, their contribution of the lateral force resistance to the lateral force resisting system should not be ignored. The modeling technique of bearing walls was the same as the shear walls. The backbone curve and parameters of pinching4 material were based on the bearing wall test results. The complete set of Pinching4 parameters used for bearing walls is listed in Table 5.5.

Table 5.5 - Pinching4 Material Parameters Used for Bearing Wall

ePd1	ePd2	ePd3	ePd4	ePf1	ePf2	ePf3	ePf4
0.31	0.79	1	1.4	0.55	0.72	0.9	0.35
eNd1	eNd2	eNd3	eNd4	eNd1	eNd2	eNd3	eNd4

0.31	0.79	1	1.4	0.55	0.72	0.9	0.35
rDisp	rForce	uForce	gK1	gK2	gK3	gK4	gKlim
0.1	0.1	-0.1	-1	-0.2	0.3	0.2	0.9
gD1	gD2	gD3	gD4	gDLim	gF	gE	
0.4	0.4	2	2	0.5	0	10	

The comparison between the bearing wall simulation results and the shear wall test results is shown in Figure 5.5. It shows that they have a good match. The bearing wall model is also able to simulate the post-peak behaviors of the shear wall.

Similar to shear wall, aspect ratio adjustment was considered in the bearing wall model when the width of the bearing wall was different from the width of test specimens in the modeling.

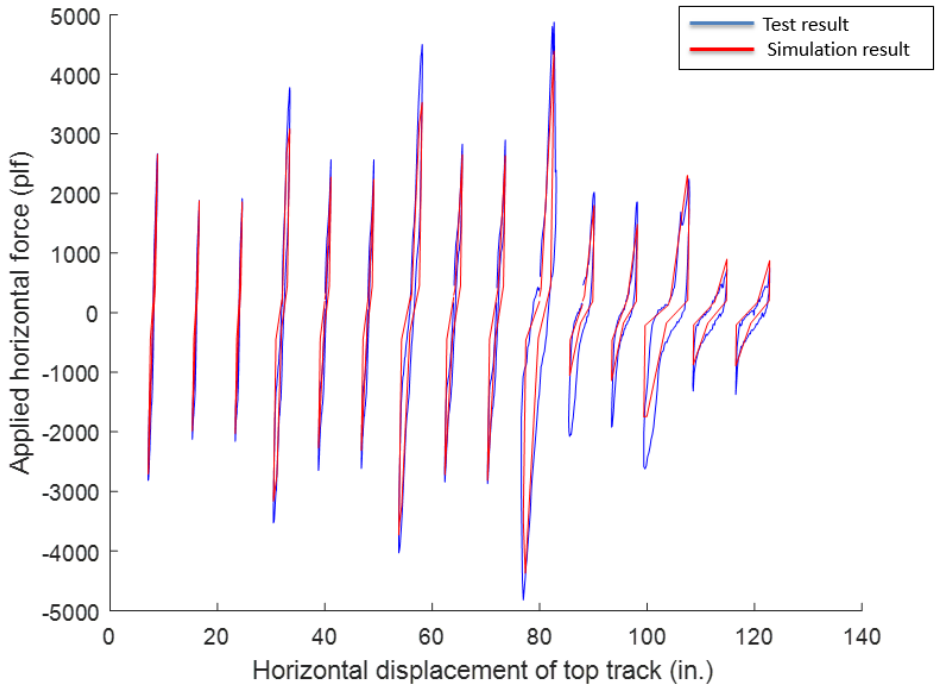

Figure 5.5 - Comparison between the Bearing Wall Simulation Results and the Test Results

5.6 Modeling of Diaphragm

In Leng's dissertation (2015), he concluded that the stiffness of diaphragms contributes greatly to the overall stiffness of 3D models and it determines the extent of coupling between shear walls. Peterman (Peterman 2014) compared shake table test results to the definition of flexible diaphragms in ASCE 7 and the design assumption of the archetype building and concluded that considering the diaphragm as semi-rigid is most consistent with observations. From the modeling guidelines of Leng's research. He concluded that modeling diaphragms as rigid is simpler and is a better initial assumption. Zhang (2016) also choose rigid diaphragm for modeling the floor and roof.

So, rigid diaphragm was chosen in this research. Rigid diaphragm was used in the model by a built-in rigid diaphragm command. It requires to define one master node and multiply slave nodes. The degrees of freedom of the slave nodes will be the same as the master node. The master node was defined on the geometry center of each floor, and all the perimeter nodes on each floor were defined as the slave nodes.

5.7 Seismic Mass and Gravity Load

For office building, total seismic mass was refer to the effective seismic mass calculated in the Design Narrative (Madsen, Nakata, Schafer, 2011). For hotel building, the seismic mass was refer to the ASCE 7-10. The mass on each floor was divided equally and lumped to the four corners of the building model.

Since gravity loads has been considered in the test, which means P-delta effects were also been considered. So, no gravity load and P-delta effects were defined in the modeling.

5.8 Nonlinear Static (Pushover) Analysis

5.8.1 Introduction of Nonlinear Static Analysis

Pushover is a nonlinear static analysis method where a structure is subjected to gravity loading and a monotonic displacement-controlled lateral load pattern which continuously increases through elastic and inelastic behavior until an ultimate condition is reached. Lateral load may represent the range of base shear induced by earthquake loading, and its configuration may be proportional to the distribution of mass along building height, mode shapes.

Pushover analysis was performed first in both horizontal directions, to help validate the model.

5.8.2 Results of Nonlinear Static Analysis

The objective of nonlinear static (pushover) analysis was to quantify maximum base shear strength (V_{max}), effective yield roof drift displacement $\delta_{y.eff}$ and ultimate droof isplacement, δ_u. The applied lateral force at each story level was in proportion to the fundamental mode shape of the index archetype model. Figure 5.6 shows the pushover curve of the 2-story office building in the long direction.

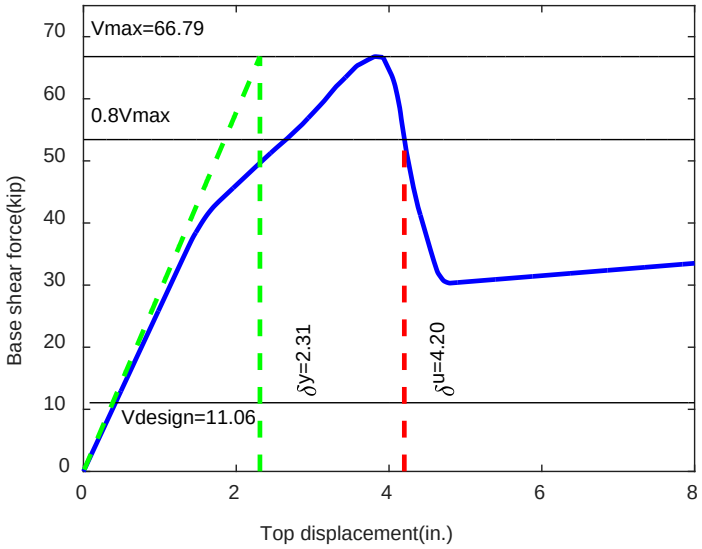

Figure 5.6 - Pushover Curve of the 2-Story Office Building in the Long Direction

The overstrength factor for a given index archetype model, Ω, is defined as the ratio of the maximum base shear strength, V_{max}, to the design base shear, V:

$$\Omega = \frac{V_{max}}{V}$$

The period-based ductility is defined as the ratio of ultimate roof drift displacement, δ_u, to the effective yield roof drift displacement $\delta_{y.eff}$. The δ_u is taken as the roof displacement at the point of 20% strength loss (0.8 V_{max}).

$$\mu_T = \frac{\delta_u}{\delta_{y.eff}}$$

The effective yield roof drift displacement is given by the formula:

$$\delta_{y.eff} = C_0 \frac{V_{max}}{W} \left[\frac{g}{4\pi^2}\right] (\max(T, T_1)^2$$

Where T is the fundamental period, and T_1 is the fundamental period of the archetype model computed using eigenvalue analysis. Coefficient C_0 is based on Equation C3-4 of ASCE/SEI 41-06, as follows:

$$C_0 = \emptyset_{1,r} \frac{\sum_1^N m_x \emptyset_{1,x}}{\sum_1^N m_x {\emptyset_{1,x}}^2}$$

Where m_x is the mass at level x; and $\emptyset_{1,x}$ ($\emptyset_{1,r}$) is the ordinate of the fundamental model at level x (roof), and N is the number of levels.

Based on the formulas and equations listed above, the pushover results of the 2-story office building in the long direction is given in Table 13. Same procedure of pushover analysis applies to other building archetype simulation. Pushover analysis was performed on both horizontal direction of each building archetype, and the details of pushover analysis were given in Appendix D & E.

Table 5.6 - Pushover Results of the 2-story Office Building in the Long Direction

	T	T_1	δ_u	$\delta_{y.eff}$	V_{max}	V_{design}	δ_T	Ω
Long direction	0.244	0.470	4.2	2.31	66.79	11.06	1.82	6.04

5.9 Incremental Dynamic Analysis

5.9.1 Introduction of Incremental Dynamic Analysis

Nonlinear dynamic analysis was conducted by the concept of incremental dynamic analysis (IDA) (Vamvatsikos and Cornell, 2002), in which individual ground motions are scaled to increasing intensities until the structure reaches a collapse point. Nonlinear dynamic analyses are used to established the median collapse capacity, S_{CT}, and collapse margin ratio, CMR, for each of the index archetype model.

In this research, building archetypes were subjected to a suite of far-field ground motion records. The results of IDA are plotted by structure damage measure (DM) versus an intensity measure (IM). Story drift is the DM and the spectral acceleration of the first natural period of the structure is the intensity measure (IM). IDA analysis was performed on both horizontal directions.

5.9.2 Selection of Ground Motion Record Sets

Per FEMA P695, the criteria of ground motion record selection requires to consider the elements of source magnitude, source type, site conditions, site source, number of records per event and strongest ground motion records, etc.

The Methodology provides two sets of ground motion records for collapse assessment using nonlinear dynamic analysis, referred to as Far-Field record set and Near-Field record set. The Far-Field record set includes twenty-two pairs of horizontal ground motions from sites located greater than or equal to 10 km from fault rupture. The Near-Field record set includes twenty-eight component pairs of horizontal ground motions from sites located greater than or equal to 10 km from fault rupture. The record sets do not include the vertical component of ground motion since vertical earthquake shaking is not considered of primary importance for collapse evaluation, and is not required by the FEMA P695 Methodology for nonlinear dynamic analysis.

The Methodology specifies use of the Far-Field record set for collapse evaluation of index archetypes designed for Seismic Design Category B, C, or D. The twenty-two Far-Field record set were selected from the Pacific Earthquake Engineering Research Center (PEER) database. The twenty-two records are take from 14 events that occurred between 1971 and 1999. Of the 14 events, eight were California earthquakes and six were from five different foreign countries. The Far-Field record set was chosen for this research. Details of the 22 far-field ground motion record set is provided in Table 5.7.

Table 5.7 - Details of 22 Far-Field Ground Motion Record Set

ID No.	Earthquake			File Names – Horizontal Records		PGV (cm/s)	Normalization Factor
	M	Year	Name	Component 1	Component 2		
1	6.7	1994	Northridge	NORTHR/MUL009	NORTHR/MUL279	63	0.65
2	6.7	1994	Northridge	NORTHR/LOS000	NORTHR/LOS270	45	0.83
3	7.1	1999	Duzce, Turkey	DUZCE/BOL000	DUZCE/BOL090	62	0.63
4	7.1	1999	Hector Mine	HECTOR/HEC000	HECTOR/HEC090	42	1.09
5	6.5	1979	Imperial Valley	IMPVALL/H-DLT262	IMPVALL/H-DLT352	33	1.31
6	6.5	1979	Imperial Valley	IMPVALL/H-E11140	IMPVALL/H-E11230	42	1.01
7	6.9	1995	Kobe, Japan	KOBE/NIS000	KOBE/NIS090	37	1.03
8	6.9	1995	Kobe, Japan	KOBE/SHI000	KOBE/SHI090	38	1.1
9	7.5	1999	Kocaeli, Turkey	KOCAELI/DZC180	KOCAELI/DZC270	59	0.69
10	7.5	1999	Kocaeli, Turkey	KOCAELI/ARC000	KOCAELI/ARC090	40	1.36
11	7.3	1992	Landers	LANDERS/YER270	LANDERS/YER360	52	0.99
12	7.3	1992	Landers	LANDERS/CLW-LN	LANDERS/CLW-TR	42	1.15
13	6.9	1989	Loma Prieta	LOMAP/CAP000	LOMAP/CAP090	35	1.09
14	6.9	1989	Loma Prieta	LOMAP/G03000	LOMAP/G03090	45	0.88
15	7.4	1990	Manjiil, Iran	MANJIL/ABBAR--L	MANJIL/ABBAR--T	54	0.79
16	6.5	1987	Superstition Hills	SUPERST/B-ICC000	SUPERST/B-ICC090	46	0.87
17	6.5	1987	Superstition Hills	SUPERST/B-POE270	SUPERST/B-POE360	36	1.17
18	7	1992	Cape Mendocino	CAPEMEND/RIO270	CAPEMEND/RIO360	44	0.82
19	7.6	1999	Chi-Chi, Taiwan	CHICHI/CHY101-E	CHICHI/CHY101-N	115	0.41
20	7.6	1999	Chi-Chi, Taiwan	CHICHI/TCU045-E	CHICHI/TCU045-N	39	0.96
21	6.6	1971	San Fernando	SFERN/PEL090	SFERN/PEL180	19	2.1
22	6.5	1976	Friuli, Italy	FRIULI/A-TMZ000	FRIULI/A-TMZ270	31	1.44

5.9.3 Results of Incremental Dynamic Analysis

The median collapse intensity, S_{CT}, is defined as the ground motion intensity where half of the ground motions in the record set cause collapse of an index archetype model. The ratio between the median collapse intensity (S_{CT}) and the MCE intensity (S_{MT}) is the CMR. CMR is the primary parameter used to evaluate the collapse safety of the building design. The tests showed that the sheet-in shear wall could reach 7.5% drift without collapse. FEMA P695 (2009) adopted 7% as the collapse drift limit for the light-framed wood shear wall system. Since the building codes (IBC 2015, ASCE7 2016) consider the light framed wood and steel shear wall systems to have the same seismic performance, the authors conservatively chose 7% as the drift limit for the sheet-in shear wall system in incremental dynamic analysis.

The IDA results are plotted in terms of the spectral intensity of the ground motion versus maximum story drift ratio recorded in the analysis. Figure 5.7(a) shows the 2-story office building IDA results in the long direction, each line in the Figure 5.7 represented a given ground motion scaled to increasing spectral intensity. From Figure 5.7(a), the S_{CT} is 2.42 (g), and the S_{MT} is 1.39 (g).

Another expression of IDA result is the fragility curve. Fragility curve can be defined through a cumulative distribution function, which relates the ground motion intensity to the probability of collapse. (Ibarra et al., 2002). Figure 20-b shows fragility curve of the 2-story office building analysis in the long direction by fitting a lognormal distribution through the collapse data points from Figure 5.7(a). In Figure 5.7(b), the S_{CT} corresponds the 50% collapse probability of the index archetype at the ground motion intensity S_{CT}. CMR can be calculated as:

$$CMR = \frac{S_{CT}}{S_{MT}} = \frac{2.42}{1.39} = 1.741$$

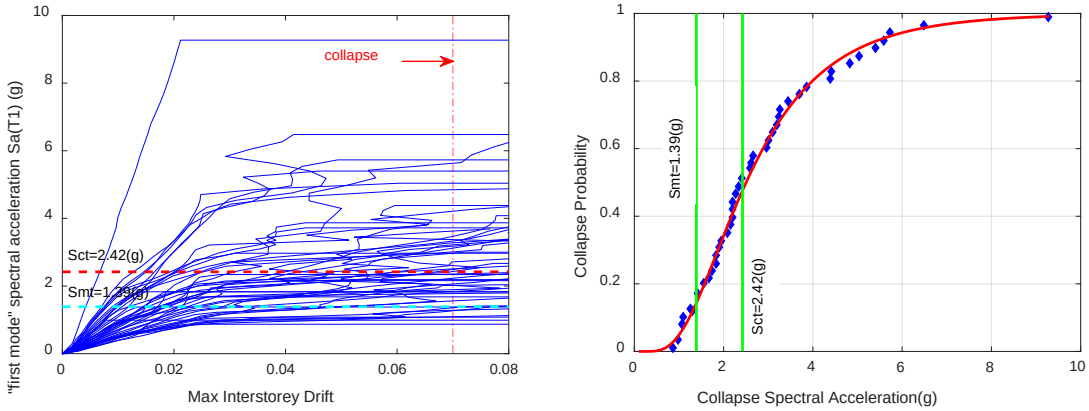

(a)IDA curve (b) Fragility curve

Figure 5.7 - IDA Results of the 2-Story Office Building in the Long Direction

Same procedure of IDA analysis applies to other building archetype simulation. Details of IDA analysis for each archetype was given in Appendices D and E.

CHAPTER 6

SEISMIC PERFORMANCE EVALUATION

Chapter 6 discusses the process of evaluating the seismic performance of newly proposed sheet-in shear wall seismic-force-resisting system, assessing the acceptable trial value of the response modification coefficient, R , and determining appropriate values of the system overstrength factor Ω_0, and the deflection amplification factor, C_d.

In general, trial values of seismic performance factors are evaluated for each building archetype. The results within each performance group are averaged to determine the value for the group, which is the primary basis for judging acceptability of the trial value.

6.1 The Process of Seismic Performance Evaluation

The process of performance evaluation includes are: (FEMA P695):

1. Obtain calculated values of system overstrength, Ω, period-based ductility, μ_T, and collapse margin ratio, *CMR*, for each index archetype, from results of nonlinear analyses (pushover analysis) (Chapter 5).
2. Calculate the adjusted collapse margin ratio, *ACMR*, for each archetype using the spectral shape factor, *SSF*, which depends on the fundamental period, *T*, and period-based ductility, μ_T.
3. Calculate total system collapse uncertainty, β_{TOT}, based on the quality ratings of design requirements and test data, and the quality rating of index archetype models.
4. Determine acceptable values of adjusted collapse margin ratio, *ACMR*10% and *ACMR*20%, respectively, based on total collapse system uncertainty, β_{TOT}.
5. Evaluate the adjusted collapse margin ratio, *ACMR*, for each archetype and average values of *ACMR* for each archetype performance group relative to acceptable values.

6. Evaluate the system overstrength factor, Ω_0.

7. Evaluate the displacement amplification factor, C_d.

If the evaluation of ACMR finds trial values of seismic performance factors were unacceptable, then the system should be redefined and reanalyzed, then re-evaluated by repeating performance evaluation process.

Here, the 2-story office building was used as an example again to demonstrate the individual index archetype performance evaluation before performing the group of index archetypes performance evaluation.

At this point, Step 1 has been completed. However, the CMR computed above did not account for the unique spectral shape (frequency content) of rare ground motions. To account for the effects of spectral shape, the CMR is adjusted to obtain an adjusted collapse margin ratio, ACMR, for each index archetype.

$$ACMR = SSF \times CMR$$

Spectral shape factors, SSF, are a function of the fundamental period, T, the period-based ductility, μ_T, and the applicable Seismic Design Category. The SSF is calculated by the interpolation method from Table 6.1.

ACMR is calculated as:

$$ACMR = SSF \times CMR = 1.12 \times 1.74 = 1.95$$

Table 6.1 - Spectral Shape Factor (SSF) for Archetypes Designed using SDC Dmax

T（s）	Period-Based Ductility,						
	1	1.1	1.5	2	3	4	6
≤0.5	1	1.05	1.1	1.13	1.18	1.22	1.28
0.6	1	1.05	1.11	1.14	1.2	1.24	1.3
0.7	1	1.06	1.11	1.15	1.21	1.25	1.32
0.8	1	1.06	1.12	1.16	1.22	1.27	1.35

0.9	1	1.06	1.13	1.17	1.24	1.29	1.37
1	1	1.07	1.13	1.18	1.26	1.31	1.39
1.1	1	1.07	1.14	1.19	1.27	1.32	1.41
1.2	1	1.07	1.15	1.2	1.28	1.34	1.44
1.3	1	1.08	1.16	1.21	1.29	1.36	1.46
1.4	1	1.08	1.16	1.22	1.31	1.38	1.49
≥1.5	1	1.08	1.17	1.23	1.32	1.4	1.51

Many sources of uncertainty contribute to variability in collapse capacity. It is important to evaluate all significant sources of uncertainty in collapse response, and to incorporate their effects in the collapse assessment process.

Four sources of uncertainty were considered in the performance evaluation process, there were record-to-record uncertainty (RTR), design requirements uncertainty (DR), test data uncertainty (TD), and modeling uncertainty (MDL).

6.1.1 Record-to-Record Uncertainty (RTR)

Record-to-record uncertainty, β_{RTR}, is due to variability in the response of index archetypes to different ground motion records. Record-to-record variability is evident in incremental dynamic response plots. Variability in response is due to the combined effects of: (1) variations in frequency content and dynamic characteristics of the various records; and (2) variability in the hazard characterization as reflected in the Far-Field ground motion record set. The record-to-record uncertainty is calculated by:

$$\beta_{RTR} = 0.1 + 0.1\mu_T \leq 0.40$$

Where β_{RTR} must be greater than or equal to 0.20.

In the 2-story office building in the long direction, the β_{RTR} is calculated as

$$\beta_{RTR} = 0.1 + 0.1 \times 1.82 = 0.282$$

6.1.2 Design Requirements Uncertainty (DR)

Design requirements uncertainty, β_{DR}, is related to the completeness and robustness of the design requirements, and the extent to which they provide safeguards against unanticipated failure modes. Design requirements-related uncertainty is quantified in terms of the quality of design requirements, rated in accordance with the requirements in Table 3-1 of FEMA P695.

6.1.3 Test Data Uncertainty (TD)

Test data uncertainty, β_{TD}, is related to the completeness and robustness of the test data used to define the system. Uncertainty in test data is closely associated with, but distinct from, modeling-related uncertainty. Test data-related uncertainty is quantified in terms of the quality of test data, rated in accordance with the requirements in Table 3-2 of FEMA P695.

6.1.4 Modeling Uncertainty (MDL)

Modeling uncertainty, β_{MDL}, is related to how well index archetype models represent the full range of structural response characteristics and associated design parameters of the archetype design space, and how well the analysis models capture structural collapse behavior through direct simulation or non-simulated component checks. Modeling-related uncertainty is quantified in terms of the quality of index archetype models, rated in accordance with the requirements in Table 5-3 of FEMA P695. Table 4-4 concluded the quality rating of the design requirements uncertainty, test data uncertainty, and modeling uncertainty. The rating of design requirements uncertainty, test data uncertainty and modeling uncertainty is summarized in Table 6.2.

Table 6.2 - Uncertainty Rating of β_{DR}, β_{TD}, and β_{MDL}.

	Superior	Good	Fair	Poor
β_{DR}	0.1	0.2	0.35	0.5
β_{TD}	0.1	0.2	0.35	0.5
β_{MDL}	0.1	0.2	0.35	0.5

For design requirements uncertainty, it was rated as good. The reason is that there are many similarities between sheet-in shear wall and the shear wall with flat sheet, the design of sheet-in shear wall can refer to the design of shear wall with flat sheet, which is certified by AISI S400-15. Also, There is a high likelihood that the manufacturer and builder will use the same method of fabrication, erection and construction of shear wall with flat sheet for sheet-in shear wall, though minor detailing needs to be changed.

For test data uncertainty, it was rated as good. The experimental evidence was sufficient, important behaviors of the shear wall (from material to system) were well understood. The results can be used to quantify all important parameters that affect design requirements and analytical modeling. Confidence level for cyclic tests were high as two identical tests were done, while confidence level for monotonic tests were medium as one test for one configuration was done. However, sufficient amount of monotonic tests has shown that the results of two identical shear wall monotonic tests were consistent, the possibility of deviation of two identical tests results was low.

For modeling uncertainty, it was rated as good. Two groups of index archetypes were designed in the modeling process. The index archetype configurations varied in a wide range as discussed in Chapter 5.3. Before performing 3D simulation, shear wall model and bearing wall model was verified first. Nonlinear model was capable of simulating pinching effects, from the onset of yielding through strength and stiffness degradation causing collapse.

Since these four random variables are assumed to be statistically independent, the lognormal standard deviation parameter, β_{TOT}, describing total collapse uncertainty, is calculated by:

$$\beta_{TOT} = \sqrt{{\beta_{RTR}}^2 + {\beta_{DR}}^2 + {\beta_{TD}}^2 + {\beta_{MDL}}^2}$$

Where:

$\beta_{TOT=}$ total system collapse uncertainty (0.275 – 0.950)

$\beta_{RTR=}$ record-to-record collapse uncertainty (0.20 – 0.40)

$\beta_{DR=}$ design requirements-related collapse uncertainty (0.10 – 0.50)

$\beta_{TD=}$ test data-related collapse uncertainty (0.10 – 0.50)

$\beta_{MDL=}$ modeling-related collapse uncertainty (0.10 – 0.50)

The β_{TOT} of the 2-story office building in the long direction is calculated as:

$$\beta_{TOT} = \sqrt{0.282^2 + 0.2^2 + 0.2^2 + 0.2^2} = 0.447$$

Acceptable values of adjusted collapse margin ratio are based on total system collapse uncertainty, β_{TOT}, and established values of acceptable probabilities of collapse. The acceptable values of ACMR is calculated by the interpolation method from Table 6.3.

Table 6.3 - Acceptable Values of Adjusted Collapse Margin Ratio

Total System Collapse Uncertainty	Collapse Probability			
	5%	10% $ACMR_{10\%}$	15%	20% （$ACMR_{20\%}$）
0.275	1.57	1.42	1.33	1.26
0.3	1.64	1.47	1.36	1.29
0.325	1.71	1.52	1.4	1.31
0.35	1.78	1.57	1.44	1.34
0.375	1.85	1.62	1.48	1.37
0.4	1.93	1.67	1.51	1.4
0.425	2.01	1.72	1.55	1.43
0.45	2.1	1.78	1.59	1.46
0.475	2.18	1.84	1.64	1.49
0.5	2.28	1.9	1.68	1.52
0.525	2.37	1.96	1.72	1.56
0.55	2.47	2.02	1.77	1.59

If the trial value of response modification coefficient, R, was acceptable, it is required that for each index archetype and each performance group meet the following two criteria:

Individual values of adjusted collapse margin ratio for each index archetype within a performance group exceeds $ACMR_{20\%}$:

$$ACMR_i \geq ACMR_{20\%}$$

The average value of adjusted collapse margin ratio for each performance group exceeds $ACMR_{10\%}$:

$$\overline{ACMR_i} \geq ACMR_{10\%}$$

The average value of archetype overstrength, Ω, is calculated for each performance group. Then, the value of the system overstrength factor, Ω_0, for use in design should not be taken as less than the largest average value of calculated archetype overstrength Ω, from any performance group.

The deflection amplification factor, C_d, is based on the acceptable value of the response modification factor, R, reduced by the damping factor, B_I, corresponding to the inherent damping of the system of interest.

$$C_d = \frac{R}{B_I}$$

Where B_I is the numerical damping coefficient given in Table 18.6-1 of ASCE 7-10 (2016).

However, the inherent damping of the newly proposed CFS framed building system with sheet-in shear wall needs to be verified by future investigations. According to the test results by Shafer (2015), the measured damping of the CFS framed building using wood sheathed shear walls varied from 4% to 9%. The author adopted 5% inherent damping in this research, which was believed to be appropriate. As a result, the damping coefficient, B_I equals to 1.0. So, C_d would be equal to R.

6.2 Seismic Performance Evaluation of Office Archetypes and Hotel Archetypes

Based on the process of seismic performance evaluation given in the Section of 6.1, this section showed the results of the performance evaluation on the two performance groups of index archetypes.

Table 18 summarized the performance evaluation results of the two groups of building archetypes. Detailed calculation of the archetypes performance evaluation can be found in Appendix C & D.

6.3 Summary of Performance Evaluation

For performance evaluation based on the good uncertainty ratings. Table 18, all individual values of adjusted collapse margin ratio (ACMR) for each index archetype within a performance group exceeded the corresponding $ACMR_{20\%}$ value. And the average value of adjusted collapse margin ratio (ACMR) for each performance group exceeded the corresponding $ACMR_{10\%}$ value. This proved that the trial value of the response modification coefficient R, 6.5, was acceptable.

The average value of overstrength factor, Ω_0, for each performance group was 3.73 and 3.35. According to the Section 7.6 in FEMA P695, a practical limit on the value of Ω_0 is about 3.0, which is consistent with the largest value of this factor specific in Table 12.2-1 of ASCE 7-10 for all current approved seismic-force-resisting systems. In addition, the Example 9.4 provided in FEMA P695 chose 3.0 for overstrength factor as the average values being greater than 3.0 in that Example. Hence, author proposed the use of 3.0 for overstrength factor due to the the average value of each performance group was bigger than 3.0.

The deflection amplification factor, C_d, was equal to R, which has been discussed in the previous section.

However, it would be safer to perform another performance evaluation based on the fair uncertainty ratings. Table 6.4 summarizes the results of performance evaluation based on the fair uncertainty ratings. All individual values of adjusted collapse margin ratio (ACMR) for each index archetype within a performance group exceeded the corresponding $ACMR_{20\%}$ value. However, the average value of adjusted collapse margin ratio (ACMR) for each performance group failed to exceed the corresponding $ACMR_{10\%}$ value.

Table 6.4 - Performance Evaluation Results of the Two Groups of Building Archetypes (Good Uncertainty)

		Ω_0	δ_T	S_{CT}	S_{MT}	CMR	SSF	ACMR	β_{TOT}	Accept ACMR(20%)	Accept ACMR(10%)
Office building	2-story-long	6.04	1.82	2.42	1.39	1.741	1.119	1.948	0.447	1.458	1.775
	2-story-short	4.24	1.77	2.42	1.39	1.741	1.116	1.943	0.444	1.441	1.742
	3-story-long	4.1	1.83	2.83	1.39	2.036	1.12	2.279	0.448	1.458	1.775
	3-story-short	3.22	1.62	2.53	1.39	1.82	1.107	2.015	0.434	1.441	1.742
	5-story-long	2.67	2.52	2.53	1.39	1.82	1.156	2.104	0.494	1.513	1.886
	5-story-short	2.1	2.19	2.31	1.39	1.662	1.141	1.896	0.471	1.485	1.83
Mean of Office Performance Group		3.73	1.96	2.51	1.39	1.803	1.127	2.031	0.456	1.466	1.792
Hotel building	2-story-long	4.8	1.8	2.46	1.5	1.64	1.118	1.834	0.445	1.454	1.768
	2-story-short	5.48	1.82	2.42	1.5	1.613	1.119	1.805	0.447	1.456	1.773
	4-story-long	2.47	1.04	2.35	1.5	1.567	1.02	1.598	0.402	1.402	1.674
	4-story-short	2.5	1.09	2.35	1.5	1.567	1.045	1.637	0.405	1.406	1.68
	5-story-long	2.22	3	2.71	1.5	1.807	1.184	2.139	0.529	1.565	1.97
	5-story-short	2.61	1.83	2.63	1.5	1.753	1.13	1.981	0.447	1.456	1.773
Mean of Hotel Performance Group		3.35	1.76	2.49	1.5	1.658	1.103	1.832	0.446	1.457	1.773

Table 6.5 - Performance Evaluation Results of the Two Groups of Building Archetypes (Fair Uncertainty)

		Ω_0	δ_T	S_{CT}	S_{MT}	CMR	SSF	ACMR	β_{TOT}	Accept ACMR(20%)	Accept ACMR(10%)
Office building	2-story-long	6.04	1.82	2.42	1.39	1.741	1.119	1.948	0.447	1.753	2.353
	2-story-short	4.24	1.77	2.42	1.39	1.741	1.116	1.943	0.444	1.749	2.345
	3-story-long	4.1	1.83	2.83	1.39	2.036	1.12	2.279	0.448	1.755	2.359
	3-story-short	3.22	1.62	2.53	1.39	1.82	1.107	2.015	0.434	1.742	2.328
	5-story-long	2.67	2.52	2.53	1.39	1.82	1.156	2.104	0.494	1.801	2.453
	5-story-short	2.1	2.19	2.31	1.39	1.662	1.141	1.896	0.471	1.772	2.408
Mean of Office Performance Group		3.73	1.96	2.51	1.39	1.803	1.127	2.031	0.456	1.762	2.374
Hotel building	2-story-long	4.8	1.8	2.46	1.5	1.64	1.118	1.834	0.445	1.752	2.350
	2-story-short	5.48	1.82	2.42	1.5	1.613	1.119	1.805	0.447	1.753	2.353
	4-story-long	2.47	1.04	2.35	1.5	1.567	1.02	1.598	0.402	1.708	2.272
	4-story-short	2.5	1.09	2.35	1.5	1.567	1.045	1.637	0.405	1.709	2.275
	5-story-long	2.22	3	2.71	1.5	1.807	1.184	2.139	0.529	1.841	2.533
	5-story-short	2.61	1.83	2.63	1.5	1.753	1.13	1.981	0.447	1.753	2.353
Mean of Hotel Performance Group		3.35	1.76	2.49	1.5	1.658	1.103	1.832	0.446	1.753	2.356

CHAPTER 7

CONCLUSION AND FURTURE RESEARCH

Follow up Mahdavian's (2016) and Zhang's (2016) research, this research was to evaluate the structural performance of the newly designed sheet-in shear wall lateral-force-resisting system, and its potential use for mid-rise buildings.

Compared to sheet-out shear wall, sheet-in shear wall provides a smooth surface so that it is easier for finish installation thanks to the corrugated steel sheets are installed inside the frame. In this research, it was the first time to test the sheet-in walls under combined lateral and gravity loads. The test results showed that gravity loads has negative effects on the strength and stiffness of the sheet-in shear wall due to the local buckling of the chord framing members. The test results also showed that the strength of the sheet-in bearing wall was approximately equal to one third of the strength of the sheet-in shear wall. If a structure had significant amount of bearing walls, their contribution to the lateral force resistance of the structure should not be ignored. In the monotonic tests, it was observed that both sheet-in bearing wall and shear wall were able to carry gravity load without collapse at the maximum drift of 7.5% so that 7% drift was set as the collapse drift limit for the sheet-in shear wall in the numerical model.

The seismic performance evaluation was performed on two groups of building archetypes by following the Methodology in FEMA P695. Nonlinear static and dynamic analysis were performed in both horizontal directions of each building archetype. Due to the inherent uncertainties involved throughout the process, from test data to finite element analysis, good uncertainty rating and fair uncertainty rating were selected for seismic performance evaluation. For good uncertainty rating, the results of the performance evaluation verified the seismic performance factors ($R=C_d=6.5$ and $\Omega=3.0$) were appropriate for the novel shear wall system,

which is consistent with the seismic performance factor used in CFS framed shear wall with flat steel sheet and wood-based panel. However, for fair uncertainty rating, the performance evaluation verified the seismic performance factors ($R=C_d=6.5$ and $\Omega=3.0$) could not meet the evaluation criteria with the same seismic performance factors ($R=C_d=6.5$ and $\Omega=3.0$). Implementation of the Methodology in FEMA P695 involves much uncertainty, judgment and potential for variation. All the documentations and the proposed seismic performance factors shall be reviewed by an independent peer review panel before the adoption of the proposed seismic performance factors for this newly design shear wall system.

In future research, a few of studies could be done for further improving the structural performance of the sheet-in shear wall and its seismic performance evaluation results.

Firstly, it was observed that the strength and stiffness of the sheet-in shear wall test with gravity loads dropped compared with tests without gravity loads due to the local buckling of the chord framing members. As tracks are weaker than studs, reinforcement of the chord vertical tracks can be studied.

Secondly, the gravity loads applied to the wall was based on the 2-story NEES-CFS building. The configuration of the sheet-in shear wall used in this research may not resist the 3 story or higher story gravity loads. So, verification of the bearing strength of the sheet-in bearing wall and shear wall needs to be done. In addition, wider and thicker sheet-in shear wall configuration can be tested in the future, and the stronger sheet-in shear wall could be used in the lower story of a mid-rise CFS structure.

Last but not least, it is expected that the set of building archetype configurations will generally include about twenty to thirty specific structural configurations for performance evaluation. Only 6 index building archetypes were studied in this research, more configuration

design variables could be tried on the building archetype design. Also, trail value of the response modification coefficient, R, could be set to 7.0 or 7.5 to further explore the potential of the newly design shear wall system since the value of 6.5 has been verified in this research.

APPENDIX A

TEST DETAILS

Test No. 1

Opening Type: No opening

Wall Type: Bearing Wall

Test date: Sept. 2, 2016

Specimen Configuration:

Wall dimensions: 8 ft. x 4 ft. Studs: 350 T 125 - 68, 50 ksi Tracks: 350 T 150- 68, 50 ksi

Steel sheathing: Verco Decking, SV36, 22 ga, 80 ksi

Fastener: # 12 x 1 - 1/4" hex head washer self-drilling screws, 3/6 in. spacing

Hold-down: Simpson Strong Tie S/HD15S both side

Gravity loads: 5384 lbs

Test protocol: Monotonic test

Test results:

+Peak load: 4747.60 lbs

Lateral displacement of wall @ peak load: 2.55 in.

Observed Failure Mode: vertical chord tracks buckle, bottom track buckles, screw pull out, screw pull over, track buckled, sheet tearing

Screw Pull Out: No

Sheathing Tear: No

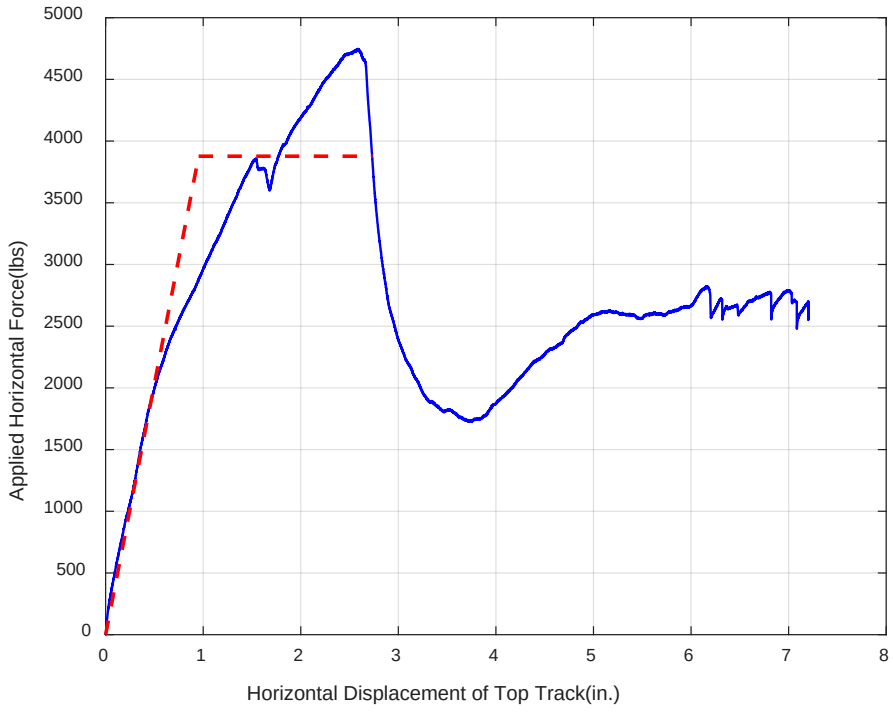

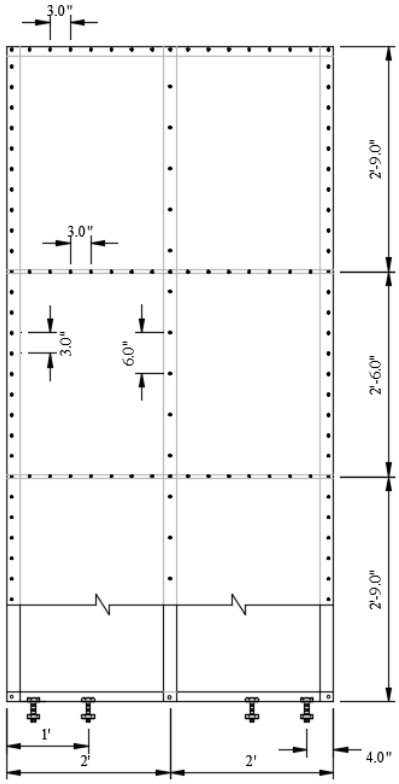
3.0"
3.0"
3.0"
6.0"
2'-9.0"
2'-6.0"
2'-9.0"
1'
2'
2'
4.0"

Test No. 2

Opening Type: No opening

Wall Type: Bearing Wall

Test date: Aug. 23, 2016

Specimen Configuration:

Wall dimensions: 8 ft. x 4 ft. Studs: 350 T 125 - 68, 50 ksi Tracks: 350 T 150- 68, 50 ksi

Steel sheathing: Verco Decking, SV36, 22 ga, 80 ksi

Fastener: # 12 x 1 - 1/4" hex head washer self-drilling screws, 3/6 in. spacing

Gravity loads: 5384 lbs

Test protocol: Cyclic test

Test results:

Average Peak load: 5520.70 lbs

Average Lateral displacement of wall @ peak load: 3.02 in.

Peak Load Cycle: 38

Observed Failure Mode: vertical chord tracks and middle buckle, screw pull out in the bottom track

Screw Pull Out: Yes

Sheathing Tear: No

Note: Negative peak load was not a valid data, the T-bar hit the testing frame.

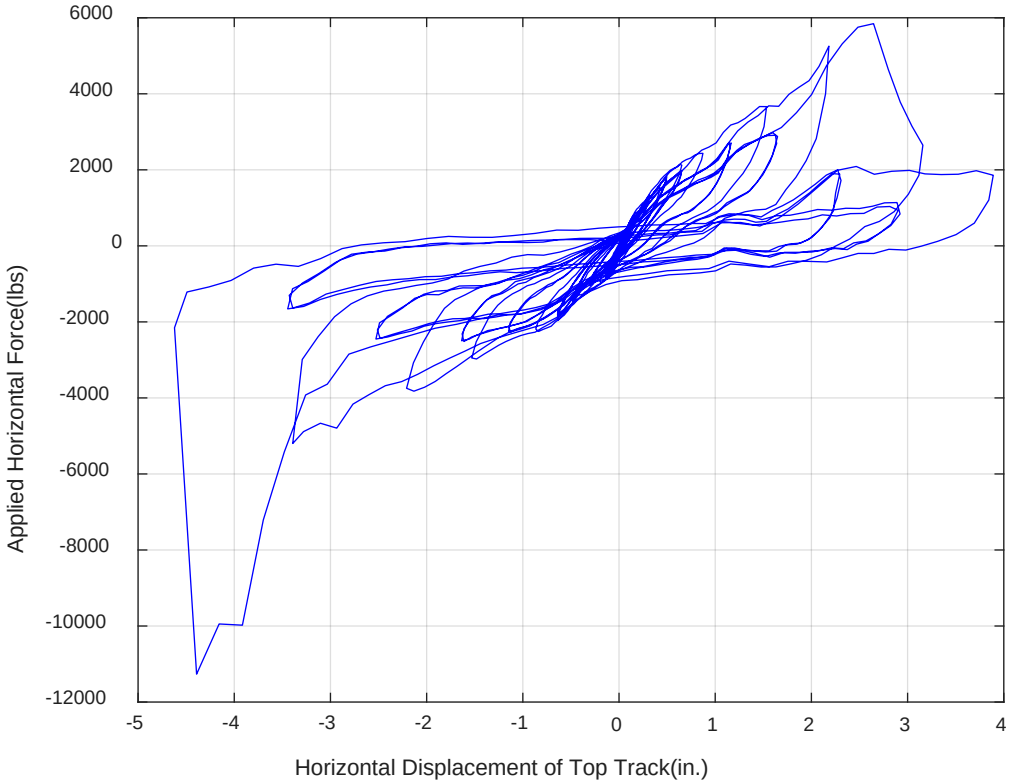

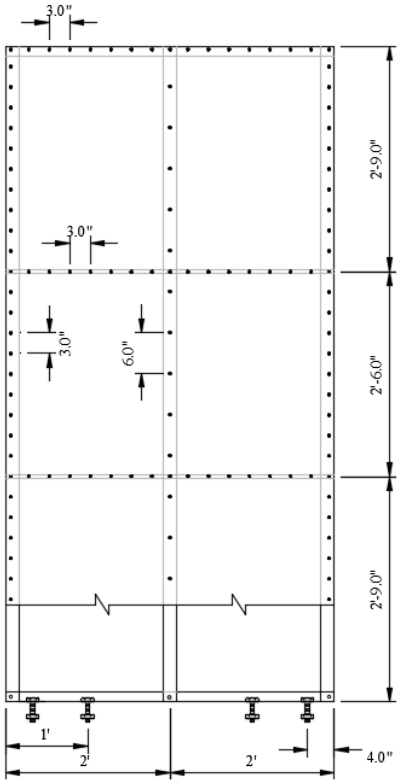

Wall Type: Bearing Wall

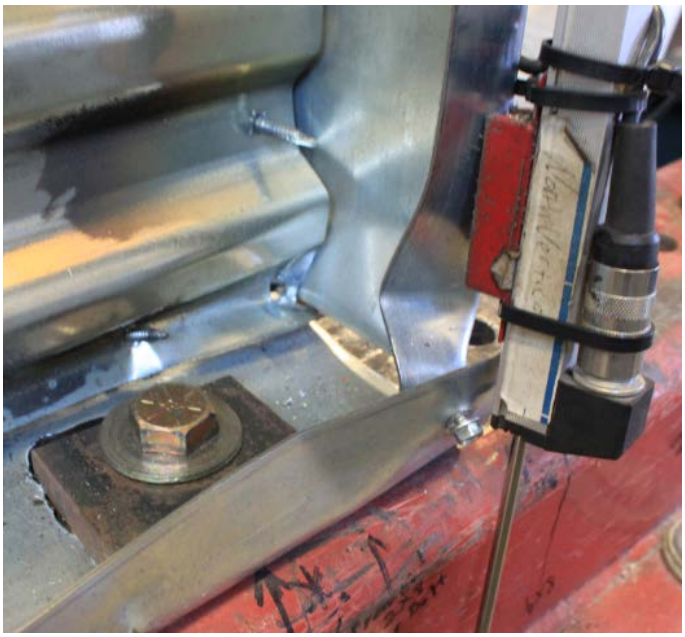

Test No. 3

Opening Type: No opening

Test date: Aug. 24, 2016

Specimen Configuration:

Wall dimensions: 8 ft. x 4 ft. Studs: 350 T 125 - 68, 50 ksi Tracks: 350 T 150- 68, 50 ksi

Steel sheathing: Verco Decking, SV36, 22 ga, 80 ksi

Fastener: # 12 x 1 - 1/4" hex head washer self-drilling screws, 3/6 in. spacing

Gravity loads: 5384 lbs

Test protocol: Cyclic test

Test results:

+Peak load: 4847.68 lbs

Lateral displacement of wall @ peak load: 2.87 in.

Peak Load Cycle: 38

Observed Failure Mode: Vertical chord tracks buckle, screws pull out in the bottom track

Screw Pull Out: Yes

Sheathing Tear: No

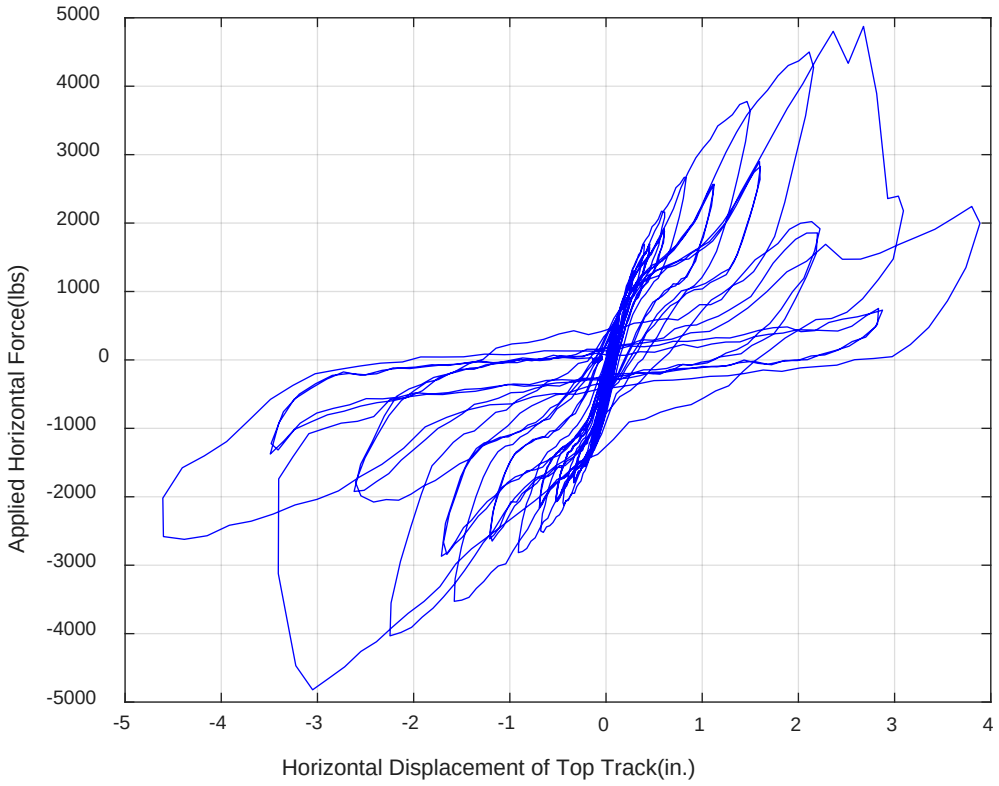

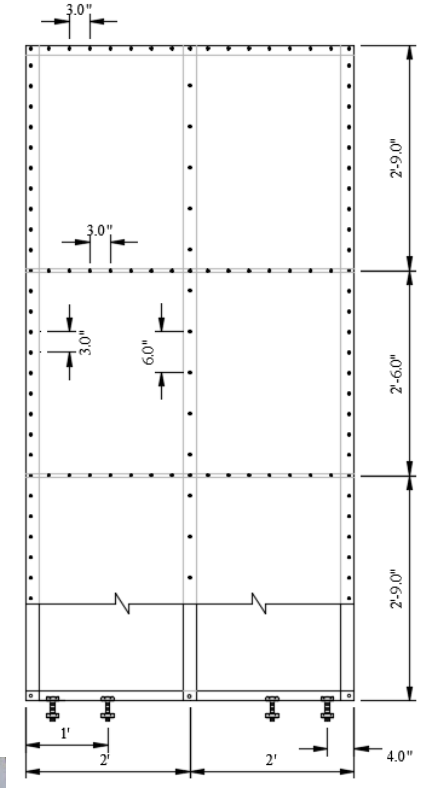
3.0"
3.0"
3.0"
6.0"
2'-9.0"
2'-6.0"
2'-9.0"
1'
2'
2'
4.0"

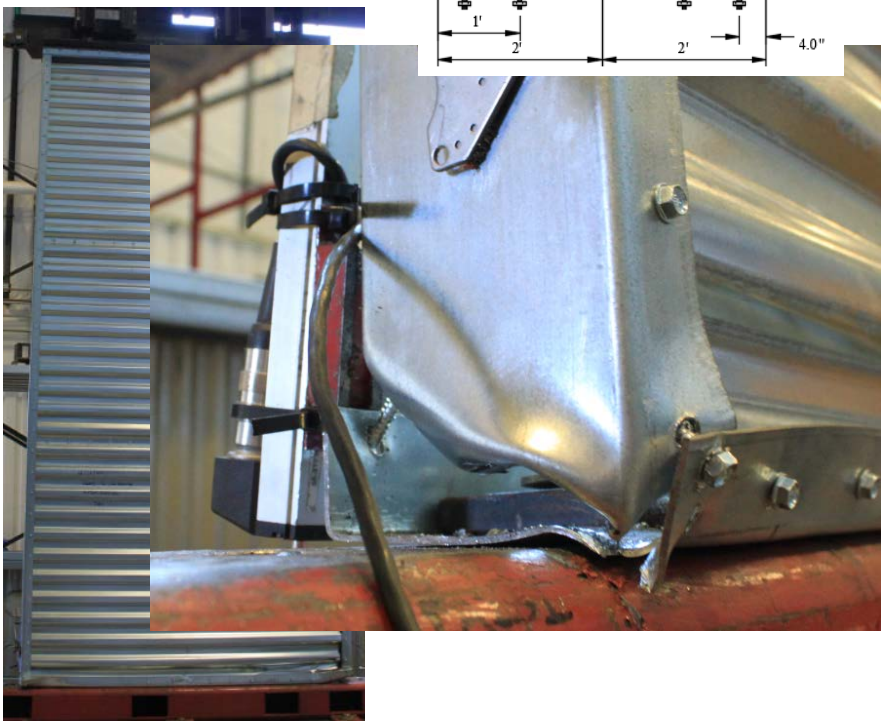

Test No. 4

Opening Type: No opening

Wall Type: Shear Wall

Test date: Sept. 9, 2016

Specimen Configuration:

Wall dimensions: 8 ft. x 4 ft. Studs: 350 T 125 - 68, 50 ksi Tracks: 350 T 150- 68, 50 ksi

Steel sheathing: Verco Decking, SV36, 22 ga, 80 ksi

Fastener: # 12 x 1 - 1/4" hex head washer self-drilling screws, 3/6 in. spacing

Hold-down: Simpson Strong Tie S/HD15S both side

Gravity loads: 5384 lbs

Test protocol: Monotonic test

Test results:

+Peak load: 13523.58 lbs

Lateral displacement of wall @ peak load: 2.30 in.

Observed Failure Mode: Vertical vertical chord tracks buckle right above the hold-down, bottom sheet tearing. Screw pull out

Screw Pull Out: Yes

Sheathing Tear: Yes

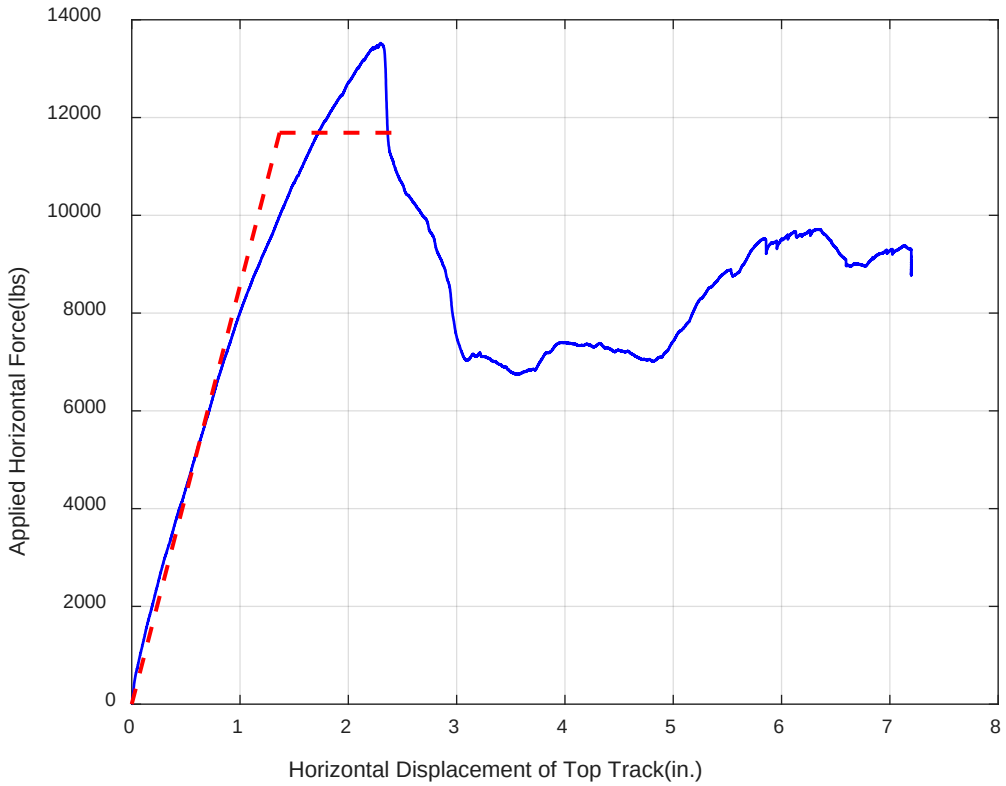

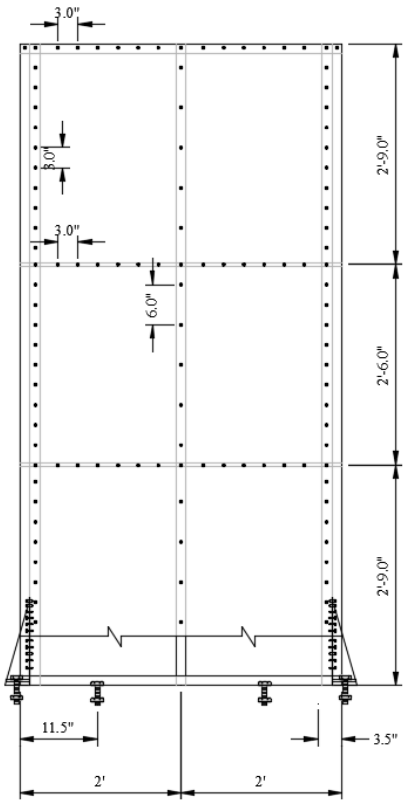

Test No. 5

Opening Type: No opening

Wall Type: Shear Wall

Test date: Sept. 9, 2016

Specimen Configuration:

Wall dimensions: 8 ft. x 4 ft. Studs: 350 T 125 - 68, 50 ksi Tracks: 350 T 150- 68, 50 ksi

Steel sheathing: Verco Decking, SV36, 22 ga, 80 ksi

Fastener: # 12 x 1 - 1/4" hex head washer self-drilling screws, 3/6 in. spacing

Hold-down: Simpson Strong Tie S/HD15S both side

Gravity loads: 5384 lbs

Test protocol: Cyclic test

Test results:

+Peak load: 13837.10 lbs

Lateral displacement of wall @ peak load: 2.12 in.

Peak Load Cycle: 35

Observed Failure Mode: Vertical vertical chord tracks buckle right above the hold-down, bottom sheet tearing, screws pull out

Screw Pull Out: Yes

Sheathing Tear: Yes

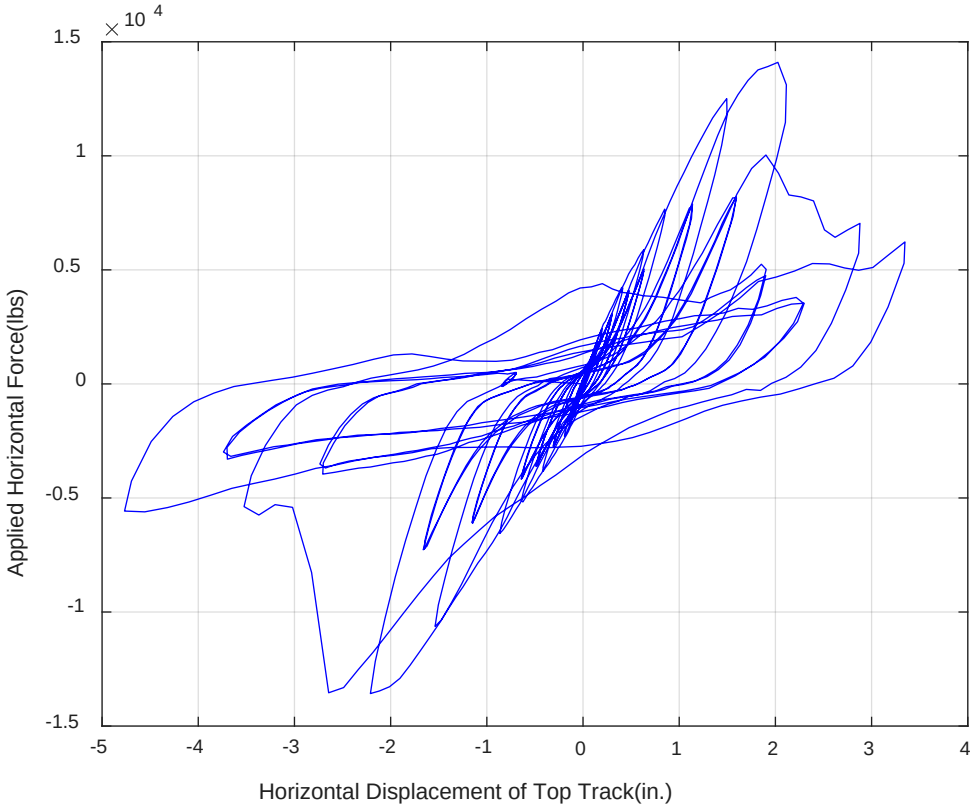

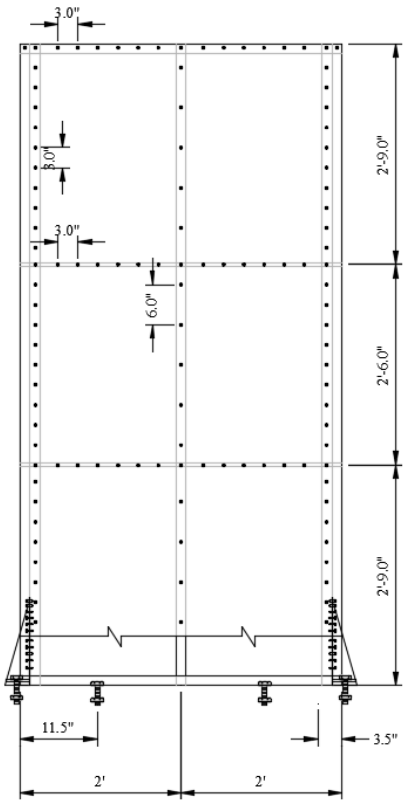

Test No. 6

Opening Type: No opening

Wall Type: Shear Wall

Test date: Jan. 12, 2017

Specimen Configuration:

Wall dimensions: 8 ft. x 4 ft. Studs: 350 T 125 - 68, 50 ksi Tracks: 350 T 150- 68, 50 ksi

Steel sheathing: Verco Decking, SV36, 22 ga, 80 ksi

Fastener: # 12 x 1 - 1/4" hex head washer self-drilling screws, 3/6 in. spacing

Hold-down: Simpson Strong Tie S/HD15S both side

Gravity loads: 5384 lbs

Test protocol: Cyclic test

Test results:

+Peak load: 14346.58 lbs

Lateral displacement of wall @ peak load: 2.10 in.

Peak Load Cycle: 35

Observed Failure Mode: Vertical vertical chord tracks slightly buckle, bottom sheet tearing, screws pull out, screws shear failure

Screw Pull Out: Yes

Sheathing Tear: Yes

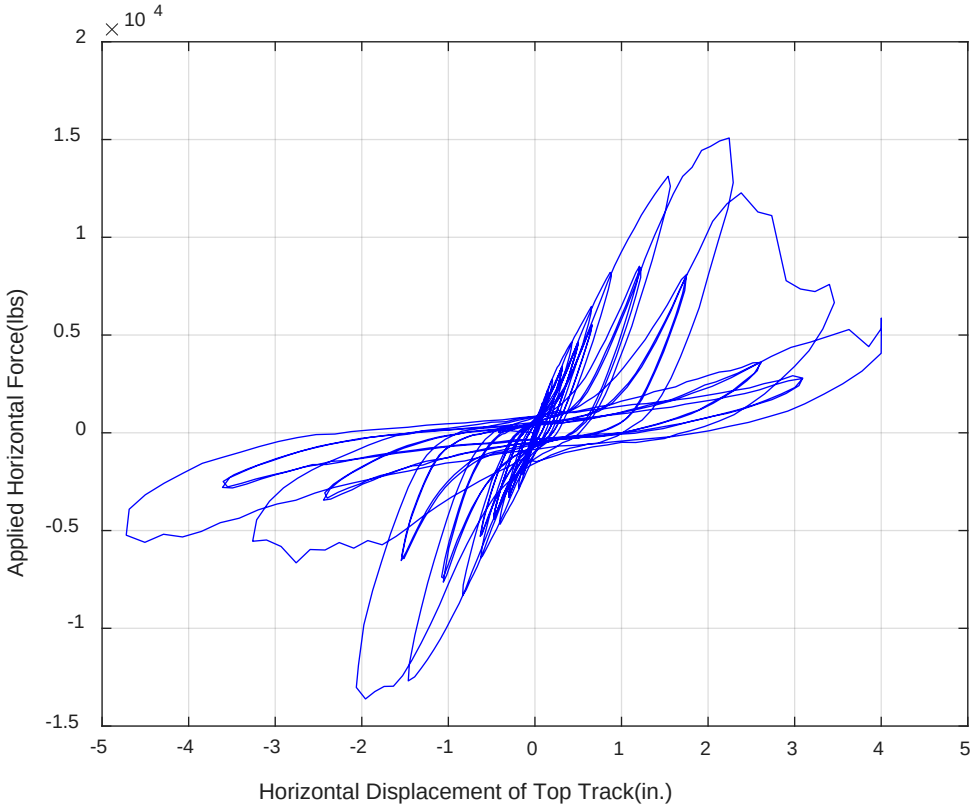

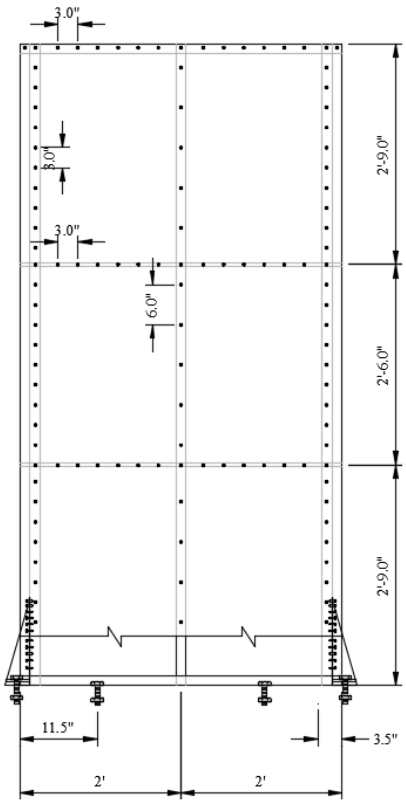
3.0"
8.0"
3.0"
6.0"
2'-9.0"
2'-6.0"
2'-9.0"
11.5"
3.5"
2'
2'

APPENDIX B

DESIGN OF SHEAR WALL FOR OFFICE BUILDING MODELS

Design Parameters for Office Building Models

Seismic Analysis (LFRS) per ASCE 7-10

Occupancy Category II

Ie = 1.0

Ss = 1.39 Fa = 1.0 (Table 11.4-1)

S1 = 0.50 Fv = 1.5 (Table 11.4-2)

Site Class D

$S_{MS} = F_a S_s =$ 1.39 (Eq. 11.4-1)

$S_{M1} = FvS_1 =$ 0.75 (Eq. 11.4-2)

$S_{DS} = 2/3 \times S_{MS} =$ 0.927 (Eq. 11.4-3)

$S_{D1} = 2/3 \times S_{M1} =$ 0.500 (Eq. 11.4-4)

Cs = 0.143 (Eq. 12.8-2)

Unit Weights

Roof 20 (psf)

Floor 18 (psf)

Walls 10 (psf)

Partitions 10 (psf)

Rooftop MEP 1200 (lb)

Parapet 1819 (lb)

Building Dimensions

Width (E-W) 49.75 (ft)

Length (N-S) 23.00 (ft)

Story Height 9.00 (ft)

Roof Wx based on Roof DL, Rooftop MEP, Parapet and 1/2 of Upper Walls

2nd Level wx based on 2nd Floor DL, Less Clerestory, + 0.5 x (Upper Walls + Lower Walls)

Figure 21 illustrates three types of shear wall layouts for office building model

(a)

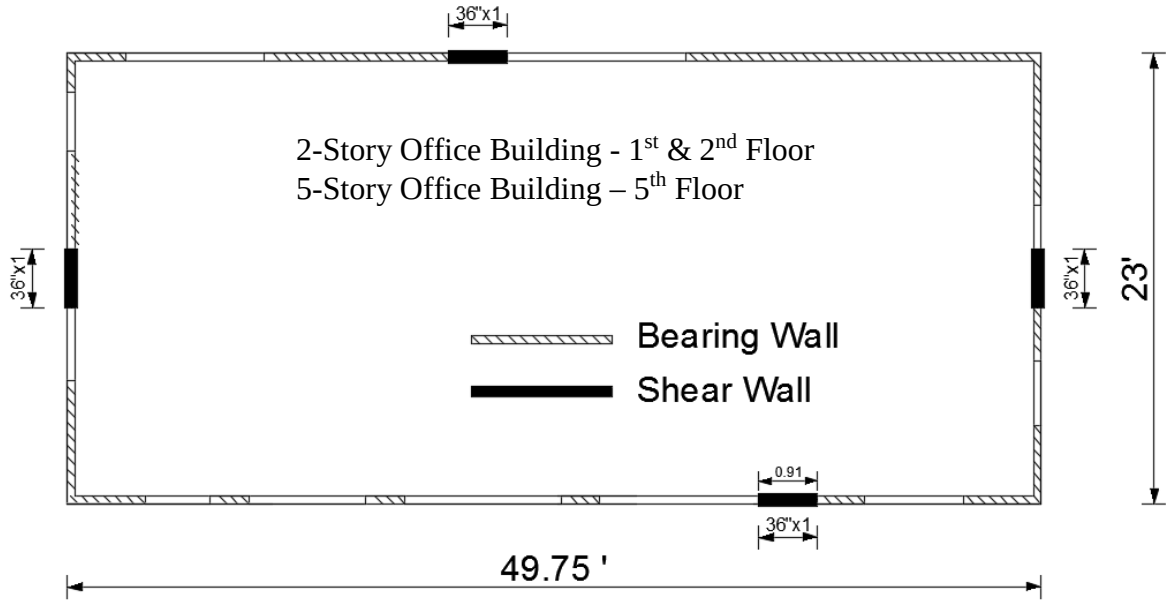

(b)

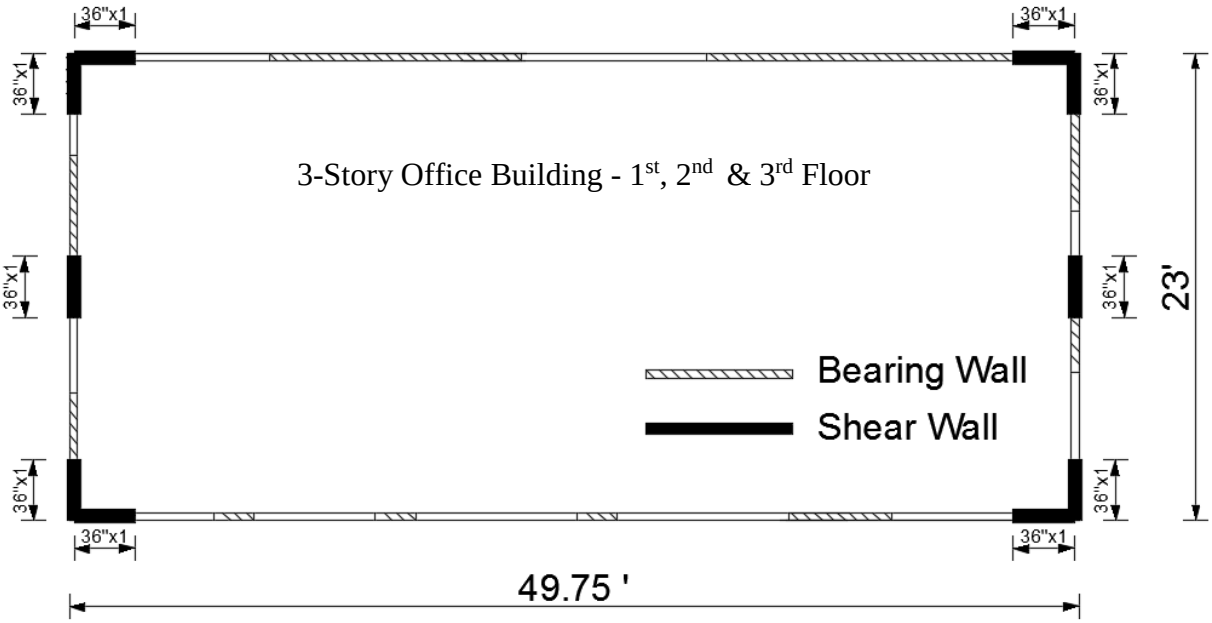

(c)

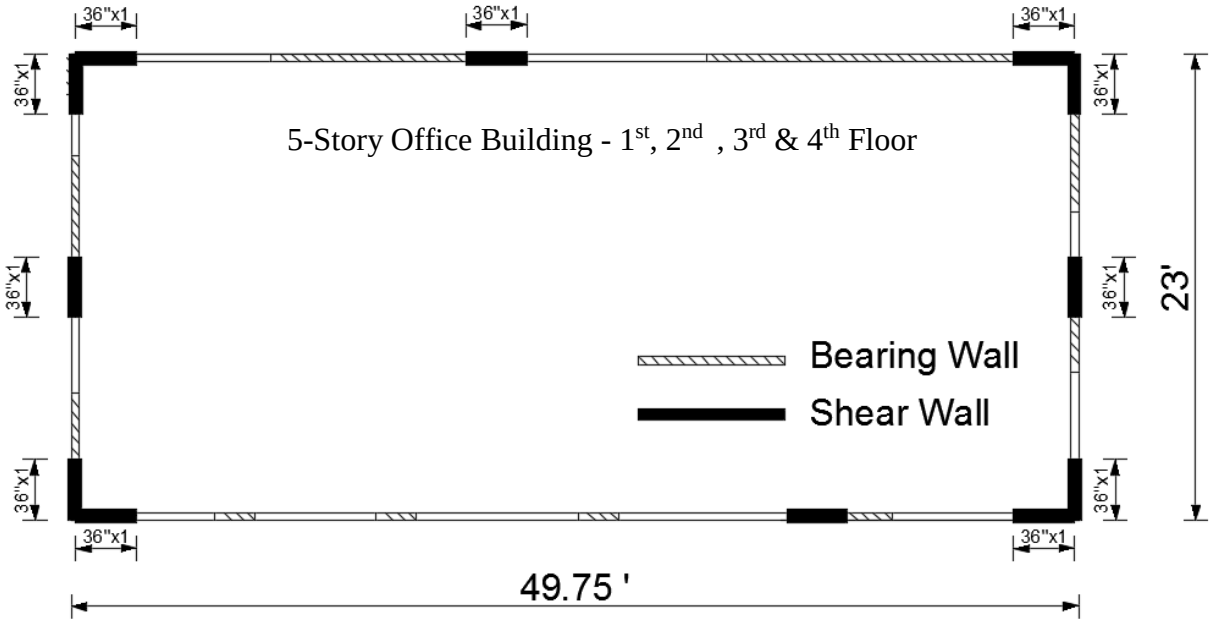

Figure B.1 - Three Types of Shear Wall Layouts for Office Building Model

B1. Shear Wall Design of the 2-Story Office Building Model

Table B.1 - Vertical Distribution of Seismic Forces in 2-Story Office Building Model

Floor Level	Effective Seismic Weight W_x (lbs)	Height h_x (ft)	$w_x h_x^k$	Vertical Distribution Factor C_{vx}	Seismic Force F_x (lb)
Roof	32451	18	584123	0.59	6524
2nd	45134	9	406206	0.41	4537

Table B.2 - Shear Wall Design 2-Story Office Building Model

Location	Distributed Force V (lb)	Shear Wall Width B (ft)	Design Shear Force V(lb/ft)	Nominal Strength Vn(lb/ft)	H (ft)	Adjustment Factor (2w/h)	Design Strength φVn(lb/ft)	V/(φVn)
2S	3262	3.5	932	3584	9	0.778	1673	0.557
2N	3262	3.5	932	3584	9	0.778	1673	0.557
2W	3262	3.5	932	3584	9	0.778	1673	0.557
2E	3262	3.5	932	3584	9	0.778	1673	0.557
1S	5530	3.5	1580	3584	9	0.778	1673	0.945
1N	5530	3.5	1580	3584	9	0.778	1673	0.945
1W	5530	3.5	1580	3584	9	0.778	1673	0.945
1E	5530	3.5	1580	3584	9	0.778	1673	0.945

Note: 1-2 floor shear wall layout for 2-story office building model illustrated in Figure 21-a

B2. Shear Wall Design of the 3-Story Office Building Model

Table B.3 - Vertical Distribution of Seismic Forces in 3-Story Office Building Model

Floor Level	Effective Seismic Weight W_x (lb)	Height h_x (ft)	$w_x h_x^k$	Vertical Distribution Factor C_{vx}	Seismic Force F_x (lb)
Roof	32451	27	897784	0.424	7470
3rd	45134	18	812412	0.384	6760
2nd	45134	9	406206	0.192	3380

Table B.4 - Shear Wall Design for 3-Story Office Building Model

Location	Distributed Force V (lb)	Shear Wall Width B (ft)	Design Shear Force V(lb/ft)	Nominal Strength Vn(lb/ft)	H (ft)	Adjustment Factor (2w/h)	Design Strength φVn(lb/ft)	V/(φVn)
3S	3735	3.5	1067	3584	9	0.778	1673	0.638
3N	3735	3.5	1067	3584	9	0.778	1673	0.638
3W	3735	3.5	1067	3584	9	0.778	1673	0.638
3E	3735	3.5	1067	3584	9	0.778	1673	0.638
2S	7115	3.5x2	1016	3584	9	0.778	1673	0.608
2N	7115	3.5x2	1016	3584	9	0.778	1673	0.608
2W	7115	3.5x2	1016	3584	9	0.778	1673	0.608
2E	7115	3.5x2	1016	3584	9	0.778	1673	0.608
1S	8805	3.5x2	1258	3584	9	0.778	1673	0.752
1N	8805	3.5x2	1258	3584	9	0.778	1673	0.752

1W	8805	3.5x2	1258	3584	9	0.778	1673	0.752
1E	8805	3.5x2	1258	3584	9	0.778	1673	0.752

Note: 1-3 floor shear wall layout for 3-story office building model illustrated in Figure 21-b

B3. Shear Wall Design of the 5-Story Office Building Model

Table B.5 - Vertical Distribution of Seismic Forces in 5-Story Office Building Model

Floor Level	Effective Seismic Weight W_x (lbs)	Height h_x (ft)	$w_x h_x^k$	Vertical Distribution Factor C_{vx}	Seismic Force F_x (lb)
Roof	33251	45	1496306	0.269	8205
5th	45134	36	1624824	0.292	8909
4th	45134	27	1218618	0.219	6682
3rd	45134	18	812412	0.146	4455
2nd	45134	9	406206	0.073	2227

Table B.6 - Shear Wall Design for 5-Story Office Building Model

Location	Distributed Force V (lb)	Shear Wall Width B (ft)	Design Shear Force V(lb/ft)	Nominal Strength Vn(lb/ft)	H (ft)	Adjustment Factor (2w/h)	Design Strength φVn(lb/ft)	V/(φVn)
5S	4102	3.5	1172	3584	9	0.778	1673	0.701
5N	4102	3.5	1172	3584	9	0.778	1673	0.701
5W	4102	3.5	1172	3584	9	0.778	1673	0.701
5E	4102	3.5	1172	3584	9	0.778	1673	0.701

4S	8557	7	1222	3584	9	0.778	1673	0.731
4N	8557	7	1222	3584	9	0.778	1673	0.731
4W	8557	7	1222	3584	9	0.778	1673	0.731
4E	8557	7	1222	3584	9	0.778	1673	0.731
3S	11898	10.5	1133	3584	9	0.778	1673	0.678
3N	11898	10.5	1133	3584	9	0.778	1673	0.678
3W	11898	10.5	1133	3584	9	0.778	1673	0.678
3E	11898	10.5	1133	3584	9	0.778	1673	0.678
2S	14126	10.5	1345	3584	9	0.778	1673	0.804
2N	14126	10.5	1345	3584	9	0.778	1673	0.804
2W	14126	10.5	1345	3584	9	0.778	1673	0.804
2E	14126	10.5	1345	3584	9	0.778	1673	0.804
1S	15239	10.5	1451	3584	9	0.778	1673	0.868
1N	15239	10.5	1451	3584	9	0.778	1673	0.868
1W	15239	10.5	1451	3584	9	0.778	1673	0.868
1E	15239	10.5	1451	3584	9	0.778	1673	0.868

Note: 1-4 floor shear wall layout for 5-story office building model illustrated in Figure 21-c
5^{th} floor shear wall layout for 5-story office building model illustrated in Figure 21-a

APPENDIX C

DESIGN OF SHEAR WALL FOR HOTEL BUILDING MODELS

Seismic Analysis (LFRS) per ASCE 7-10

Occupancy Category II

Ie = 1.0

Ss = 1.50 Fa = 1.0 (Table 11.4-1)

S1 = 0.60 Fv = 1.5 (Table 11.4-2)

Site Class D

$S_{MS} = F_a S_s =$ 1.5 (Eq. 11.4-1)

$S_{M1} = FvS_1 =$ 0.75 (Eq. 11.4-2)

$S_{DS} = 2/3 \times S_{MS} =$ 1.00 (Eq. 11.4-3)

$S_{D1} = 2/3 \times S_{M1} =$ 0.60 (Eq. 11.4-4)

Cs = 0.154 (Eq. 12.8-2)

Unit Weights

Roof 20 (psf)

Floor 18 (psf)

Walls 10 (psf)

Rooftop MEP 3400 (lb)

Parapet 2933 (lb)

Building Dimensions

Width (E-W) 66.60 (ft)

Length (N-S) 49.80 (ft)

Story Height 9.84 (ft)

Roof Wx based on Roof DL, Rooftop MEP, Parapet and 1/2 of Upper Walls

2nd Level wx based on 2nd Floor DL, Less Clerestory, + 0.5 x (Upper Walls + Lower Walls)

Figure C.1 illustrate three types of Shear Wall Layouts for Office Building Model

(a)

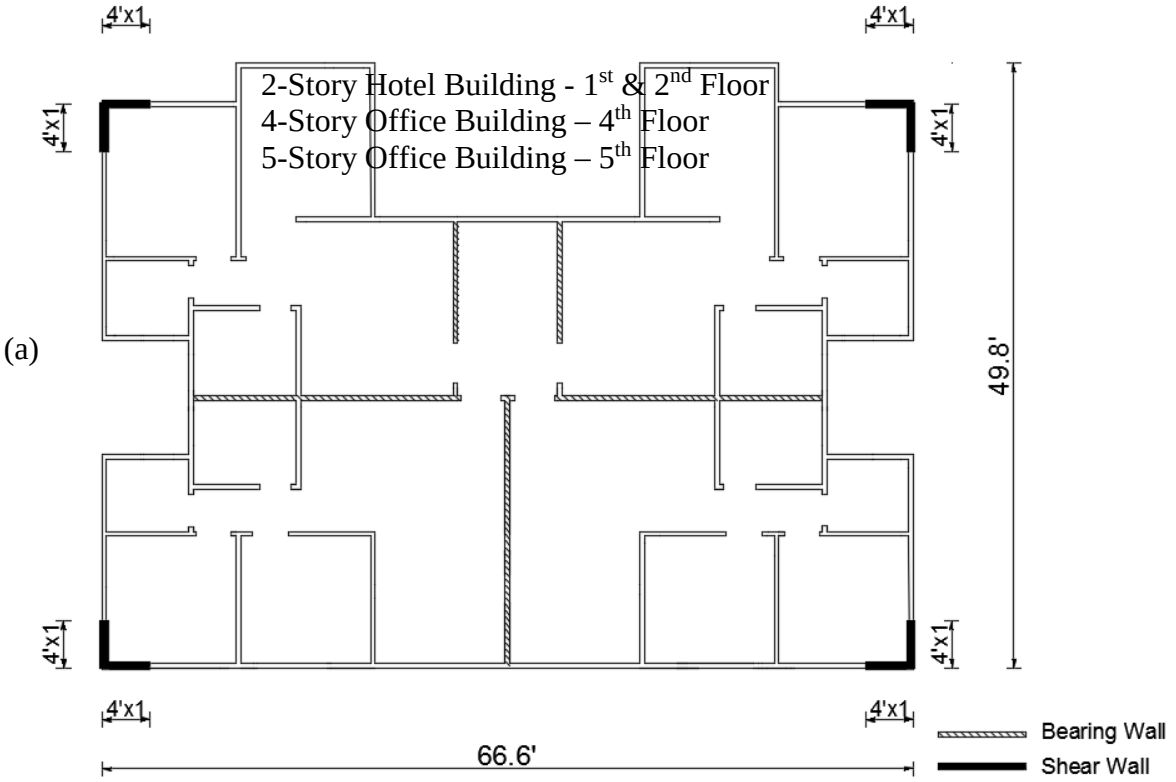

(b)

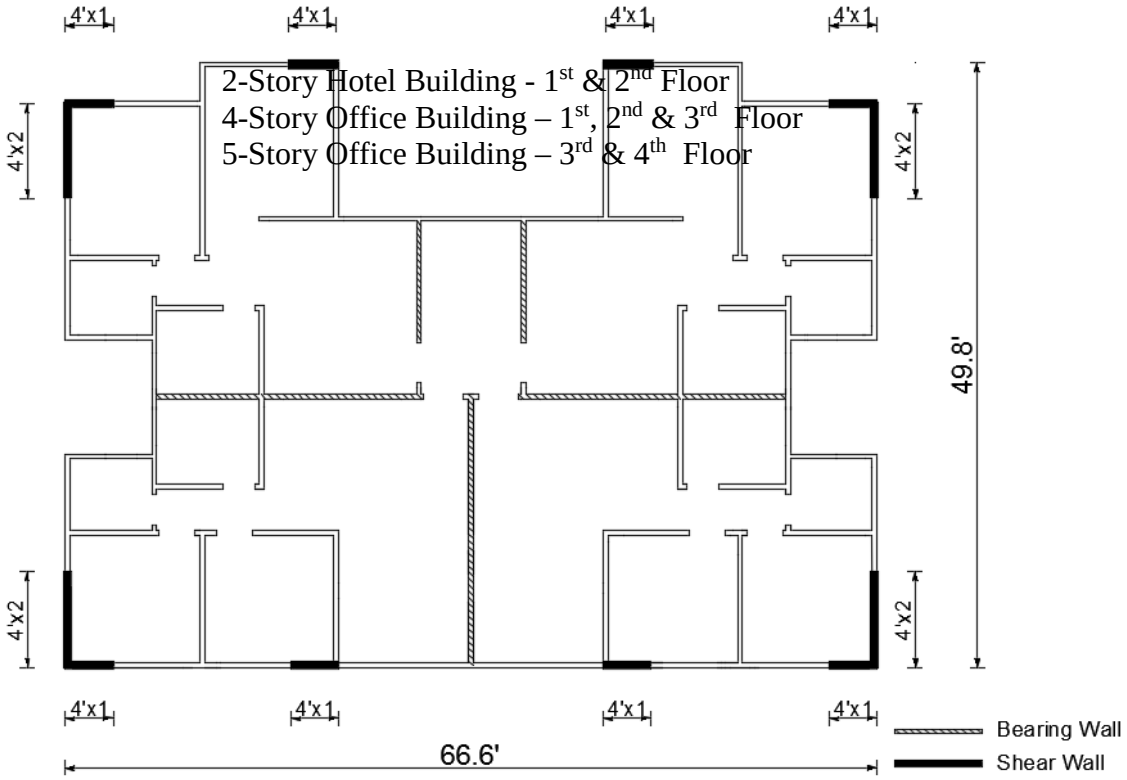

(c)

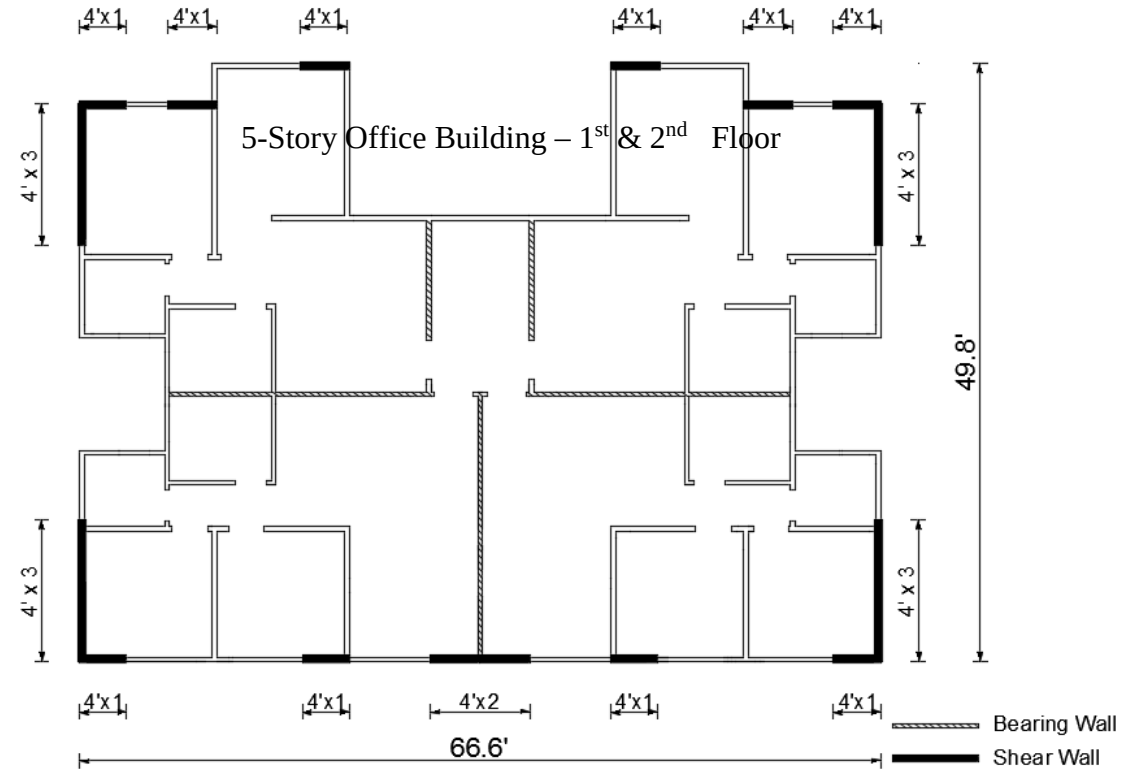

Figure C.1 - Three Types of Shear Wall Layouts for Office Building Model

C1. Shear Wall Design of the 2-Story Hotel Building Model

Table C.1 - Vertical Distribution of Seismic Forces in 2-Story Hotel Building Model

Floor Level	Effective Seismic Weight W_x (lbs)	Height h_x (ft)	$w_x h_x^k$	Vertical Distribution Factor C_{vx}	Seismic Force F_x (lb)
Roof	85343	19.68	1679547	0.671	17453
2nd	83806	9.84	824649	0.329	8570

Table C.2 - Shear Wall Design for 2-Story Office Building Model

Location	Distributed Force V (lb)	Shear Wall Width B (ft)	Design Shear Force V(lb/ft)	Nominal Strength Vn(lb/ft)	H (ft)	Adjustment Factor (2w/h)	Design Strength φVn(lb/ft)	V/(φVn)
2S	8727	8	1091	3584	9.84	0.813	1748	0.624
2N	8727	8	1091	3584	9.84	0.813	1748	0.624
2W	8727	8	1091	3584	9.84	0.813	1748	0.624
2E	8727	8	1091	3584	9.84	0.813	1748	0.624
1S	13011	8	1626	3584	9.84	0.813	1748	0.93
1N	13011	8	1626	3584	9.84	0.813	1748	0.93
1W	13011	8	1626	3584	9.84	0.813	1748	0.93
1E	13011	8	1626	3584	9.84	0.813	1748	0.93

Note: 1-2 floor shear wall layout for 2-story hotel building model illustrated in Figure 22-a

C2. Shear Wall Design of the 4-Story Office Building Model

Table C.3 - Vertical Distribution of Seismic Forces in 4-Story Hotel Building Model

Floor Level	Effective Seismic Weight W_x (lb)	Height h_x (ft)	$w_x h_x^k$	Vertical Distribution Factor C_{vx}	Seismic Force F_x (lb)
Roof	85343	39.36	3008623	0.4	22143
4th	83806	29.52	2235037	0.297	16450
3rd	83806	19.68	1508261	0.201	11101
2nd	83806	9.84	769977	0.102	5667

Table C.4 - Shear Wall Design for 4-Story Hotel Building Model

Location	Distributed Force V (lb)	Shear Wall Width B (ft)	Design Shear Force V(lb/ft)	Nominal Strength Vn(lb/ft)	H (ft)	Adjustment Factor (2w/h)	Design Strength φVn(lb/ft)	V/(φVn)
4S	11072	8	1384	3584	9.84	0.813	1748	0.792
4N	11072	8	1384	3584	9.84	0.813	1748	0.792
4W	11072	8	1384	3584	9.84	0.813	1748	0.792
4E	11072	8	1384	3584	9.84	0.813	1748	0.792
3S	19297	16	1206	3584	9.84	0.813	1748	0.69
3N	19297	16	1206	3584	9.84	0.813	1748	0.69
3W	19297	16	1206	3584	9.84	0.813	1748	0.69
3E	19297	16	1206	3584	9.84	0.813	1748	0.69
2S	24847	16	1553	3584	9.84	0.813	1748	0.888

2N	24847	16	1553	3584	9.84	0.813	1748	0.888
2W	24847	16	1553	3584	9.84	0.813	1748	0.888
2E	24847	16	1553	3584	9.84	0.813	1748	0.888
1S	27680	16	1730	3584	9.84	0.813	1748	0.99
1N	27680	16	1730	3584	9.84	0.813	1748	0.99
1W	27680	16	1730	3584	9.84	0.813	1748	0.99
1E	27680	16	1730	3584	9.84	0.813	1748	0.99

Note: 1-3 floor shear wall layout for 4-story hotel building model illustrated in Figure 22-b
4^{th} floor shear wall layout for 4-story hotel building model illustrated in Figure 22-a

C3. Shear Wall Design of the 5-Story Office Building Model

Table C.5 - Vertical Distribution of Seismic Forces in 5-Story Hotel Building Model

Floor Level	Effective Seismic Weight W_x (lbs)	Height h_x (ft)	$w_x h_x^k$	Vertical Distribution Factor C_{vx}	Seismic Force F_x (lb)
Roof	85343	49.2	4366987	0.339	21915
5^{th}	83806	39.36	3422967	0.265	17178
4^{th}	83806	29.52	2559793	0.199	12846
3^{rd}	83806	19.68	1699571	0.132	8529
2^{nd}	83806	9.84	843870	0.065	4235

Table C.6 - Shear Wall Design for 5-Story Hotel Building Model

Location	Distributed Force V (lb)	Shear Wall Width B (ft)	Design Shear Force V(lb/ft)	Nominal Strength Vn(lb/ft)	H (ft)	Adjustment Factor (2w/h)	Design Strength φVn(lb/ft)	V/(φVn)
5S	10958	8	1370	3584	9.84	0.813	1748	0.783
5N	10958	8	1370	3584	9.84	0.813	1748	0.783
5W	10958	8	1370	3584	9.84	0.813	1748	0.783
5E	10958	8	1370	3584	9.84	0.813	1748	0.783
4S	19546	16	1222	3584	9.84	0.813	1748	0.699
4N	19546	16	1222	3584	9.84	0.813	1748	0.699
4W	19546	16	1222	3584	9.84	0.813	1748	0.699
4E	19546	16	1222	3584	9.84	0.813	1748	0.699
3S	25969	16	1623	3584	9.84	0.813	1748	0.928
3N	25969	16	1623	3584	9.84	0.813	1748	0.928
3W	25969	16	1623	3584	9.84	0.813	1748	0.928
3E	25969	16	1623	3584	9.84	0.813	1748	0.928
2S	30234	24	1260	3584	9.84	0.813	1748	0.721
2N	30234	24	1260	3584	9.84	0.813	1748	0.721
2W	30234	24	1260	3584	9.84	0.813	1748	0.721
2E	30234	24	1260	3584	9.84	0.813	1748	0.721
1S	32351	24	1348	3584	9.84	0.813	1748	0.771
1N	32351	24	1348	3584	9.84	0.813	1748	0.771

1W	32351	24	1348	3584	9.84	0.813	1748	0.771
1E	32351	24	1348	3584	9.84	0.813	1748	0.771

Note: 1-2 floor shear wall layout for 5-story hotel building model illustrated in Figure 22-c
3-4 floor shear wall layout for 5-story hotel building model illustrated in Figure 22-b
5^{th} floor shear wall layout for 5-story hotel building model illustrated in Figure 22-a

APPENDIX D

DETAILS OF NONLINEAR ANALYSIS OF OFFICE ARCHETYPES

D1. 2-Story Office Building Nonlinear Analysis in the Long Direction

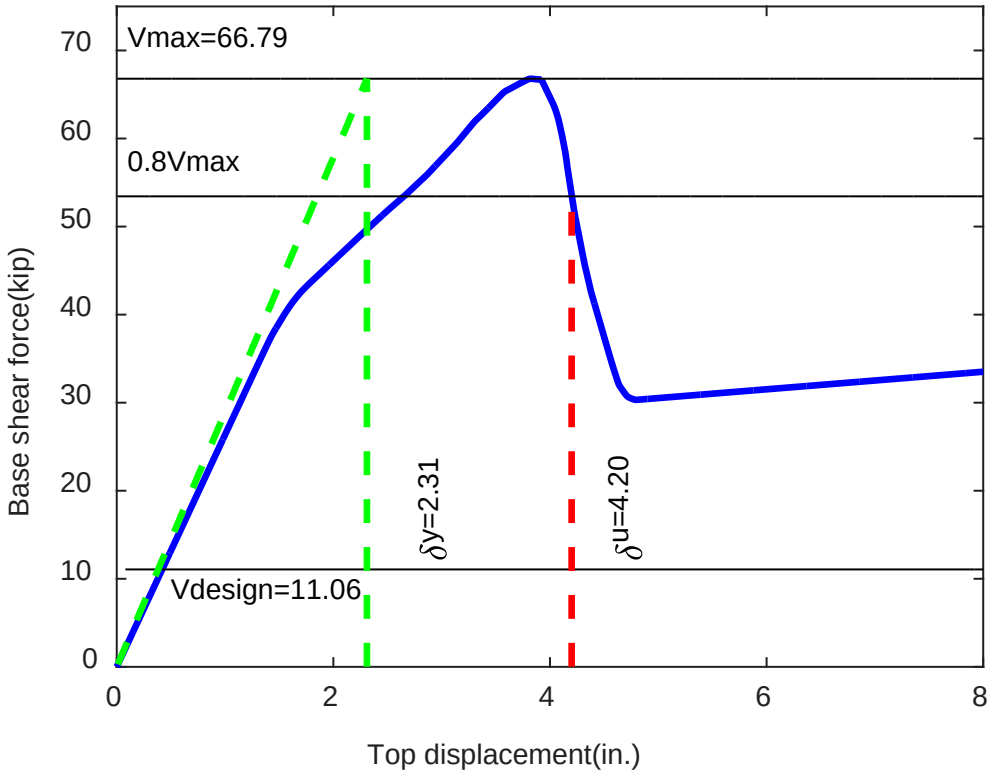

Figure D.1 - Pushover Curve of 2-Story Office Building Model in the Long Direction

Table D.1 - Pushover Results of 2-Story Office Building Model in the Long Direction

$T\ (s)$	$T1\ (s)$	$\delta_u(in.)$	$\delta_{y.eff}(in.)$	V_{max}(kips)	V_{design}(kips)	δ_T	Ω
0.244	0.470	4.2	2.31	66.79	11.06	1.82	6.04

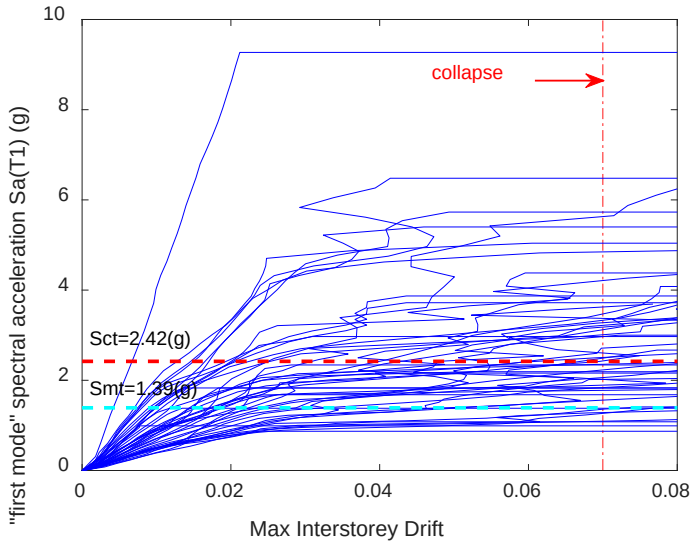

(a) IDA curve

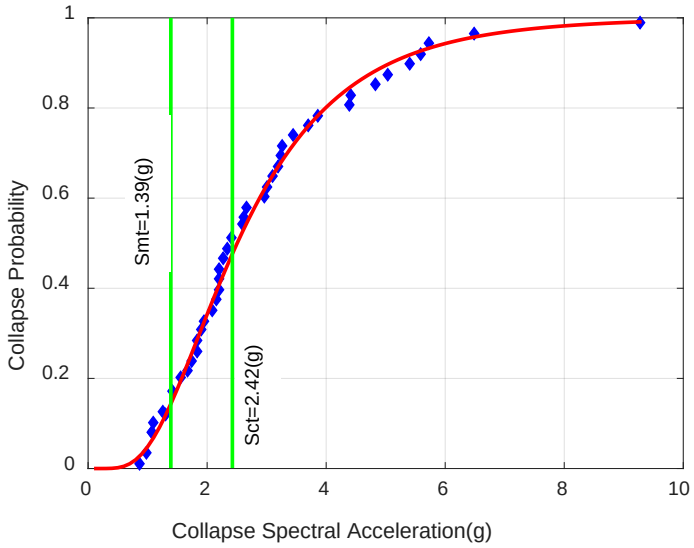

(b) Fragility curve

Figure D.2 - IDA Results of 2-Story Office Building Model in the Long Direction

Table D.2 - IDA Results of 2-Story Office Building Model in the Long Direction

S_{CT}	S_{MT}	CMR	SSF	ACMR	β_{TOT}	Accept ACMR(20%)
2.42	1.39	1.741	1.119	1.948	0.447	1.458

D2. 2-Story Office Building Nonlinear Analysis in the Short Direction

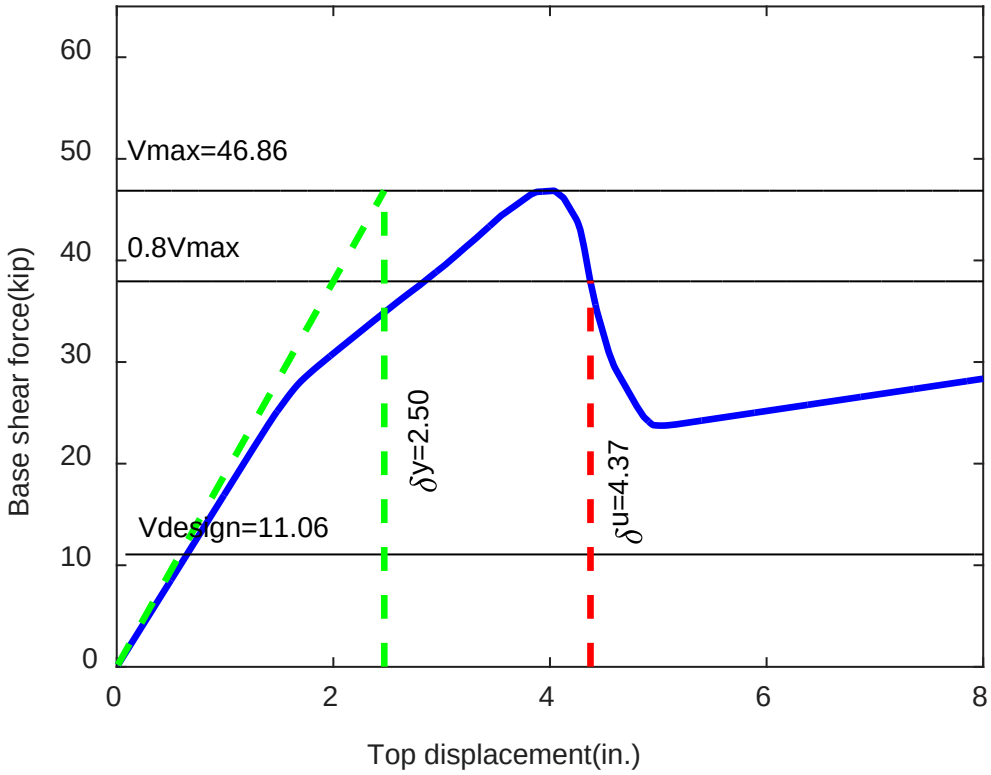

Figure D.3 - Pushover Curve of 2-Story Office Building Model in the Short Direction

Table D.3 - Pushover Results of 2-Story Office Building Model in the Short Direction

$T\ (s)$	$T1\ (s)$	$\delta_u(in.)$	$\delta_{y.eff}(in.)$	V_{max}(kips)	V_{design}(kips)	δ_T	Ω
0.244	0.580	2.47	46.86	11.06	1.77	4.24	2.47

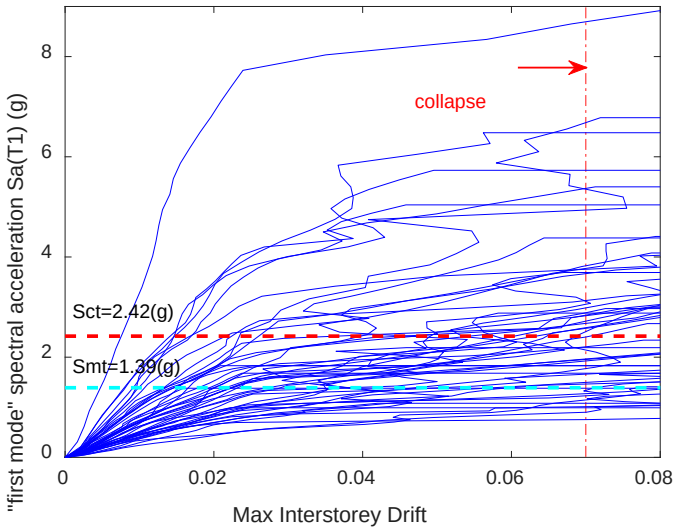

(b) IDA curve

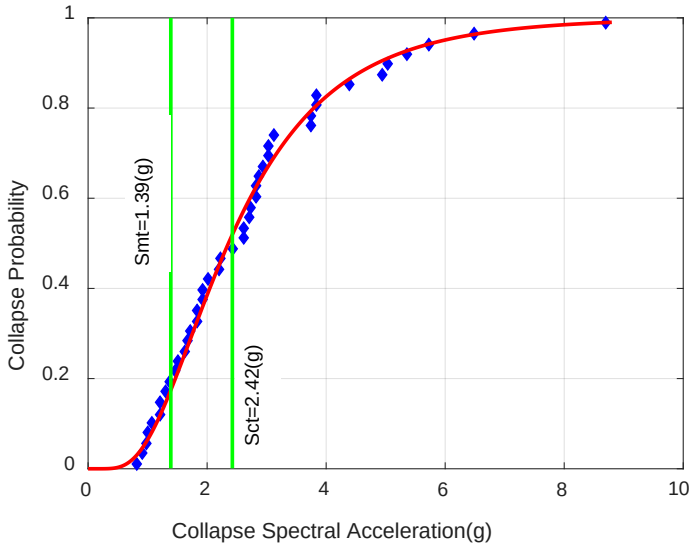

(b) Fragility curve

Figure D.4 - IDA Results of 2-Story Office Building Model in the Short Direction

Table D.4 - IDA Results of 2-Story Office Building Model in the Short Direction

S_{CT}	S_{MT}	CMR	SSF	ACMR	β_{TOT}	Accept ACMR(20%)
2.42	1.39	1.741	1.116	1.943	0.444	1.441

D3. 3-Story Office Building Nonlinear Analysis in the Long Direction

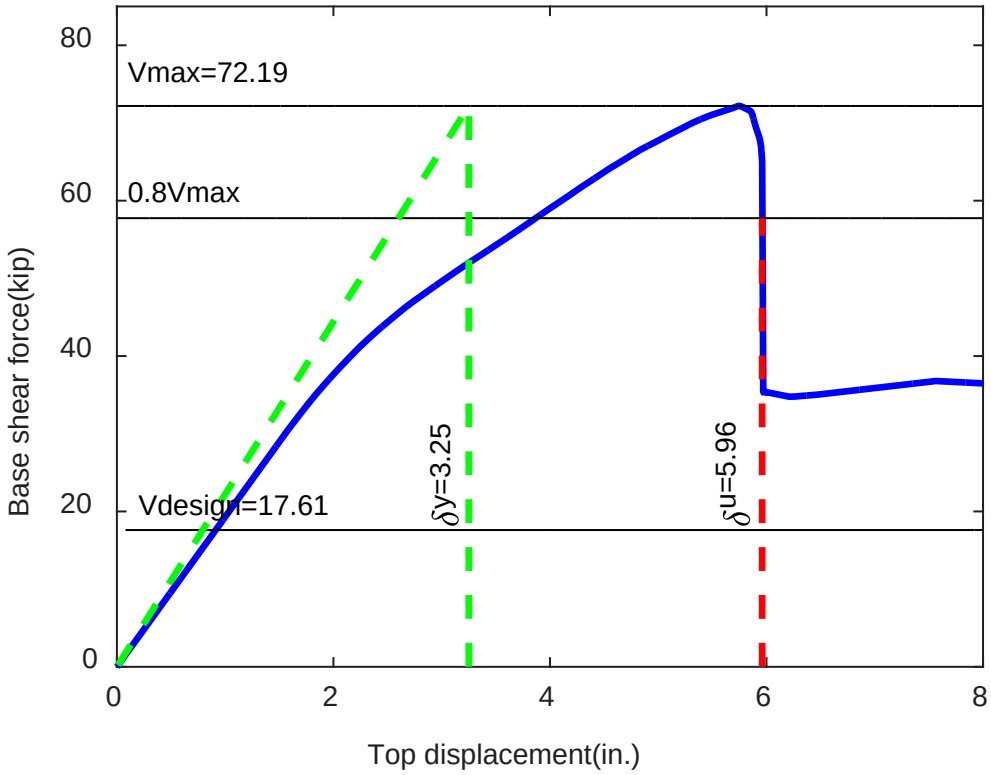

Figure D.5 - Pushover Curve of 3-Story Office Building Model in the Long Direction

Table D.5 - Pushover Results of 3-Story Office Building Model in the Long Direction

$T\ (s)$	$T1\ (s)$	$\delta_u(in.)$	$\delta_{y.eff}(in.)$	V_{max}(kips)	V_{design}(kips)	δ_T	Ω
0.332	0.650	5.96	3.25	72.19	17.61	1.83	4.10

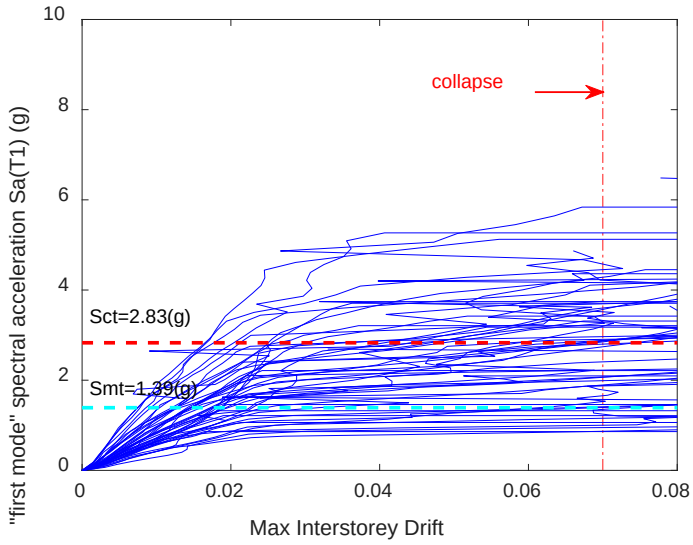

(a) IDA curve

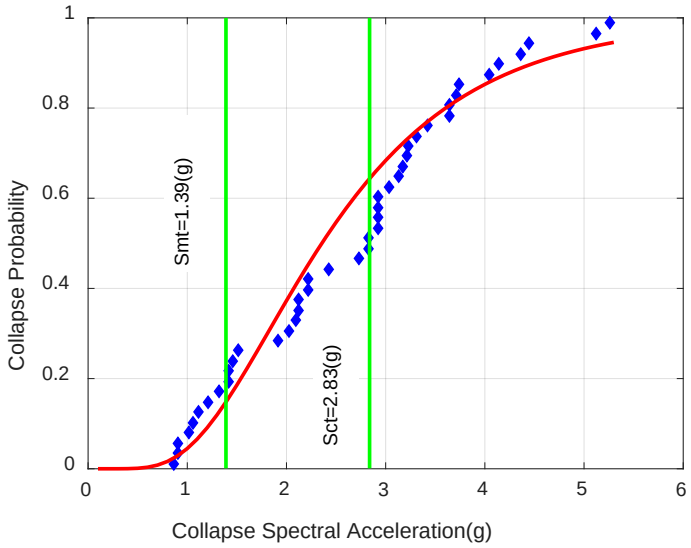

(b) Fragility curve

Figure D.6 - IDA Results of 3-Story Office Building Model in the Long Direction

Table D.6 - IDA Results of 3-Story Office Building Model in the Long Direction

S_{CT}	S_{MT}	CMR	SSF	ACMR	β_{TOT}	Accept ACMR(20%)
2.83	1.39	2.036	1.12	2.279	0.448	1.458

D4. 3-Story Office Building Nonlinear Analysis in the Short Direction

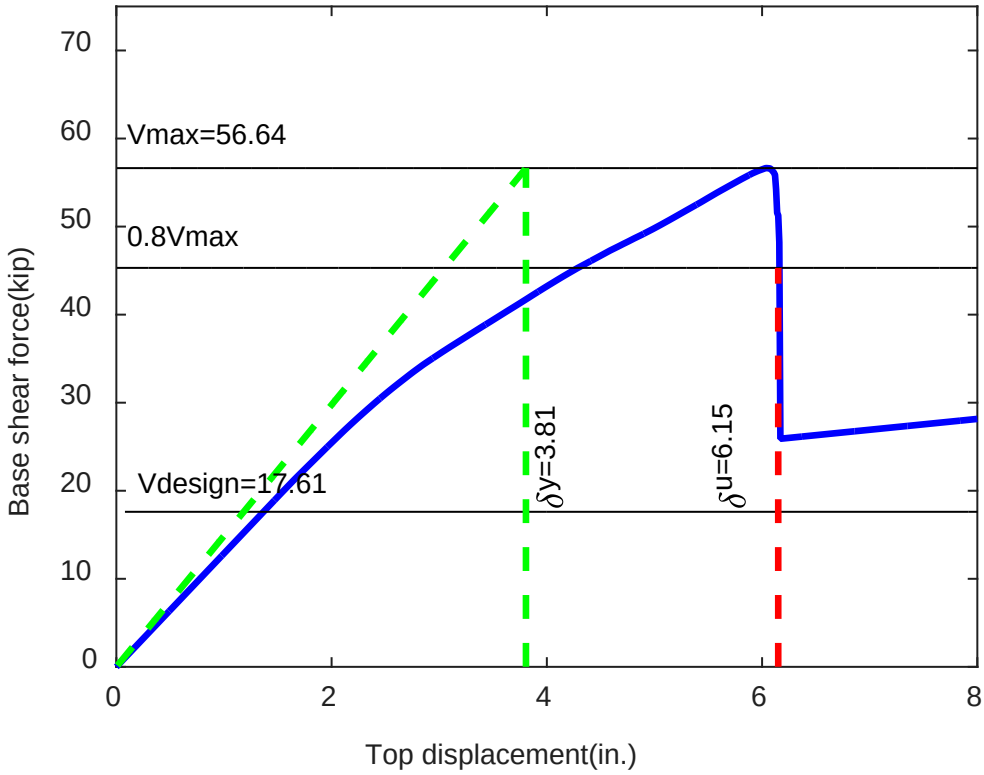

Figure D.7 - Pushover Curve of 3-Story Office Building Model in the Short Direction

Table D.7 - Pushover Results of 3-Story Office Building Model in the Short Direction

$T\ (s)$	$T1\ (s)$	$\delta_u(in.)$	$\delta_{y.eff}(in.)$	V_{max}(kips)	V_{design}(kips)	δ_T	Ω
0.332	0.794	6.15	3.81	56.64	17.61	1.62	3.22

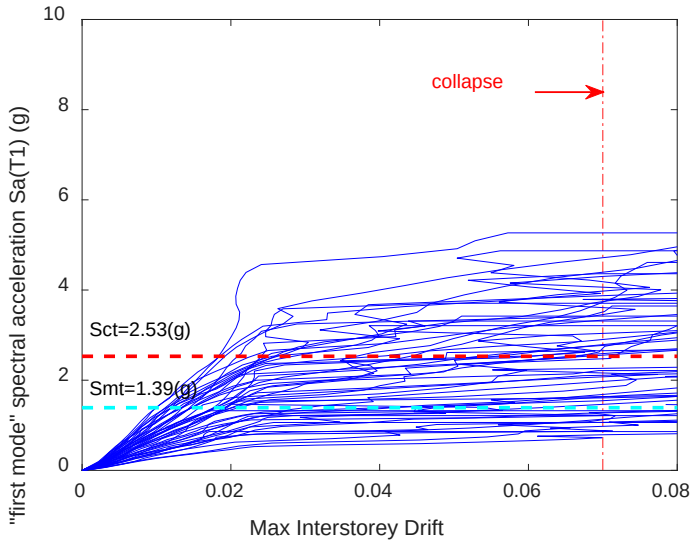

(b) IDA curve

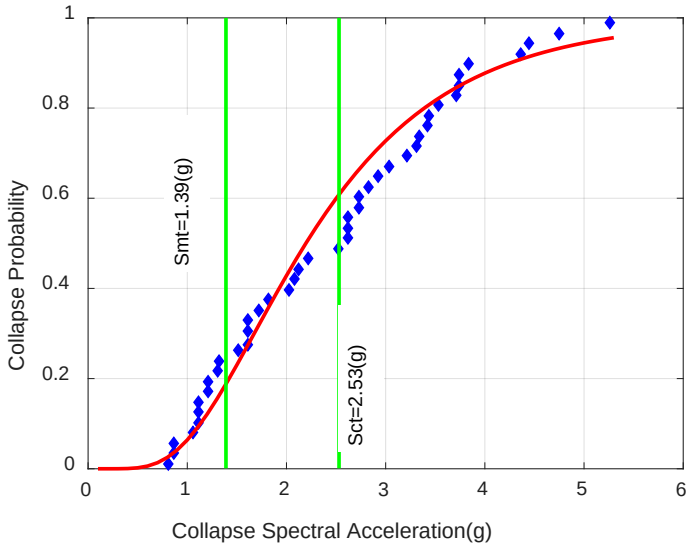

(b) Fragility curve

Figure D.8 - IDA Results of 3-Story Office Building Model in the Short Direction

Table D.8 - IDA Results of 3-Story Office Building Model in the Short Direction

S_{CT}	S_{MT}	CMR	SSF	ACMR	β_{TOT}	Accept ACMR(20%)
2.53	1.39	1.82	1.107	2.015	0.434	1.441

D5. 5-Story Office Building Nonlinear Analysis in the Long Direction

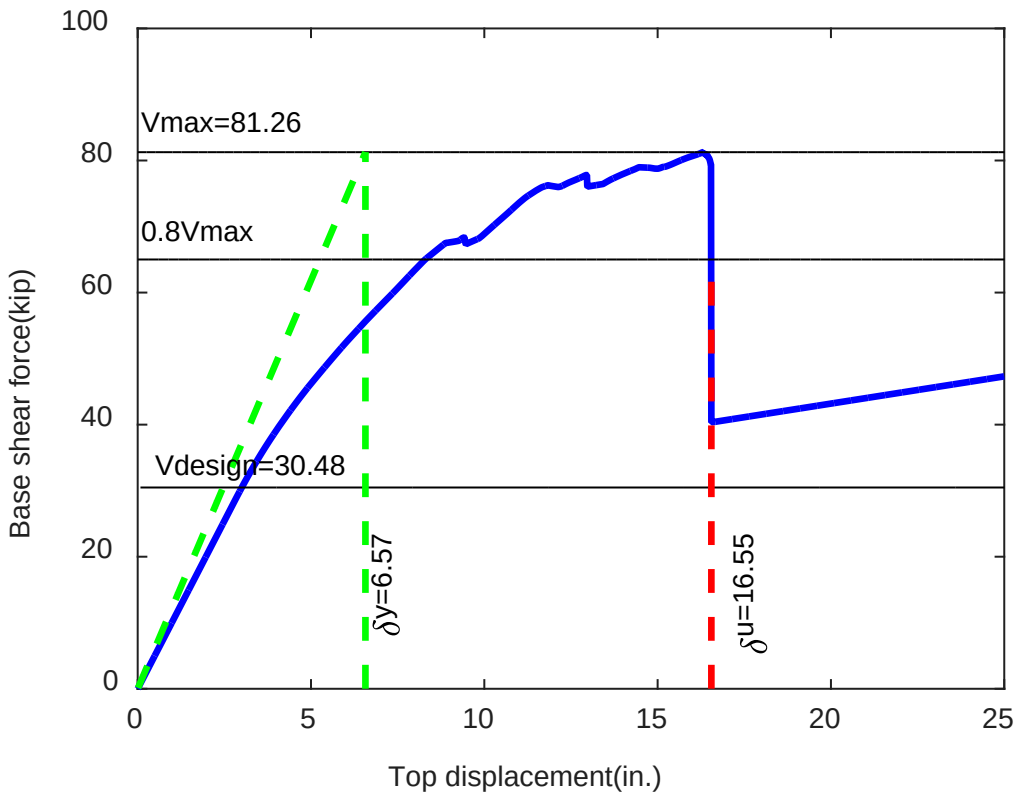

Figure D.9 - Pushover Curve of 5-Story Office Building Model in the Long Direction

Table D.9 - Pushover Results of 5-Story Office Building Model in the Long Direction

$T\ (s)$	$T1\ (s)$	$\delta_u(in.)$	$\delta_{y.eff}(in.)$	V_{max}(kips)	V_{design}(kips)	δ_T	Ω
0.486	1.117	16.55	6.57	81.26	30.48	2.52	2.67

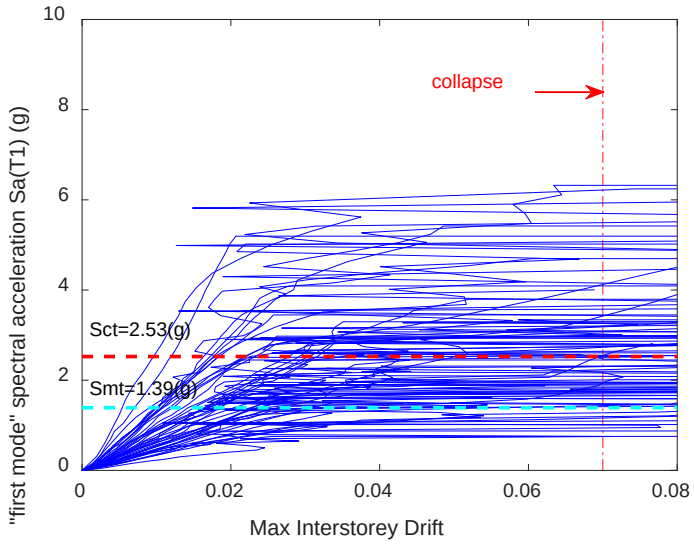

(c) IDA curve

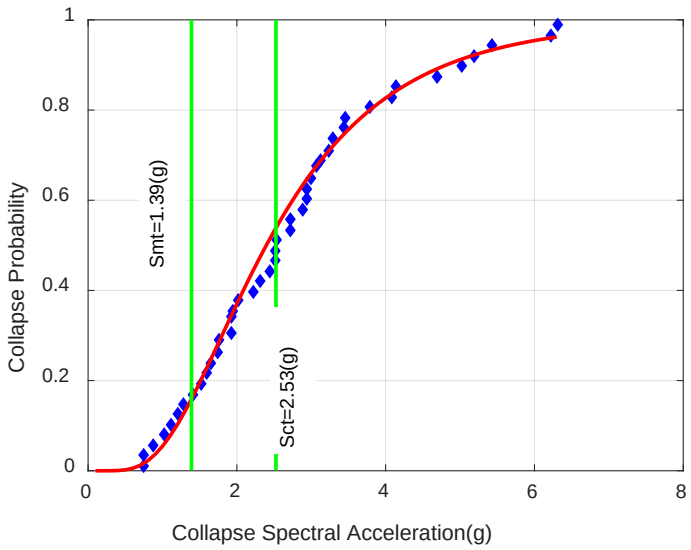

(b) Fragility curve

Figure D.10 - IDA Results of 5-Story Office Building Model in the Long Direction

Table D.10 - IDA Results of 5-Story Office Building Model in the Long Direction

S_{CT}	S_{MT}	CMR	SSF	ACMR	β_{TOT}	Accept ACMR(20%)
2.53	1.39	1.82	1.156	2.104	0.494	1.513

D6. 5-Story Office Building Nonlinear Analysis in the Short Direction

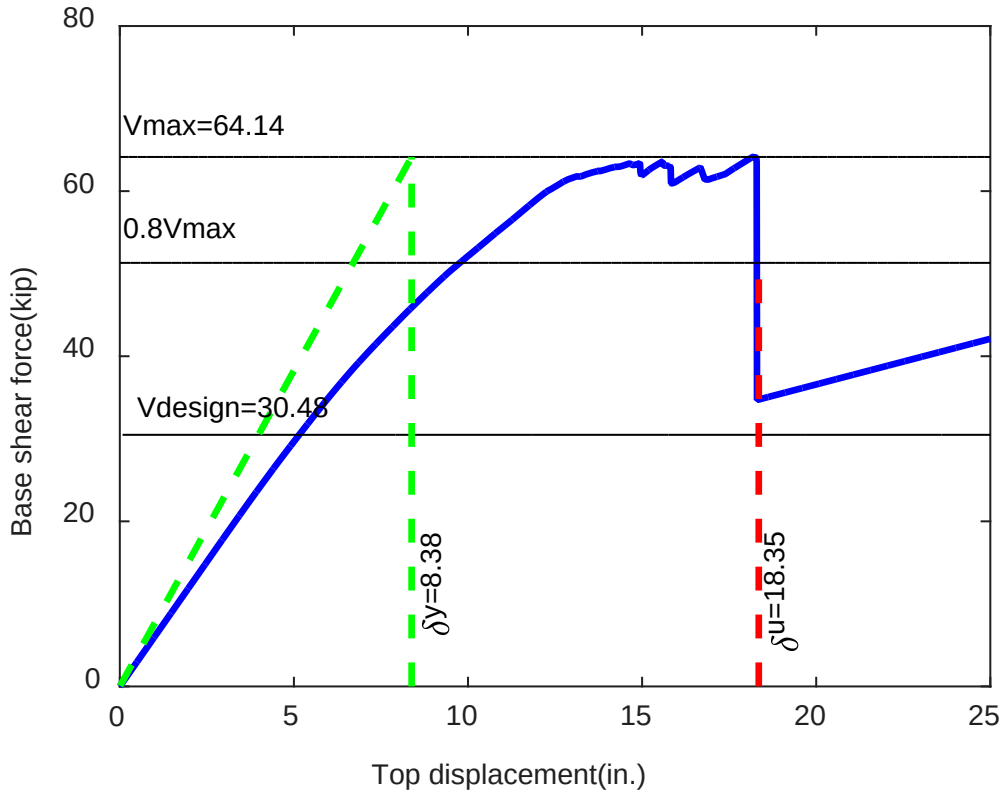

Figure D.11 - Pushover Curve of 5-Story Office Building Model in the Short Direction

Table D.11 - Pushover Results of 5-Story Office Building Model in the Short Direction

$T\ (s)$	$T1\ (s)$	$\delta_u(in.)$	$\delta_{y.eff}(in.)$	V_{max}(kips)	V_{design}(kips)	δ_T	Ω
0.486	1.42	18.35	8.38	64.14	30.48	2.19	2.10

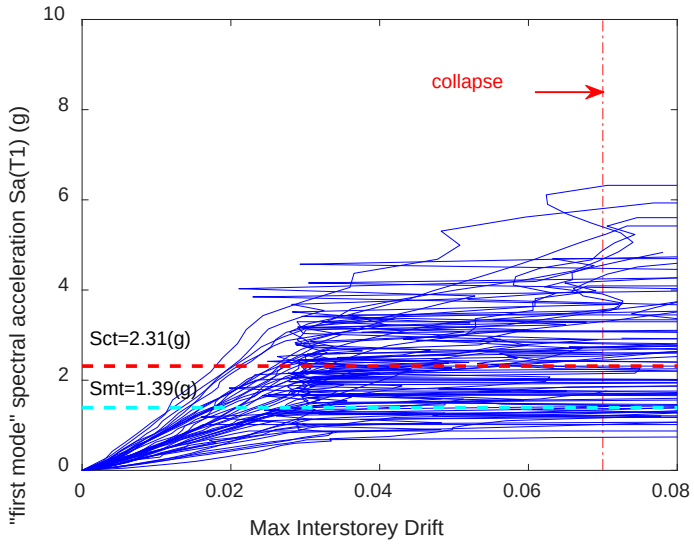

(d) IDA curve

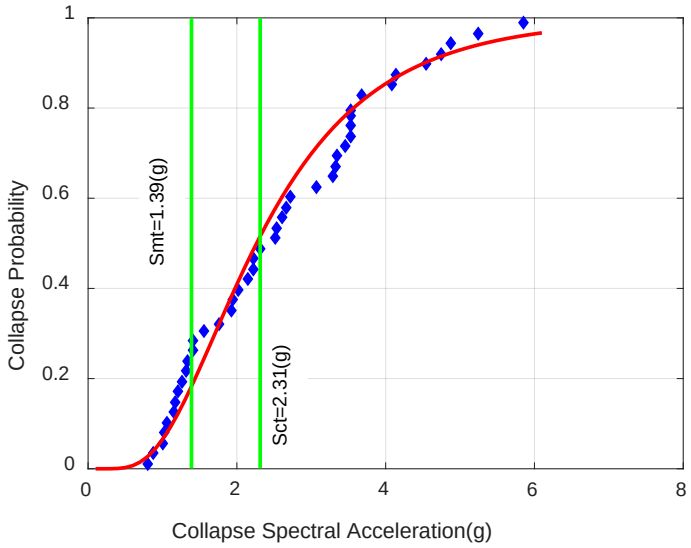

(b) Fragility curve

Figure D.12 - IDA Results of 5-Story Office Building Model in the Short Direction

Table D.12 - IDA Results of 5-Story Office Building Model in the Short Direction

S_{CT}	S_{MT}	CMR	SSF	ACMR	β_{TOT}	Accept ACMR(20%)
2.31	1.39	1.662	1.141	1.896	0.471	1.485

APPENDIX E

DETAILS OF NONLINEAR ANALYSIS OF HOTEL ARCHETYPES

E1. 2-Story Hotel Building Nonlinear Analysis in the Long Direction

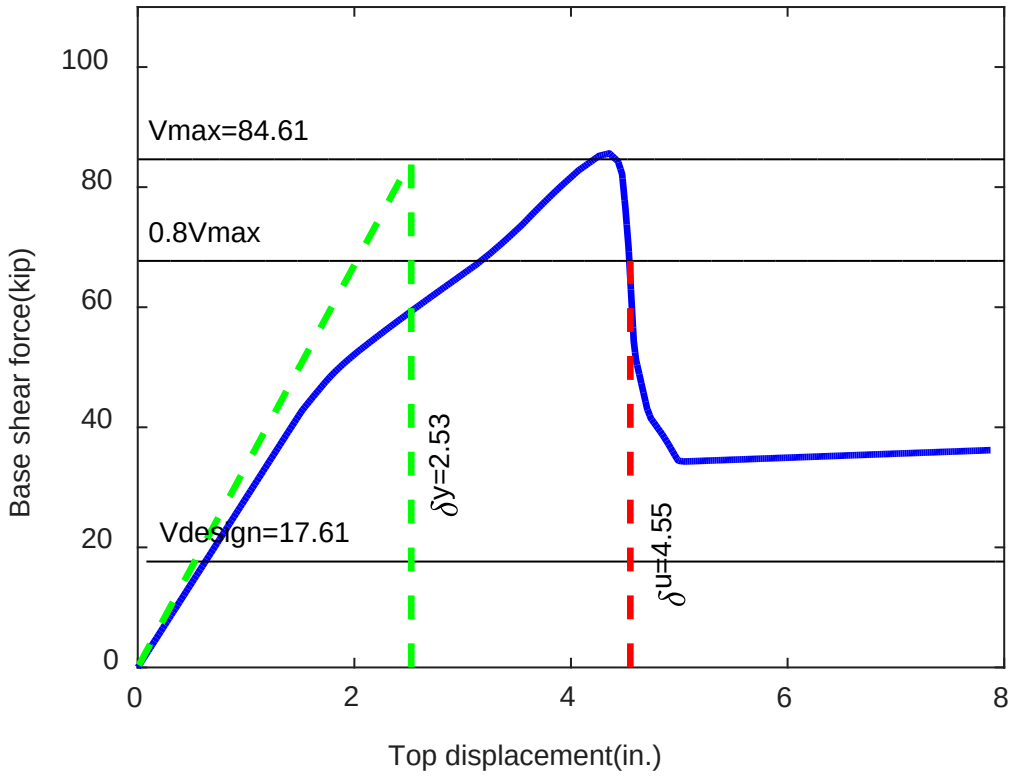

Figure E.1 - Pushover Curve of 2-Hotel Office Building Model in the Long Direction

Table E.1 - Pushover Results of 2-Hotel Office Building Model in the Long Direction

$T\ (s)$	$T1\ (s)$	$\delta_u(in.)$	$\delta_{y.eff}(in.)$	V_{max}(kips)	V_{design}(kips)	δ_T	Ω
0.262	0.656	4.548	2.525	84.61	17.61	1.80	4.80

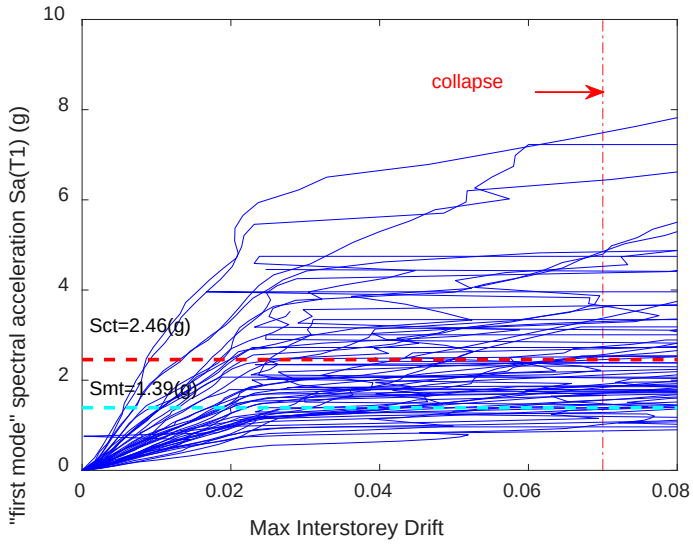

(a) IDA curve

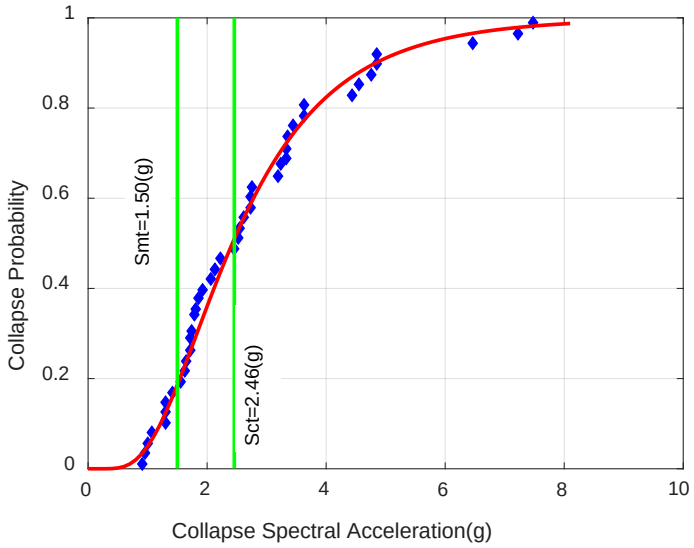

(b) Fragility curve

Figure E.2 - IDA Results of 2-Hotel Office Building Model in the Long Direction

Table E.2 - IDA Results of 2-Hotel Office Building Model in the Long Direction

S_{CT}	S_{MT}	CMR	SSF	ACMR	β_{TOT}	Accept ACMR(20%)
2.46	1.5	1.64	1.118	1.834	0.445	1.454

E2. 2-Story Hotel Building Nonlinear Analysis in the Short Direction

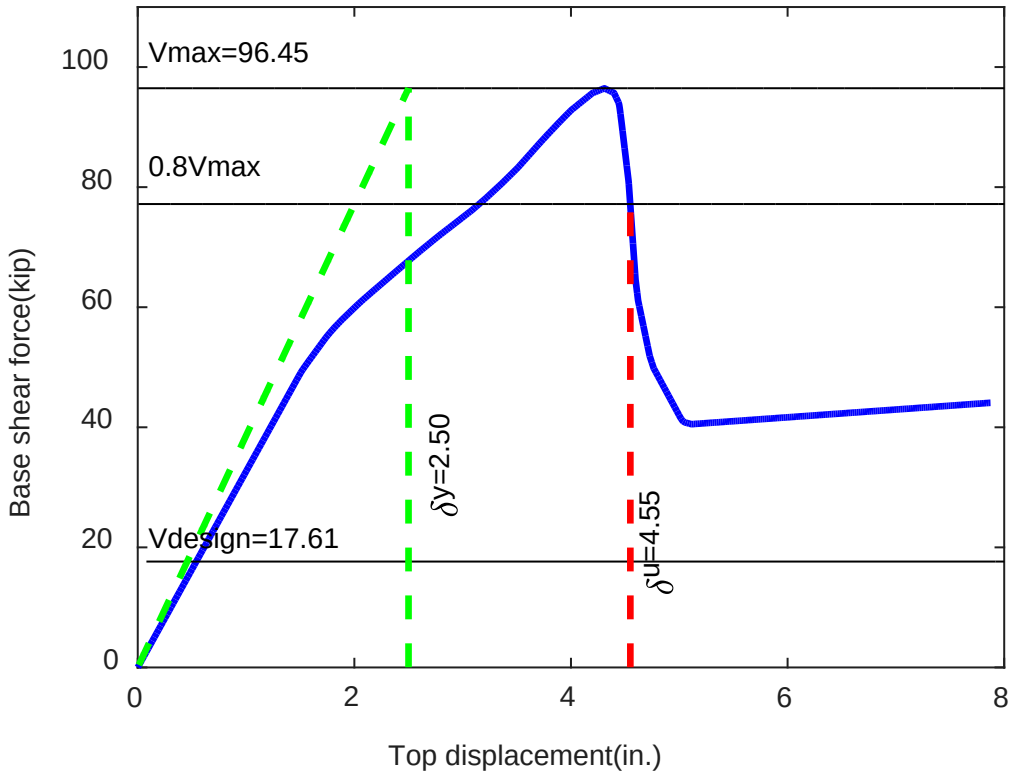

Figure E.3 - Pushover Curve of 2-Hotel Office Building Model in the Short Direction

Table E.3 - Pushover Results of 2-Hotel Office Building Model in the Short Direction

$T\ (s)$	$T1\ (s)$	$\delta_u(in.)$	$\delta_{y.eff}(in.)$	V_{max}(kips)	V_{design}(kips)	δ_T	Ω
0.262	0.611	4.548	2.50	96.45	17.61	1.82	5.48

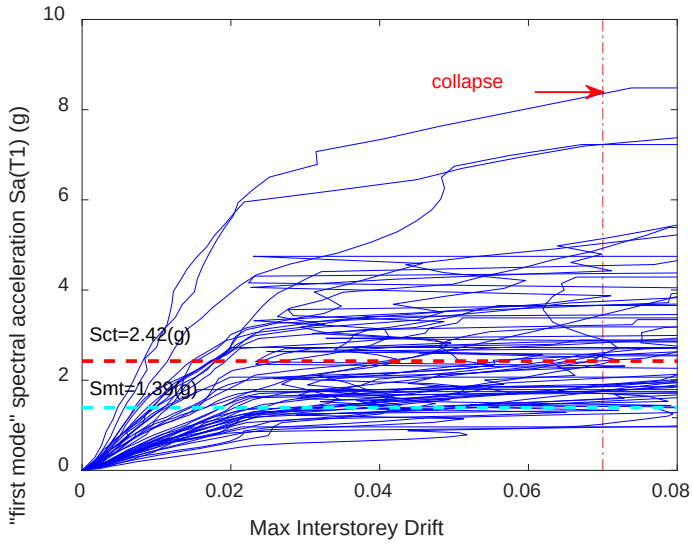

(a) IDA curve

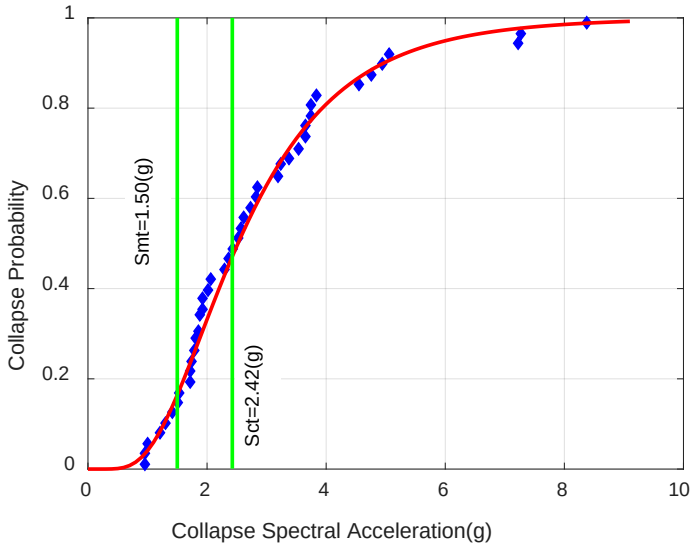

(b) Fragility curve

Figure E.4 - IDA Results of 2-Hotel Office Building Model in the Short Direction

Table E.4 - IDA Results of 2-Hotel Office Building Model in the Short Direction

S_{CT}	S_{MT}	CMR	SSF	ACMR	β_{TOT}	Accept ACMR(20%)
2.42	1.5	1.613	1.119	1.805	0.447	1.456

E3. 4-Story Hotel Building Nonlinear Analysis in the Long Direction

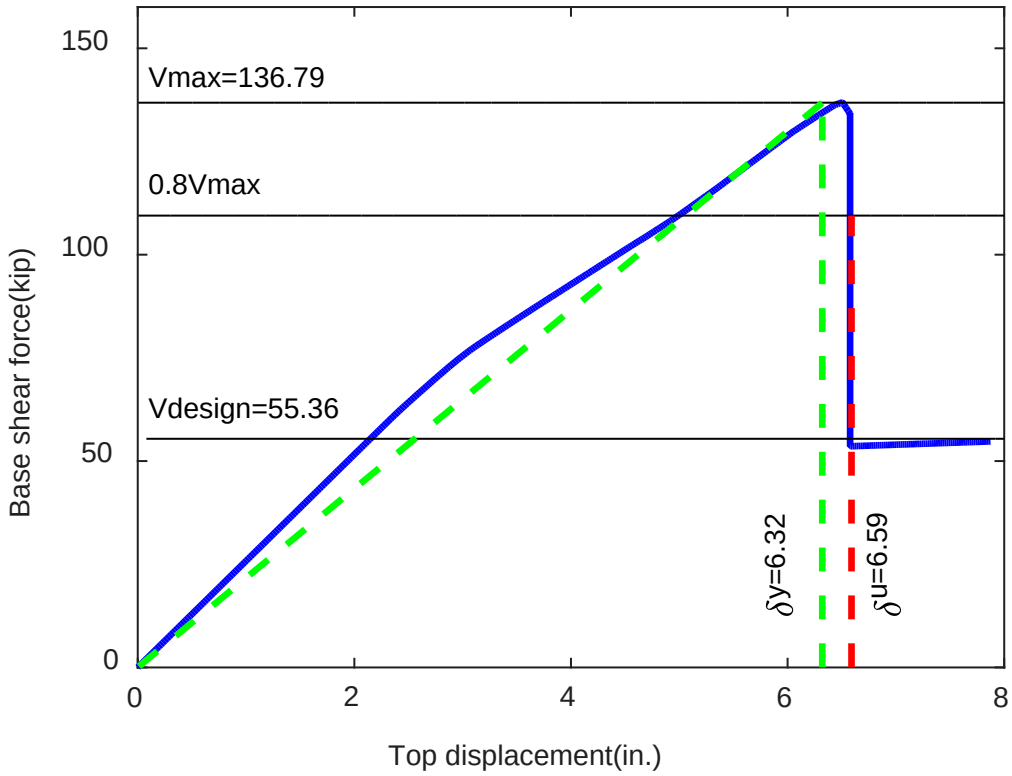

Figure E.5 - Pushover Curve of 4-Hotel Office Building Model in the Long Direction

Table E.5 - Pushover Results of 4-Hotel Office Building Model in the Long Direction

$T\ (s)$	$T1\ (s)$	$\delta_u(in.)$	$\delta_{y.eff}(in.)$	V_{max}(kips)	V_{design}(kips)	δ_T	Ω
0.440	1.131	6.588	6.321	136.79	55.36	1.04	2.47

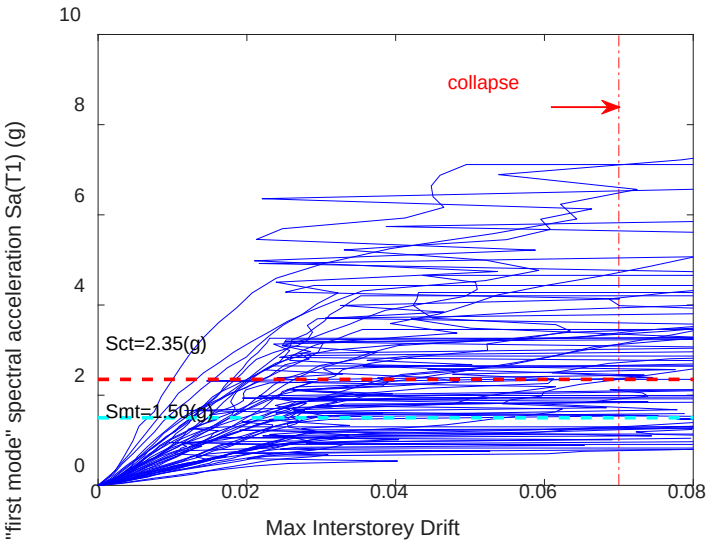

(a) IDA curve

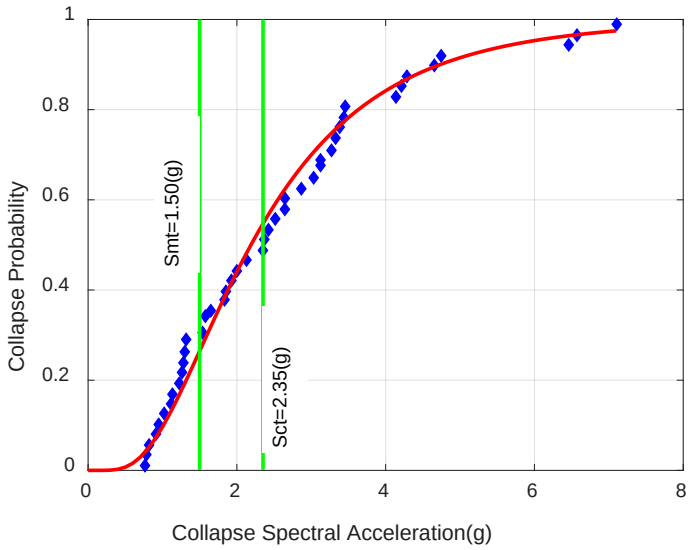

(b) Fragility curve

Figure E.6 - IDA Results of 4-Hotel Office Building Model in the Long Direction

Table E.6 - IDA Results of 4-Hotel Office Building Model in the Long Direction

S_{CT}	S_{MT}	CMR	SSF	ACMR	β_{TOT}	Accept ACMR(20%)
2.35	1.5	1.567	1.02	1.598	0.402	1.402

E4. 4-Story Hotel Building Nonlinear Analysis in the Short Direction

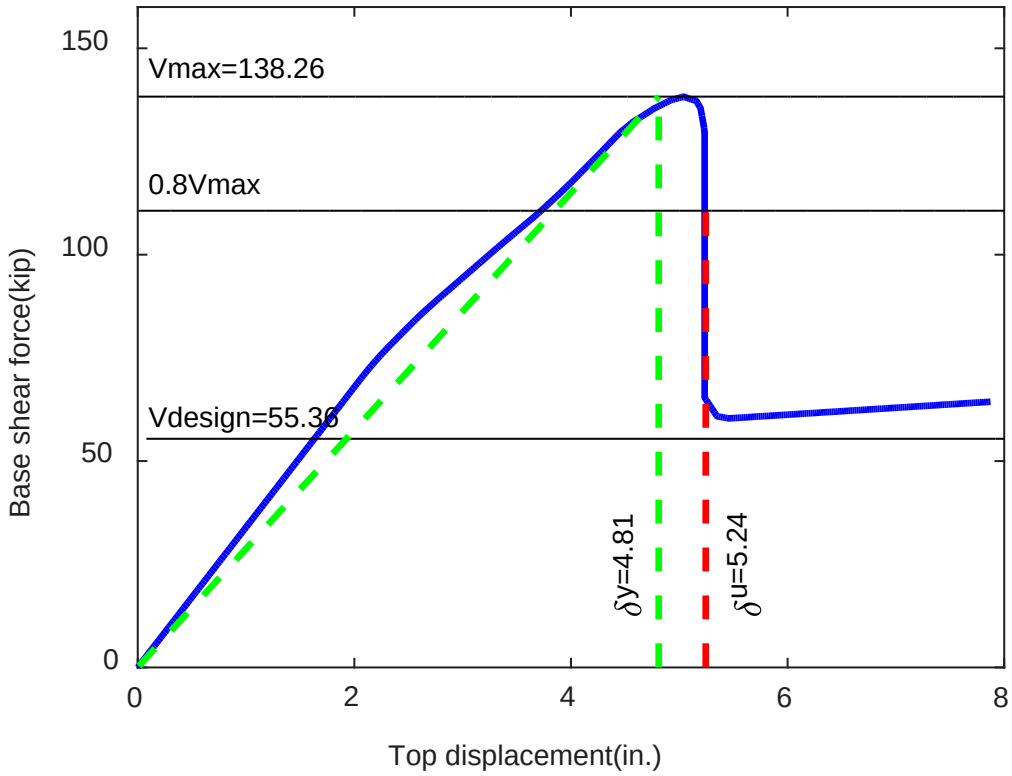

Figure E.7 - Pushover Curve of 4-Hotel Office Building Model in the Short Direction

Table E.7 - Pushover Results of 4-Hotel Office Building Model in the Short Direction

$T\ (s)$	$T1\ (s)$	$\delta_u(in.)$	$\delta_{y.eff}(in.)$	V_{max}(kips)	V_{design}(kips)	δ_T	Ω
0.440	0.981	5.244	4.81	138.26	55.36	1.09	2.50

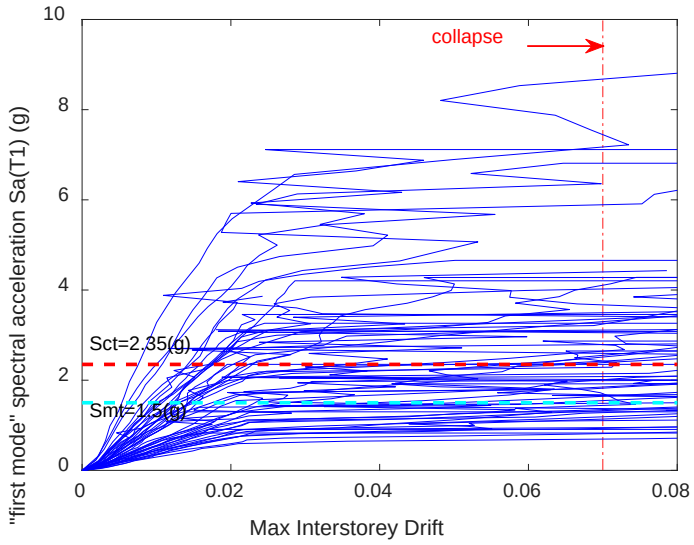

(a) IDA curve

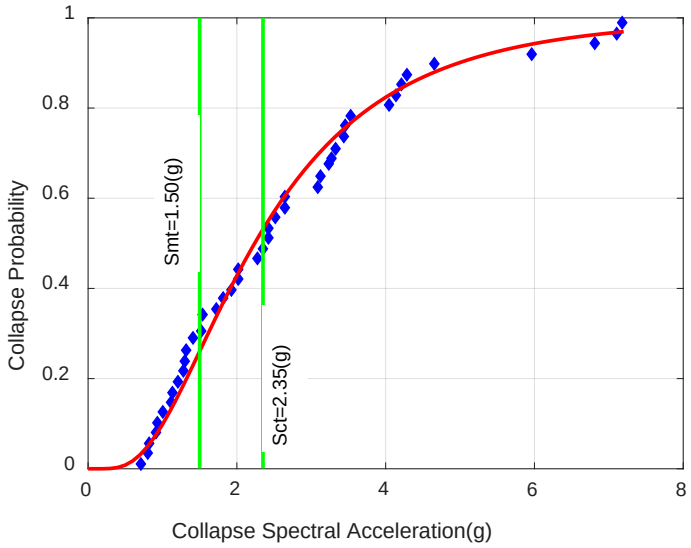

(b) Fragility curve

Figure E.8 - IDA Results of 4-Hotel Office Building Model in the Short Direction

Table E.8 - IDA Results of 4-Hotel Office Building Model in the Short Direction

S_{CT}	S_{MT}	CMR	SSF	ACMR	β_{TOT}	Accept ACMR(20%)
2.35	1.5	1.567	1.045	1.637	0.405	1.406

E5. 5-Story Hotel Building Nonlinear Analysis in the Long Direction

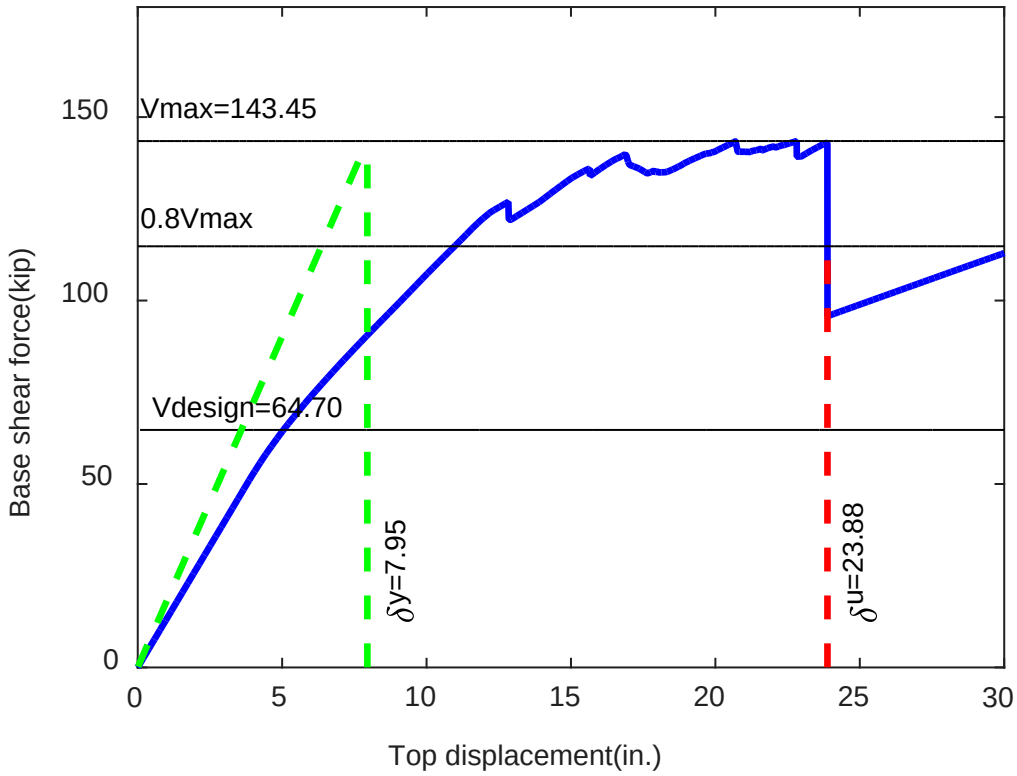

Figure E.9 - Pushover Curve of 5-Hotel Office Building Model in the Long Direction

Table E.9 - Pushover Results of 5-Hotel Office Building Model in the Long Direction

$T\ (s)$	$T1\ (s)$	$\delta_u(in.)$	$\delta_{y.eff}(in.)$	V_{max}(kips)	V_{design}(kips)	δ_T	Ω
0.520	1.336	23.88	7.95	143.45	64.7	3.00	2.22

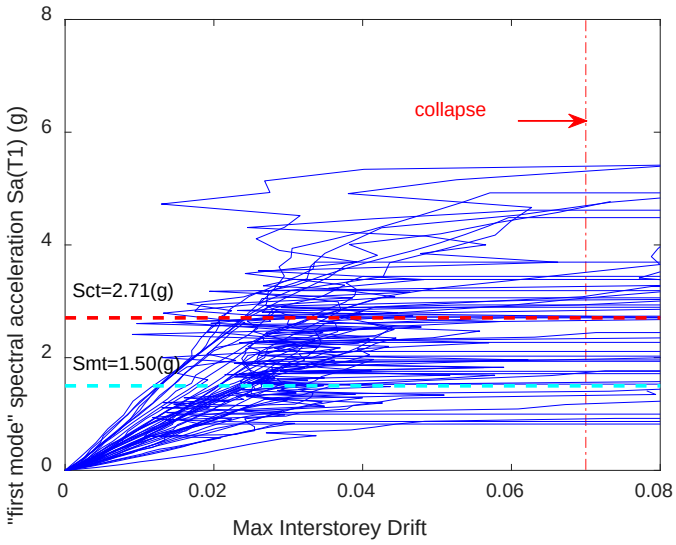

(a) IDA curve

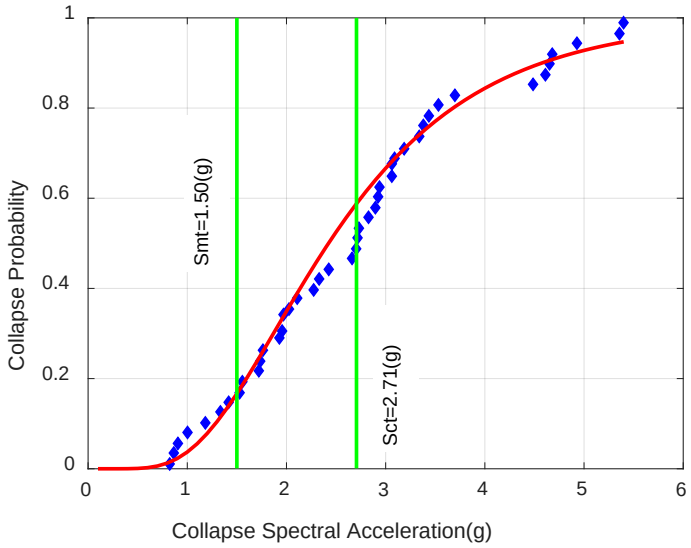

(b) Fragility curve

Figure E.10 - IDA Results of 5-Hotel Office Building Model in the Long Direction

Table E.10 - IDA Results of 5-Hotel Office Building Model in the Long Direction

S_{CT}	S_{MT}	CMR	SSF	ACMR	β_{TOT}	Accept ACMR(20%)
2.71	1.5	1.807	1.184	2.139	0.529	1.565

E6. 5-Story Hotel Building Nonlinear Analysis in the Short Direction

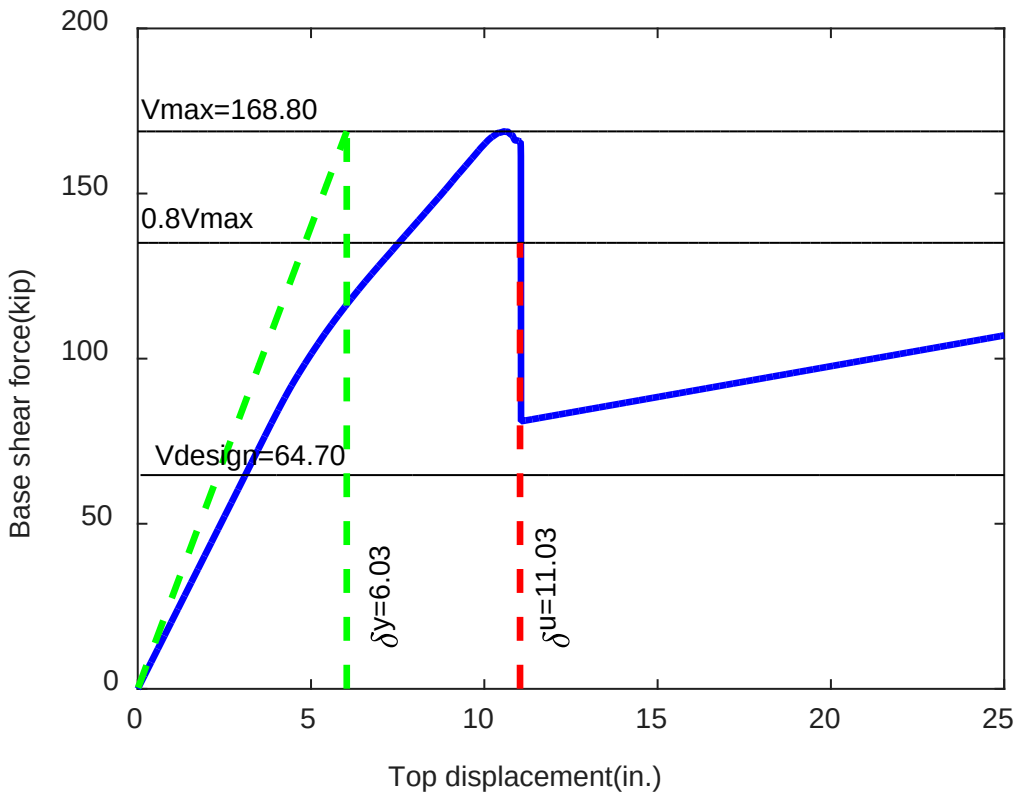

Figure E.11 - Pushover Curve of 5-Hotel Office Building Model in the Short Direction

Table E.11 - Pushover Results of 5-Hotel Office Building Model in the Short Direction

$T\ (s)$	$T1\ (s)$	$\delta_u(in.)$	$\delta_{y.eff}(in.)$	V_{max}(kips)	V_{design}(kips)	δ_T	Ω
0.520	1.072	11.03	6.03	168.8	64.7	1.83	2.61

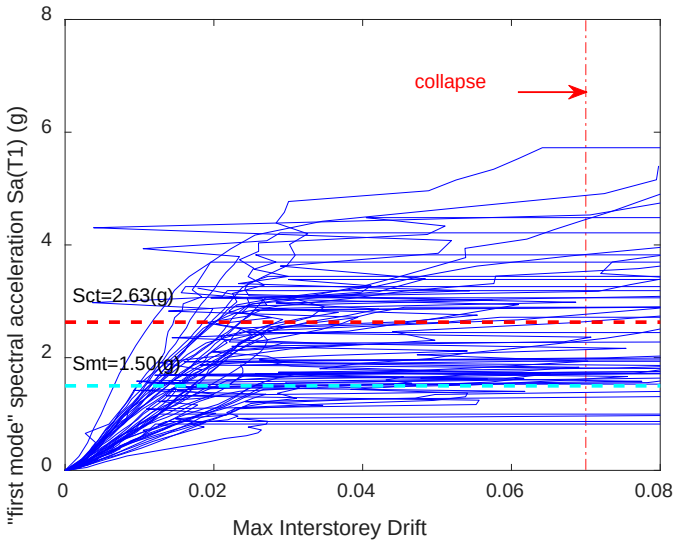

(a) IDA curve

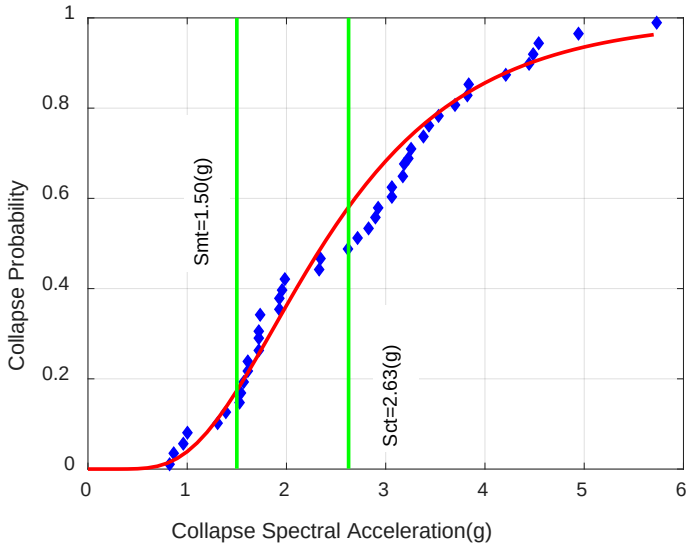

(b) Fragility curve

Figure E.12 - IDA Results of 5-Hotel Office Building Model in the Short Direction

Table E.12 - IDA Results of 5-Hotel Office Building Model in the Short Direction

S_{CT}	S_{MT}	CMR	SSF	ACMR	β_{TOT}	Accept ACMR(20%)
2.63	1.5	1.753	1.13	1.981	0.447	1.456

REFERENCES

AISI S100(2012). *North American specification for the design of cold formed steel structural members.* Washington, D.C.: American Iron and Steel Institute.

AISI S240(2015). *North American Standard for Cold-Formed Steel Structural Framing.* Washington, D.C.: American Iron and Steel Institute.

AISI S400(2015). *North American Standard for Seismic Design of Cold-Formed Steel Structural Systems.* Washington, D.C.: American Iron and Steel Institue.

ASCE 7 (2010). *Minimum design loads for buildings and other structures.* Reston, VA: American Society of Civil Engineers.

ASTM A325 (2007). *A325-07 Standard Specification for Structural Bolts, Steel, Heat Treated, 120/105 ksi Minimum Tensile Strength.* West Conshohocken, PA.: American Society for Testing and Materials.

ASTM A370(2006). *A370-06 Standard Test Methods and Definitions for Mechanical Testing of Steel Products.* West Conshohocken, PA.: American Society for Testing and Materials.

ASTM A490(2008). *A490-08 Standard Specification for Structural Bolts, Steel, Heat Treated, 150 ksi Minimum Tensile Strength.* West Conshohocken, PA: American Society for Testing and Materials.

ASTM E564(2012). *Standard Practice for Static Load Test for Shear Resistance of Framed Walls for Buildings.* West Conshohocken, PA.: American Society for Testing and Materials.

Data, A. P. (2012). *AISI Standard for Cold-Formed Steel Framing _ Product Data 2012 Edition.* Washington, D.C.: American Iron and Steel Institute.

Dubina, F. a. (2004). *Performance of wall-stud cold-formed shear panels under monotonic and cyclic loading Part I: Experimental research*. Thin-Walled Structures, 42 (2004) 321-338.

FEMA P695 (2009). *Qualifications of Building Seismic Performance Factors.* Washington, D.C.: Federal Emergency Management Agency.

Foliente GC, *Issues in seismic performance testing and evaluation of timber structural systems*[C]. International wood engineering conference, New Orleans LA, 1996, 1:29-36.

IBC (2015). *International Building Code, 2015 Edition.* Washington, D.C.: International Code Council.

Leng, J. (2015). *Simulation of Cold-formed Steel Structures.* Baltimore, MD: PhD Dissertation, Johns Hopkins University.

Madsen, R. N. (2011). *CFS-NEES Building Structural Design Narrative.* www.ce.jhu.edu/cfsness.

Mahdavian, M. (2016). *Innovative Cold-Formed Steel Shear Walls With Corrugated Steel Sheathing.* Denton, TX: Master Thesis, University of North Texas.

McKenna, F. e. (2015). *Open system for earthquake engineering simulation (OpenSees).* Berkeley, CA: Pacific Earthquake Engineering Research Center.

Park, *Evaluation of ductility of structures and structural assemblages from laboratory testing*. Bulletin of the New Zealand national Society of Earthquake Engineering, 1989, 22(3): 155-166.

Peterman, K. D. (2014). *Experimental seismic behavior of the CFS-NEES building: system-level performance of a full-scale two-story light steel framed building*. Proceedings of 22nd International Specialty Conference on Cold-Formed Steel Structures, (pp. 887-901). St. Louis, MO.

Stojadinovic and Tipping(2007). *Structural testing of corrugated sheet steel shear walls.* Ontario, CA: Report submitted to Charles Pankow Foundation.

Yu, C., Huang, Z., Vora, H.(2009). *Cold-Formed Steel Framed Shear Wall Assemblies with Corrugated Sheet Steel Sheathing*. Proceedings of the Annual Stability Conference. Phoenix, AZ: Structural Stability Research Council.

Yu, G. (2013). *Cold-Formed Steel Framed Shear Wall Sheathed with Corrugated Steel Sheet.* Denton, TX: Master Thesis, University of North Texas.

Zhang, W. Mahdavian, M., Li, Y., and Yu, C. (2016). *Experiments and Simulations of Cold-Formed Steel Wall Assemblies Using Corrugated Steel Sheathing Subjected to Shear and Gravity Loads*. Journal of Structural Engineering, Vol. 143, Issue 3.

Zhang, W. Mahdavian, M., Li, Y., and Yu, C. (2017). *Seismic Performance Evaluation of Cold-Formed Steel Shear Walls Using Corrugated Sheet Sheathing*. Journal of Structural Engineering, (Under Review).